DEPARTMENT OF MECHANICAL ENGINEERING

Nanoparticle/Biopolymer Systems for Medical Applications

Nanopartikel/Biopolymer-Systeme für Medizinische Anwendungen

a thesis

presented by

Constantin Alexander Nowald

TECHNISCHE UNIVERSITÄT MÜNCHEN

Fakultät für Maschinenwesen

Professur für Biomechanik

Nanoparticle/Biopolymer Systems for Medical Applications

Constantin Alexander Nowald

Vollständiger Abdruck der von der Fakultät für Maschinenwesen der Technischen Universität München zur Erlangung des akademischen Grades eines

Doktors der Naturwissenschaften (Dr. rer. nat.)

genehmigten Dissertation.

Vorsitzender: Univ.-Prof. Dr. Sonja Berensmeier

Prüfer der Dissertation:

1. Univ.-Prof. Dr. Oliver Lieleg
2. Univ.-Prof. Dr. Cordt Zollfrank

Die Dissertation wurde am 17.11.2016 bei der Technischen Universität München eingereicht und durch die Fakultät für Maschinenwesen am 20.03.2017 angenommen.

Summary

Hydrogels comprising biopolymers have been employed as an emerging and promising tool for *in vitro* cell culture studies, and play an important role for the development of wound gels, since they usually feature a high biocompatibility. A crucial point of wound gels are their mechanical properties: they should readily wet and cover the entire area of an uneven wound before gelation takes place *in situ*, i.e. before they form a stiff protection layer. Once a wound gel formulation that provides these required mechanical properties is generated, bioactive compounds can be integrated. Mucins, the key components of native mucus, are such bioactive compounds and serve as an initial barrier in the human body against microbial attack: they are able to prevent bacterial adhesion and can trap viruses. So far, only the weak mechanical properties of mucin solutions have prevented their application in a physiological environment, e.g. as a wound gel. In addition to the anti-microbial-properties brought about by the hydrogel itself, therapeutic agents which are of benefit to wound healing should be released from a wound gel. Here, for many pharmaceutical applications, it is important that different drugs are present in the human body at distinct time points. Typically, this is achieved by a sequential administration of different therapeutic agents. A much easier alternative would be the application of a drug enriched hydrogel that serves as a therapeutic agent delivery system containing a whole set of medically active compounds which are liberated in an orchestrated and controlled manner.

In this thesis, first commercially available basal lamina hydrogels are analyzed to study the effect of the biochemical composition of these extracellular matrix (ECM) gels on their biophysical properties, the ECMs have all been purified according to the same protocol. Nevertheless, in those gels, strong differences in the migration behavior of leukocyte cells as well as in the Brownian motion of nanoparticles could be detected. It could be shown that these differences correlate with the mechanical properties and the microarchitecture of the gels which in turn arise from small variations in their biochemical composition. In the next part of this thesis, the aim was to develop a mucin based wound gel, therefore a (mechanical) adjuvant was needed to overcome the mechanical limitation of mucin. ECM could not be employed as such an adjuvant since ECM gels are quite expensive and do not provide the required mechanical properties. Instead methylcellulose (MC) biopolymers are used to meet the mechanical requirements, thus generating a thermoresponsive methylcellulose/mucin hybrid system. The developed hybrid material combines the selective permeability properties brought about by mucins with the thermal autogelation properties of methylcellulose. As a consequence, triggered by contact with body-warm surfaces, the hybrid material rapidly forms a gel at physiological conditions, and this external temperature stimulus can also be harnessed to stimulate drug release from incorporated

thermosensitive liposomes. In addition, the hybrid gel selectively retards the release of embedded molecules which can be used to further control and prolong drug release from the gel. However, to achieve orchestrated drug release this is not sufficient. Instead it is demonstrated in this thesis, how two molecular mechanisms can be combined to solve this problem: i.e. a build-up of osmotic pressure by the depletion of a control molecule and triggered disaggregation of nanoparticle clusters by synthetic DNA sequences. The efficiency of these molecular mechanisms was investigated employing a simple hydrogel matrix, in which - due to the increased pore size and the inert character of the matrix, steric effects and electrostatic interactions with the drugs that could alter the outcome, can be excluded. Instead, with this approach, spatio-temporal control over the release of molecules and nanoparticles from the gel environment could be gained.

The findings presented here extend our knowledge of how the biochemical composition of biopolymer gels can affect their microarchitecture and mechanical properties. In addition, the development of a thermoresponsive MC/mucin hybrid gel and the strategy presented for achieving an orchestrated drug release have strong implications for developing complex anti-microbial drug delivery systems for medical applications such as wound treatment. The nanoparticle/hydrogel system developed here could also be used for the sustained release of pharmaceuticals overcoming the problem of burst drug release and will lower the need for multiple drug administrations.

Content

1 Introduction

Hydrogels are three-dimensional network structures obtained from polymers carrying hydrophilic domains or groups which can absorb and retain a significant amount of water.[1] Hydrogels have been employed as an emerging and promising tool in cell culture studies and tissue engineering, to support cell proliferation, morphogenesis and differentiation, and they play an important role for the development of wound gels.[2, 3] They facilitate the transport of oxygen, nutrients and cellular waste, as well as water soluble growth factors.[4] Typically, hydrogels are formed from aqueous solutions of polymers by a mechanism called gelation.

Both the gelation kinetics and the gel strength are determined by the polymers of the gel, the solvent and the environmental conditions. The gelation kinetics are very important for the practical applicability: e.g., *in situ* formed hydrogels applied to damaged tissue have to be able to form a gel within a short period of time to remain on site. Gel strength is at least as important as gelation kinetics, not only for the stability of the gel itself but also for cells embedded into such a gel: hydrogels used as cellular scaffolds can influence cellular mechanotransduction (the conversion of mechanical information form the microenvironment into biochemical signaling) and cell differentiation.[5, 6] Different types of hydrogel gelation mechanisms are summarized in **Figure 1**. Gelation can be a result of either intermolecular forces creating physical gels, intramolecular forces resulting in chemical gels, or a combination of both. Physical gels can be subdivided into weak and strong physical gels. Weak physical gels have reversible links formed from temporary associations between polymer chains established by e.g. weak intermolecular forces such as weak hydrogen bonds, hydrophobic or ionic associations. Strong physical gels require strong intermolecular forces, between polymer chains and are effectively permanent at a given set of environmental conditions.[7] A typical example of a strong physical gel is the gelatin gel: here, helical structures forming the network are stabilized by a multitude of interchain hydrogen bonds.[8] On the other hand, chemical gels are a result of the formation of covalent bonds leading to strong gels. The three main chemical gelation processes include condensation polymerization (where molecules join together, with elimination of water or other small byproducts), additive polymerization (which involves the reaction of unsaturated monomers, leaving no side products) and cross-linking.[7]

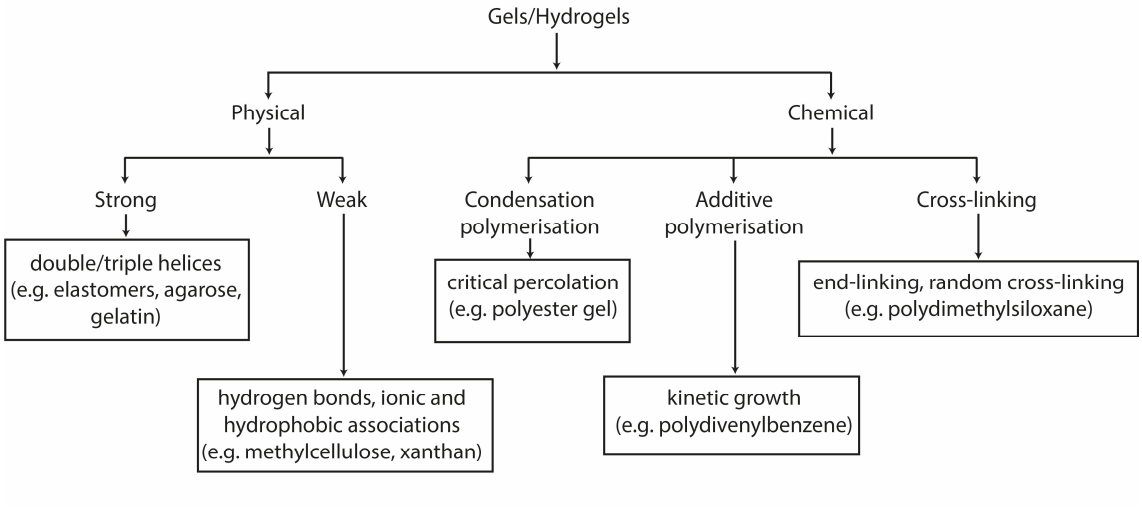

Figure 1 Classification of gelation mechanism and relevant examples.[1]

In general, two different types of scaffolds are used for cell culture studies and wound gels: reconstituted matrices comprising purified biomacromolecules such as e.g. collagen, fibrin or hyaluronic acid obtained from natural biological sources,[9-12] or synthetic extracellular matrices (ECM), e.g. composed of polyethylene glycol (PEG), polyvinyl alcohol and poly-2-hydroxy methacrylate.[13-15] Purified biomacromolecules are promising substrates primarily for biodegradable, temperature- and pH-responsive scaffolds and typically lead to physical gels (as long as no disulfide bridges are involved). Designed synthetic ECM, on the other hand, utilize intermolecular forces or intramolecular forces depending on the requirements. Both biomacromolecules and synthetic ECMs are often employed as thin coatings for 2D cell culture studies, which can provide important insights into many aspects of cellular behavior. The true strength of both systems is, however, that they can be applied as a 3D environment for embedding cells to offer a more *in vivo*-like environment than a 2D system.[16-18] Hydrogels composed of biopolymers offer the additional benefit that they usually feature a high biocompatibility which is a basic prerequisite for investigating cell behavior. Of course, biocompatibility is equally important in the context of wound treatment, especially with respect to internal injuries, where wound gels cannot be removed after treatment. A major advantage of an engineered synthetic scaffold is the opportunity to tune certain physical parameters, such as the mechanical properties or the permeability of the matrix and to investigate the influence of certain stimuli at well-defined conditions. On the other hand, ECM extracts of biological origin may be better suited to

[1] Figure adapted from: Syed K. H. Gulrez, Saphwan Al-Assaf and Glyn O Phillips (2011). Hydrogels: Methods of Preparation, Characterisation and Applications, Progress in Molecular and Environmental Bioengineering - From Analysis and Modeling to Technology Applications, Prof. Angelo Carpi (Ed.), ISBN: 978-953-307-268-5, InTech

approximate an *in vivo* environment in detail, especially if the biopolymers used to construct the scaffold are obtained from the same organism and tissue as the cells that are integrated into the matrix.[19-21]

One of the simplest biopolymer model systems in use for constructing such 3D scaffolds, mainly for cell culture studies, is a reconstituted hydrogel formed by collagen type I fibers. Macromolecules of the collagen family compromise 25 % (by dry weight) of the total protein content *in vivo*,[22] and are key constituents of various tissues including the connective tissue (collagen type I, triple helical fibers), the basal lamina (collagen type IV, fibers) and cartilage (collagen type II, fibrils).[23-25] However, they are not the only macromolecular components in those tissues, so the predictive strength of results obtained from experiments with such simple collagen matrices is limited. Also, the degree of variability and the ensuing range of biophysical properties of a scaffold comprising only one specific macromolecular component is much lower compared to a scaffold consisting of a variety of components. A more complex *in vivo*-like multi-component ECM model system is given by basal lamina gels that are typically purified from murine tumor tissue. The basal lamina is an extracellular matrix that supports epithelia, muscle fibers, blood vessels and peripheral nerves and separates endothelial or epithelial cells from the connective tissue. This specialized ECM is composed of three main macromolecular constituents, i.e. laminin 56 %, collagen IV 31 % and the perlecan complex, the latter of which combines three heparin sulfate chains into a finger-like structure which is attached to the biopolymer network. In addition to those macromolecular components and other minor components, basal lamina gels contain about 8 % of the cross-linker protein entactin (nidogen) which connects the laminin macromolecules with the collagen network (see **Figure 2**).[26] Thus, such a basal lamina gel offers a much higher complexity and biologically more relevant environment than simple collagen gels.[24, 27-29]

The complexity of such multi-component hydrogels is, in many cases, at the same time the weak point of experiments conducted with these kind of matrices. Commercially available basal lamina variants, e.g. those purified from the same murine tissue following the identical protocol established by Kleinman, [30, 31] should be very similar and differ only minimally in their protein composition. Though these deviations may appear negligibly small, but they can nevertheless have a large impact on e.g. the mechanics, permeability and bioactivity of the gel matrix. Such unwanted differences in the protein composition of basal lamina gels from four different vendors have been used in this thesis to investigate how the biophysical properties of such gels depend on their biochemical composition (see chapter 3.1). Therefore, the precise composition of the four basal lamina variants was identified and the influence on cell migration and particle diffusion was

investigated. With this approach, a detailed understanding of how variations in the biophysical properties of those gels are regulated on a molecular level was obtained. Such information will not only simplify the interpretation of future cell culture experiments but also provides important insights for the design of artificial hydrogel scaffolds.

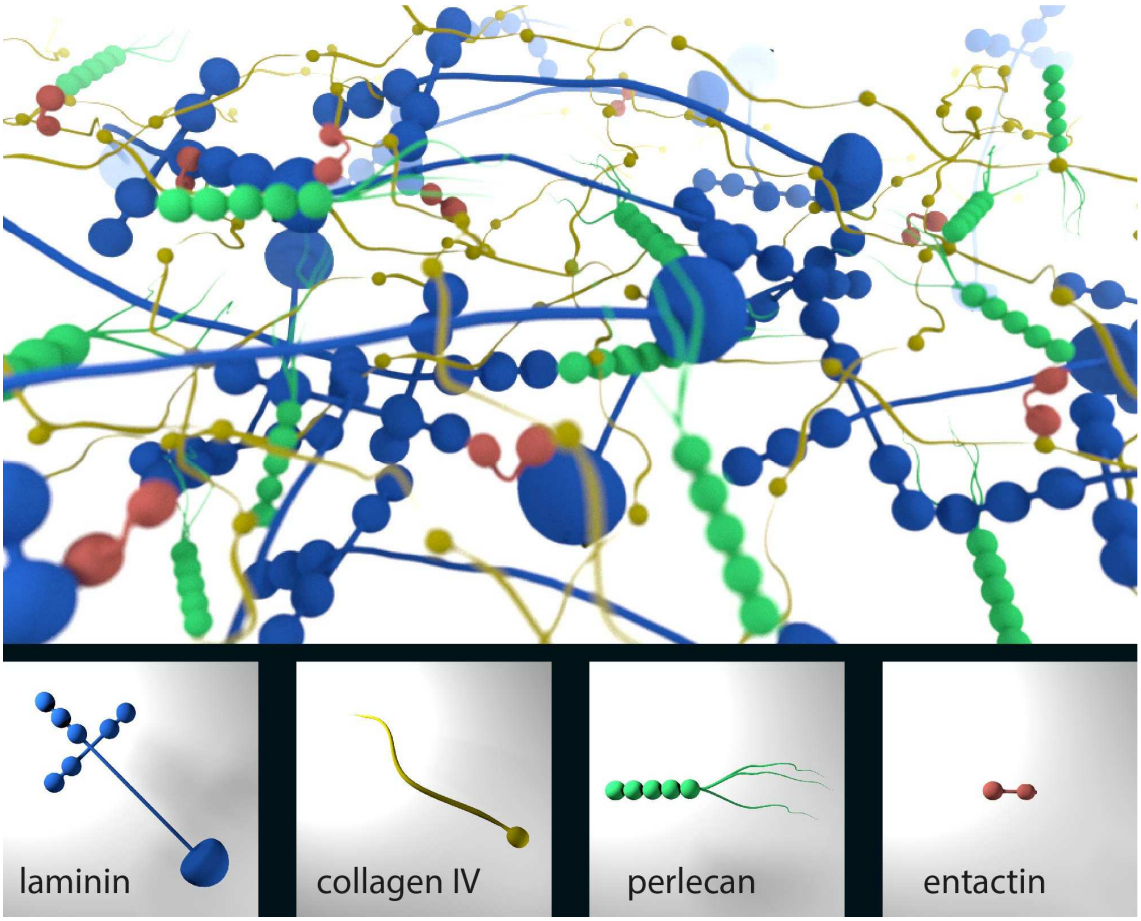

Figure 2 Molecular structure of basal lamina: The main components laminin and collagen IV self-assemble into networks which are connected via entactin and perlecan. (I want to thank Iris König-Decker for designing the 3D model of the basal lamina which provided the basis for this schematic visualization.)

In the second part of this thesis, a bioactive hydrogel was developed that can serve as a wound gel with tailored mechanical properties. As the name indicates, hydrogels have a high water content which is important for maintaining a moist environment and thus permits optimal healing rates for a wound.[32] Furthermore, hydrogels are applied as wound gels especially in cases where a conventional dressing is difficult to apply e.g. on deep and irregular lesions. Simple wound gels offer mechanical wound protection and are able to prevent, to a certain extent, microbial infections. The latter ability is becoming more and more important due to the increasing number of bacterial strains that are resistant to modern antibiotics. As of today, despite modern medicine, bacterial and viral infections still represent a major cause of disease that may lead to severe illness

or even death. Each year in the US alone, at least 2 million people are confronted with bacterial infections that are resistant to modern antibiotics, and of those over 23,000 are lethal (status 2013).[33] In particular, patients suffering from an open wound, where the skin (our first natural barrier against such microbial infections) is compromised, have a drastically increased risk of contracting an infectious disease. [34, 35] The same is true during and after surgery, where the vulnerable core of the human body is exposed to microbial attacks, even though surgery is performed under as sterile conditions as possible. Examples for pathogens causing such nosocomial infections include Hepatitis B and C, HIV, *Staphylococcus aureus*, *Proteus mirabilis*, *Klebsiella pneumoniae*, and *Acinetobacter*.[36] For instance, a study performed at a Korean hospital between April 1991 and March 1992 on 789 surgery patients showed that the Hepatitis C infection rate was more than 10-fold higher for patients that had undergone surgery compared to the control group.[37]

One approach to enhance the antimicrobial quality of wound gels is engineering bioactive hydrogels. This type of wound dressings are made of materials that can play an active role in wound protection and healing.[38] One example for such a bioactive hydrogel in the human body is the mucus layer covering the surface of wet epithelia, a natural gel that offers many properties desired for wound healing.[39] The major macromolecular constituents of mucus are large, highly glycosylated macromolecules called mucins. Mucin molecules have a protein core rich in thiol groups and contain both hydrophobic and charged domains. The cysteine rich regions contain domains that possess sequence similarity to C-terminal cystine knot domains, and von Willebrand factor (vWF) C and D domains.[40-42] These regions of the mucin molecule have been shown to be involved in mucin dimerization and subsequent polymerization to form multimers via disulfide bonds.[43] In addition, carbohydrates such as N-acetylgalactosamine, N-acetylglucosamine, fucose, galactose, sialic acid and traces of mannose and sulfate are attached to the protein backbone. These oligosaccharides consist of up to 15 monomers, provide intramolecular and intermolecular hydrogen bonding capabilities and are arranged in a “bottle brush” configuration (see **Figure 3**).[44] Mucin glycoproteins that have been manually purified from natural sources still exhibit their native inherent glycosylation pattern. In contrast to commercially purified (and partially degraded) mucins, those native mucins have recently been demonstrated to have a broad range of medically highly relevant properties, which would be of great benefit for any kind of wound gel: Mucins reduce bacterial adhesion when used as surface coatings,[45, 46] and they can also serve as a potent shielding layer reducing the infection rate of various viruses.[47] Moreover, the abundant glycosylation of the protein backbone, which can make up to 75 % of the weight,[48] give mucins considerable water-binding capacity and make them quite resistant to proteolysis. Thus, they are ideal components for hydrogels.

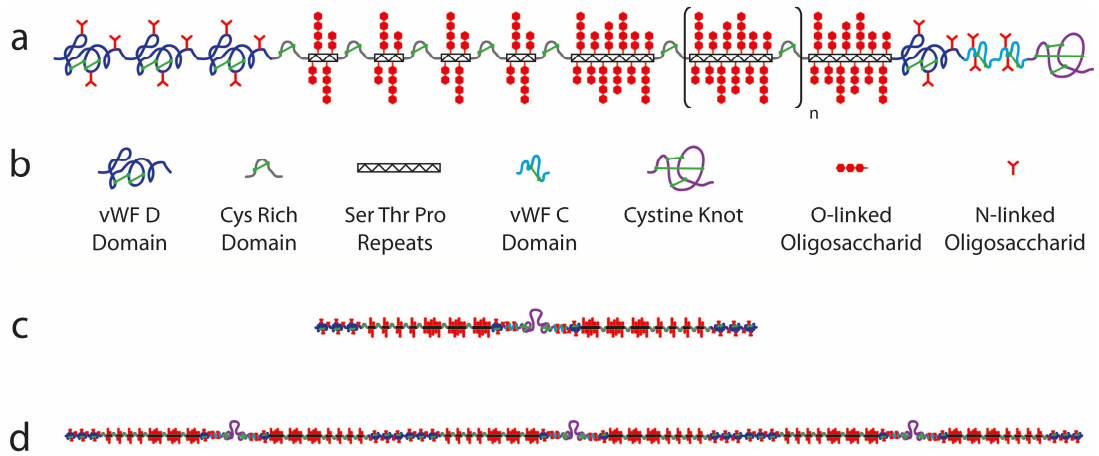

Figure 3 (a) Schematic visualization of the porcine gastric mucin monomer consisting of a core protein which is highly glycosylated in the middle and is flanked by regions of low glycosylation. (b) The symbols indicate the different domains of the drawing in (a). (c) A dimer can be formed by two monomeric subunits linked through disulfide bonds in the low-glycosylated regions, (d) which can be further linked via disulfide bonds to form longer multimers.[2]

A source from which sufficient quantities of mucins can be purified is the porcine gastric mucosa. However, special attention has to be paid to maintain the glycosylation motifs, since they are critical for the medically interesting properties of mucins. [49, 50] These purified and lyophilized mucins can be reconstituted at different concentrations and pH conditions as desired,[51, 52] and they possess buffering capabilities themselves.[53, 54] However, due to their unsatisfactory mechanical performance, reconstituted mucin solutions are not suitable for a direct application as a wound gel: Whereas reconstituted mucin solutions are able to form a weak gel with a shear stiffness on the order of a few Pascal, this gelation only occurs at acidic pH (≤ pH 4) and at low ionic strength (≤ 100 mM NaCl).[55] Ideally, the final shear stiffness of a wound gel should be on the order of the stiffness of cells and soft tissues, which is in the range of a few to tens of kPa.[56] Moreover, both conditions, i.e. low pH and low ionic strength, are not compatible with the physiological environment of a wound. Thus, to develop a bioactive mucin hydrogel in order to benefit from the anti-microbial properties of mucins, the viscoelastic properties of mucin solutions needed to be improved. Crouzier and coworkers were able to produce a mucin hydrogel with a shear stiffness similar to that of soft mammalian tissue, serving as a platform for sustained drug delivery.[57] There, gelation was triggered by ultraviolet light in the presence of a free radical photoinitiator, resulting in a covalently crosslinked hydrogel of methacrylate-modified mucin. Unfortunately, none of these conditions are suitable for an application in a physiological

[2] Figure adapted from: Bansil, R. and B.S. Turner, *Mucin structure, aggregation, physiological functions and biomedical applications.* Current Opinion in Colloid & Interface Science, 2006. **11**(2–3): p. 164-170.

environment: neither ultraviolet light, nor the free radical photoinitiator can be used, if gelation should take place *in situ*, i.e. on a wound.

The idea pursued in this thesis was to develop a hybrid gel consisting of a nontoxic base material providing the required mechanical properties (i.e. a gelation mechanism suitable for application on a patient's wound) and to incorporate mucin into this base material (see chapter 3.2). The addition of small amounts of mucins should be sufficient, since it is known from literature that mucin solutions as diluted as 1 % (w/v) exhibit high antiviral activity.[47] This concentration is also a good approximation for the concentration of mucins in native mucus gels.[58-60] Ideally, the hybrid gel should still be fluid enough so it can cover even the most difficult and uneven areas of a wound. At the same time, the mixture is required to form a stiff gel within seconds upon contact with the wound. Employing the previously examined basal lamina as an adjuvant to receive the desired mechanical properties would offer the requested gelation kinetics but a shear stiffness of only a few Pascal. Furthermore, this approach would involve unnecessarily high costs as commercial basal lamina is purified from murine tumor tissue. Instead, methylcellulose (MC) biopolymers were chosen as a mechanical adjuvant to provide the mixture with the required gelation properties. MC is nontoxic, biocompatible, cheap and forms a gel at high temperatures. [61, 62] The use of MC enabled the development of a MC/mucin hybrid wound gel, capable of forming a stiff gel at physiological temperatures and possessing selective permeability properties similar to those of mucus. Since hydrogel wound gels are increasingly also employed as drug reservoirs to support the wound healing process, temperature sensitive liposomes were added to the MC/mucin gel. Thus the same temperature trigger responsible for quick gelation can also initiate prolonged drug release from liposomes stored in the macromolecular MC/mucin matrix (see **Figure 4**).

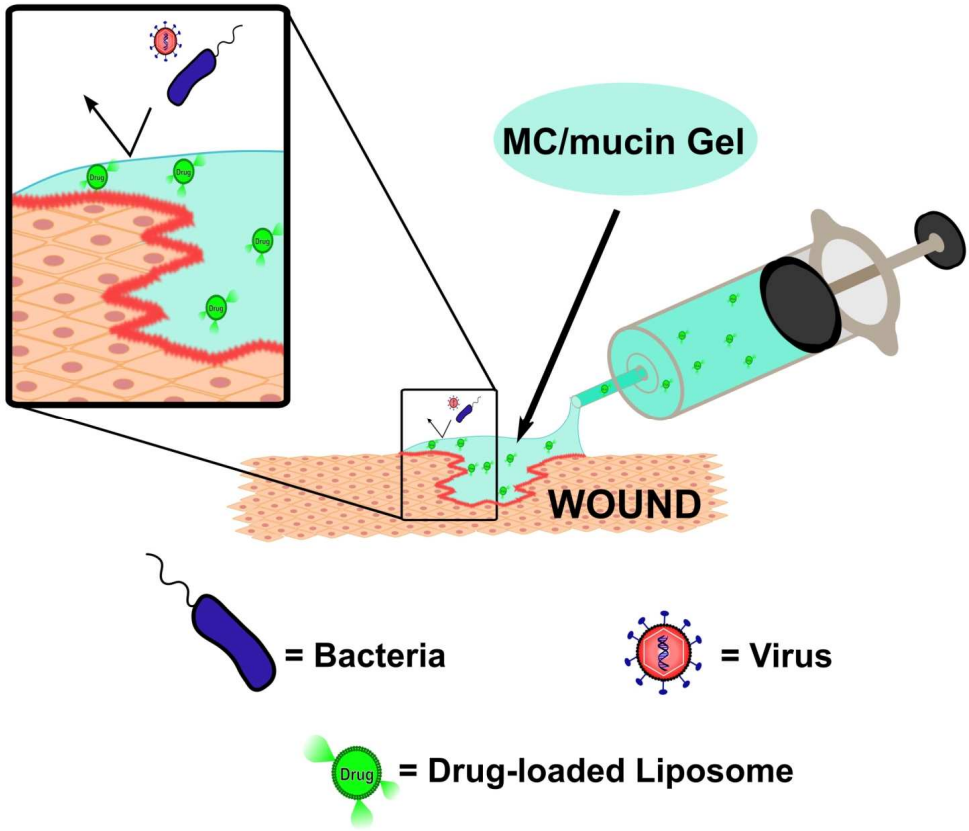

Figure 4 Schematic visualization of a lesion covered with the MC/mucin hybrid gel for successful wound healing. Here, the MC/mucin hybrid gel acts as a protective layer against bacteria and viruses and can be enriched with drug-loaded nanoparticles.

In the final part of this thesis, the aim was to achieve control over drug release kinetics from hydrogels (see chapter 3.3). To some extent, this was already possible with the MC/mucin hybrid gel system in combination with temperature sensitive liposomes. For many pharmaceutical applications, it is important that different drugs are present in the human body at distinct time points. Typically, this is achieved by a sequential administration of different therapeutic agents. A much easier alternative would be to develop a drug delivery system containing a whole set of medically active compounds which are released in a pre-defined manner. One example of a complex biological process requiring the orchestrated action of multiple molecules, which could benefit from such a hydrogel, is wound healing: Here, the regeneration of lost or inflammated tissue is more effective if growth factors are released sequentially within narrow time windows when they are needed.[63] After an injury, a finely tuned and well-timed healing cascade takes place: Different kinds of cytokines are required at certain points in time, including the platelet-derived growth factor (PDGF), transforming growth factor-beta (TGF-ß) and vascular endothelial cell growth factor (VEGF). PDGF initiates the chemotaxis of a variety of cell types such as neutrophils, macrophages, smooth muscle cells and fibroblasts – a process that is critically needed

to initiate wound healing. TGF-ß is also required during the early stage of the healing cascade, as it stimulates fibroblast proliferation, collagen synthesis,[64] attracts macrophages and stimulates them to secrete additional cytokines.[65-67] VEGF, in contrast, is the most important cytokine of the angiogenic cascade which takes place at a later stage of wound healing.[68, 69] This example involving only three different cytokines already illustrates the complexity of the wound healing process. It also shows that the three growth factors need to be available at different time points to ensure that the process correctly runs its course.

To support the natural wound healing abilities of the human body after injuries or to compensate for a pathological defect in the wound healing cascade of certain patients, medical products loaded with a set of therapeutic agents can be used. Typically, a gel enriched with molecules beneficial for the wound healing process is applied to the damaged tissue area.[70-73] In many cases, it is necessary to replace such wound gels several times during the healing process or to apply different liquids or gel formulations – each containing another set of bioactive molecules providing optimal support of each stage.[74, 75] Even though certain medical treatments are more efficient when drugs are administered sequentially,[76] this is not easily possible when repeated access to the tissue area is restricted, e.g. in the case of internal wounds after surgery. Here, all relevant therapeutic agents are typically applied at the same time[77, 78] – although their individual function is required at different time points. Moreover, even for easily accessible lesions avoiding the unpleasant procedure of wound gel replacement would be beneficial, as this would lower the risk of infections and contribute to the patient's well-being.

One existing strategy for establishing control over the release kinetics of therapeutic agents from gels targets the chemical composition of the gels to tune their pore size [79, 80] or the binding affinity of the drug to the gel constituents.[80] However, this strategy requires a tailored gel matrix for each drug. Examples for such an optimized drug/gel release system include the release of lidocaine from poloxamer 407 or sodiumcarboxymethyl cellulose gels,[81] or the release of doxorubicin from acrylate-based hydrogels[82]. Another approach makes use of the liberation of molecules from nanoparticles; here, the type and architecture of the nanoparticle determines the release kinetics of the encapsulated drug.[83]

When liposomes are used as drug carriers, variations in the lipid composition result in different release kinetics.[84] Anorganic porous nanoparticles on the other hand such as mesoporous silica nanoparticles (MSNs) and titanium dioxide (TiO_2) particles possess a stable, uniform and porous structure, high surface area, tunable pore sizes and well defined surface properties. When such porous nanoparticles are loaded with drugs, they release their cargo by diffusion.[85-89] Surface modifications of porous nanoparticles such as amination make use of electrostatic interactions to

achieve high loading rates and sustained drug release of negatively charged drugs like Ibuprofen and Aspirin.[90, 91] A different drug release mechanism from nanoparticles require polymer based nanoparticles and utilizes a combination of diffusion of cargo molecules from the nanoparticles and nanoparticle degradation.[92] Examples for such polymeric nanoparticles include chitosan,[93, 94] dextran[95, 96] and poly(methyl methacrylate) based nanoparticles.[97]

For medical applications such as wound treatment, such nanoparticles are typically incorporated into hydrogels. This is done to ensure that particles remain in place and to allow possible retardation of the release of the incorporated drugs by two mechanisms: release from the nanoparticle and subsequent release from the gel.[98, 99] Yet, whereas this combined strategy is sufficient to achieve prolonged drug release, always the same molecule is liberated. Therefore, drug co-delivery systems based on the encapsulation of multiple therapeutic agents into nanoparticles or embedding multiple nanoparticle species into a hydrogels have been developed.[100, 101]

As complex as those release approaches already are, they still share a key disadvantage: drug release can be prolonged but is immediately initiated for all molecules at the same time, i.e. after the gel sample is prepared (see **Figure 5**). Yet, there is a clear need for devising a control mechanism which allows for coordinating the release of the different incorporated drugs, e.g. liberating a second drug only when a another one has already left the gel.

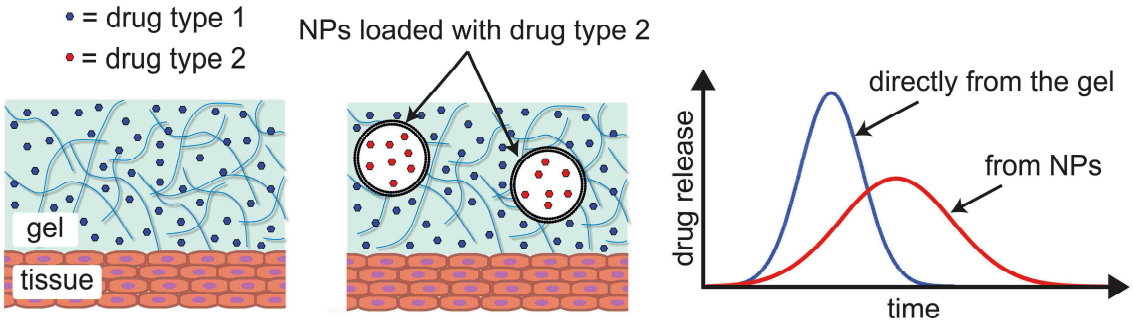

Figure 5 Schematic illustration of current drug release mechanisms from hydrogels: On the left side a simple setup, for the release of a bare drug form the hydrogel to the surrounding tissue, is depicted. In the middle, in addition to the first drug, the setup is supplemented by nanoparticles loaded with a second type of drug. The right side of the figure shows a schematic, illustrating the simultaneously starting drug release, of drug type1 and drug type 2 over time, corresponding to the setup in the middle.

To address this issue, a complex drug release mechanism from a hydrogel was developed that combines two different kind of nanoparticles. The first kind of nanoparticle was designed to release its cargo by a physiological trigger, the released cargo, in turn, initiated the disaggregation of clusters formed by a second nanoparticle species and thus the retarded release of those nanoparticles from the hydrogel.

2 Materials and Methods

The following chapter follows in part the publication: "The biophysical properties of basal lamina gels depend on the biochemical composition of the gel" published 2015 in Plos One.[102]

2.1 Biochemical Composition and Biophysical Properties of Basal Lamina Gels

Commercially available basal lamina preparations for *in vitro* studies (purified from the Engelbreth-Holm-Swarm sarcoma of mice according to the protocol established by Kleinman)[30, 31] were purchased from different vendors. Divergent results obtained from these different ECMs suggested that they vary in their composition. This gave the incentive for the first part of this thesis, i.e. to study the effect of the biochemical composition of these ECM gels on their biophysical properties.

2.1.1 Basal Lamina Gels

All basal lamina gels used in this thesis were growth factor reduced (gfr) but could due to the particular purification process still contain minor amounts of molecules that originate from other tissue types[103] in addition to the main macromolecular components 56 % laminin, 31 % collagen IV and 8 % entactin.[3] The gels were purchased from the following four suppliers: Sigma-Aldrich, Schnelldorf, Germany (ECM1), BD Bioscience, Heidelberg, Germany (ECM2), Trevigen, Gaithersburg, USA (ECM3) and Life Technologies, Carlsbad, USA (Invitrogen) (ECM4). The protein concentration of the ECMs varied from c = 7.37 mg/mL (ECM1) to c = 15.65 mg/mL (ECM3), but was adjusted for all experiments to 3.5 mg/mL by dilution with Iscove's Modified Dulbecco's Medium (IMDM, PAA Laboratories GmbH, Pasching, Austria) or Dulbecco's Modified Eagle's Medium (DMEM, Life Technologies). All experimental results have been verified with a second batch of gels, except ECM1 from Sigma-Aldrich, since it was not possible to obtain a second gfr gel batch from Sigma. Thus, as an alternative, a non-gfr gel from Sigma-Aldrich was used to repeat all experiments except the cell migration studies, since it could not be excluded that the additional growth factors would alter the results.

[3] According to the manufacturer's information

2.1.2 Polystyrene Particles for Diffusion Experiments

Fluorescent [(Ex/Em) (580 nm/605 nm)] polystyrene latex particles, carboxyl-terminated (COOH) or amine-terminated (NH_2) with a diameter of 200 nm were obtained from Invitrogen. A polyethylene glycol (PEG, M_w = 750 Da, Rapp Polymere, Tübingen, Germany) coating shielding the negative surface charge of fluorescent 200 nm carboxyl-terminated latex beads was performed using a carbodiimide-coupling protocol [104]. Successful PEGylation was verified by determining the zeta-potential of the particles suspended in 20 mM Tris-(hydroxymethyl)-aminomethanhydrochlorid (Tris/HCl, Carl Roth, Karlsruhe, Germany), 10 mM sodium chloride (NaCl, Carl Roth) buffer at pH 7.3, using dynamic light scattering implemented in a Zetasizer ZS (Malvern Instruments, Herrenberg, Germany). A zeta-potential of ζ = -34.7 ± 1.0 mV was measured for the carboxylated particles before PEGylation and ζ = -11.4 ± 1.6 mV after PEGylation proving that a least a partial PEGylation was achieved. For the aminated particles, a positive zeta-potential of +7.5 ± 1.7 mV was measured.

2.1.3 Particle Diffusion Experiments

For particle diffusion experiments carboxyl-terminated, amine-terminated and PEGylated particles as described in section 2.1.2 were embedded into ECM gels. First, ECM gels were thawed on ice and afterwards diluted with IMDM to a final protein concentration of 3.5 mg/mL in presence of the respective test particles before gelation was induced at 37 °C for 30 min. Dehydration of the samples and drift within the sample was prevented by sealing the diffusion chamber, consisting of an object slide and a cover glass, with vacuum grease which also served as a spacer. Particle trajectories were obtained and analyzed as described before in Arends *et al* [105]. In brief, movies of particles were acquired with a digital camera (Orca Flash 4.0 C11440, Hamamatsu, Japan) at frame rates of about 16 fps using the software Hokawo provided by Hamamatsu on an Axiovert 200 (Zeiss, Oberkochen, Germany) fluorescence microscope with a 32 x objective (Zeiss). Particle trajectories were obtained using the image analysis software OpenBox developed at TU München:[106] Particle positions were determined for each frame by fitting a Gaussian to the x- and y-section of the intensity profile of each individual particle. Then, the mean-square displacement (MSD) was determined from the trajectory $\vec{r}(t)$ of a particle, as follows:

$$MSD(\tau) = \frac{1}{N}\sum_{i=1}^{N}[\vec{r}(i\Delta t + \tau) - \vec{r}(i\Delta t)]^2 \quad \textbf{(1)}$$

where $r(t)$ is the position of the particle at time t, and τ is the lag time between two positions. Assuming normal diffusion, the mean-square displacement is related to the diffusion coefficient D via $MSD(\tau) = 2nD\tau$, where $n = 2$ applies for the quasi-two-dimensional trajectories $\vec{r}(t) = \big(x(t), y(t)\big)$, since all trajectories obtained are 2-dimensional projections of 3-dimensional particle movements. All particles with an apparent diffusion coefficient lager than $D_{cut} = 1\ \mu m^2/s$, which is half the diffusion coefficient of a 200 nm-sized particle in pure water, were classified as "diffusing". In every sample, particles from at least three different fields of view were analyzed, with some spatial distance to each border to avoid spatial restriction. Every experiment was repeated three times so that a total of at least 1000 particles have been analyzed for each particle species.

2.1.4 Liposome Generation and Loading

Liposomes were generated by means of lipid film hydration as follows. First, the needed amount of lipids dissolved in chloroform were mixed and transferred into a glass vial. The chloroform was then evaporated overnight, and the remaining lipid film could be hydrated with any buffer of intrest, typically containing everything the liposome should be loaded with. Only in the case of doxorubicin hydrochloride (Dox) loading, the loading process took place after liposome formation (see section 2.2.9). During hydration, thorough vortexing led to the formation of large multilamellar liposomes. Subsequently, an ultra-sonication step was added to obtain unilamellar liposomes of decreased size. Afterwards, the size of the liposomes was adjusted using a mini-Extruder (Avanti Polar Lipids, Alabaster, USA) equipped with a polycarbonate membrane possessing a pore size matching the desired liposome diameter. Finally, free molecules which were not enclosed within the liposomes were removed by means of dialysis using dialysis tubes (Carl Roth) or by SEC with an appropriate cut-off.

2.1.5 Liposomes of Varying Charge

Unilamellar liposomes of neutral, negative and positive charge with a size of 100 nm were produced according to section 2.1.4. Therefore, 1 µmol of the following lipid mixtures were used: neutral liposomes (DOPC (+/-) liposomes): 85 mol% 1,2-dioleoyl-*sn*-glycero-3-phosphocholine (DOPC), 5 mol% 1,2-dioleoyl-3-trimethylammonium-propane (DOTAP) and 5 mol% 1,2-dioleoyl-sn-glycero-3-phosphoethanolamine-N-(lissamine rhodamine B sulfonyl) (DOPE-Rhod); negative liposomes (DOPG (-) liposomes): 90 mol% 1,2-dioleoyl-sn-glycero-3-phospho-(1'rac-glycerol) (DOPG), 10 mol% DOPE-Rhod; positive liposomes (DOTAP (+) liposomes): 90 mol% DOTAP, 10 mol% DOPE-Rhod and rehydrated in 300 µl IMDM (all lipids were purchased from Avanti Polar Lipids, Alabaster, USA). Dynamic light

scattering was used to determine the zeta-potential of the different charged liposomes on a Nano ZS zetasizer (Malvern Instruments). Liposome concentration was determined, after image acquisition using ImageJ 1.47d. Therefore, the liposome solution was diluted and loaded onto a thoma counting chamber possessing a depth of 0.005 mm, before images were taken on an Orca Flash 4.0 C11440 digital camera mounted onto an Axiovert 200 (Zeiss, Oberkochen, Germany) fluorescence microscope with a 32 x objective (Zeiss).

2.1.6 Cell Migration within Different ECMs

For cell migration experiments, the human promyelocytic leukemia cell line HL-60 (CCL-240, ATCC, Wesel, Germany) was used. This cell line is a simple model system developed to study neutrophil cell migration without the need to derive cells from primary tissue [107]. HL-60 cells have several advantages over primary neutrophils, which include a higher reproducibility in their behavior and a significantly longer life span. HL-60 cells are maintained as suspension cell line in culture, and can be terminally differentiated into adherent migration-competent neutrophil-like cells (dHL-60) using, for example, dimethylsulfoxide (DMSO, Carl Roth). In brief, HL-60 cells were cultivated in IMDM supplemented with 15 % (v/v) heat-inactivated fetal bovine serum (FBS, PAA Laboratories GmbH, Pasching, Austria) at 37 °C and 5 % carbon dioxide (CO_2) and passaged when cell density of 1-2x10^6 cells/mL was reached. To differentiate cells, 1.3 % (v/v) DMSO was added to 2x10^5 cells/mL suspended in fresh IMDM+FBS. Upon differentiation, cells underwent clear morphological changes which were followed using a light microscope in phase contrast mode. Since cells are most active 4-5 days post-differentiation they were used after 4 days for cell migration studies. Respectively, 1x10^4 dHL-60 cells were suspended in ice-cold ECM samples as obtained from the four different suppliers and diluted with IMDM supplemented with N-formyl-methionine-leucine-phenylalanine (fMLP, Sigma-Aldrich) to a final concentration of 3.5 mg/mL ECM and 50 nM fMLP. The uniformly distributed chemoattractant fMLP was added to trigger spatially homogeneous cell migration. A volume of 50 µL of each ECM/cell mixture was then transferred into one lane of a µ-Slide VI 0.4 (ibidi, Planegg/Martinsried, Germany) while avoiding bubbles and incubated for 30 min at 37 °C and 5 % CO_2 in a cell incubator to allow for gel formation. After gelation, 50 µL of IMDM supplemented with 50 nM fMLP were added on top of the gel both at the inlet and outlet of the lane to allow for continuous nutrient supply and to minimize dehydration of the samples. Images for the migration experiments were acquired on a motorized Axiovert 200M microscope (Zeiss) using a 10x objective (Zeiss). A heating- and CO_2-chamber mounted onto the microscope was used to control temperature and CO_2 concentration. Movies of migrating cells were recorded with an AxioCam digital camera (Zeiss) and the software AxioVision V.4.8.20 (Zeiss). To avoid artefacts arising from gel swelling

often occurring at the beginning, an initial adjustment time of 4 h was provided. Then, phase contrast images were acquired every minute for 2 h at different locations in the gel. The x-y-position of the cells in the gel matrices were determined manually with ImageJ 1.47d for every frame of the migration video, and the migration velocity was then calculated by multiplying the average migrated distance per frame with the frame rate. The Euclidean distance (*ED*) between the start and the end position of each cell of the evaluation was calculated with a Chemotaxis and Migration Tool V2.0 (ibidi) and averaged over all cells in the respective gel.

2.1.7 Cell Migration in ECM Gels in Presence of Liposomes of Different Charge

ECM2 gels were loaded with either neutral, negatively or positively charged liposomes and analyzed for effects on dHL-60 cell migration. Therefore, ECM2, fMLP, dHL-60 cells and liposomes (final liposome concentration within the gel: 10^{10} liposomes/µL) were mixed before gelation. Gel production as well as image acquisition and evaluation was performed according to section 2.1.6.

2.1.8 Western Blots

Detection and quantification of specific proteins in each ECM sample by means of western blot was performed by K. Pflieger at the Department of Pharmacy—Center for Drug Research of the Ludwig Maximilians University of Munich in the group of Prof. S. Zahler. The following primary antibodies were used: mouse monoclonal anti-fibronectin C6F10 (1:200), rat monoclonal anti-nidogen ELM1 (1:500) (sc-73611, sc-33706; Santa Cruz, Heidelberg, Germany), rabbit polyclonal anti-collagen type IV (1:200) (AB756P; Millipore, Darmstadt, Germany) and rabbit polyclonal anti-laminin (1:500) (L9393; Sigma-Aldrich). The following secondary antibodies were used: anti-mouse IgG, horseradish peroxidase-linked (HRP-linked, 1:2000) (7076; Cell Signaling Technologies, Cambridge, UK), anti-rabbit IgG (H+L), HRP-linked (1:2000) (111-035-144; Dianova, Hamburg, Germany), anti-rat IgG (H+L), HRP-linked (1:2000) (6180-05; SouthernBiotech, Birmingham, USA) and anti-rabbit IgG (H+L), IRDye 800 (1:5000) (611-132-122; Rockland, Gilbertsville, USA). The ECM gels were thawed on ice and heated in Laemmli buffer at 95 °C for 5 min before equal amounts of total protein were loaded on polyacrylamide gels. The proteins were separated according to their size by sodium dodecyl sulfate polyacrylamide gel electrophoresis (SDS-PAGE) and transferred to nitrocellulose membranes using tank blotting. For the detection of protein levels, the ECL detection system (Amersham Pharmacia Biotech, Uppsala, Sweden) or Odyssey Infrared system version 2.1 (LI-COR Biosciences, Lincoln, USA) was used.

2.1.9 Confocal Microscopy

Confocal microscopy was performed as well in collaboration with K. Pflieger from the group of Prof. S. Zahler. The following antibodies were used for imaging applications: goat polyclonal anti-collagen type IV (1:100) (sc-167526; Santa Cruz, Heidelberg, Germany) and Alexa Fluor 680 donkey anti-goat IgG (H+L) (1:200) (A-21084; Life Technologies). To investigate the gel microarchitecture by means of confocal microscopy, the ECMs were thawed on ice and afterwards diluted with DMEM to a final concentration of 3.5 mg/mL. The gels were stained in µ-Slide Chemotaxis^{3D} (ibidi), therefore 6 µL of each ECM was injected into the observation channel of the slide and incubated for 30 minutes at 37 °C and 5 % CO_2 to allow for gel formation. Afterwards, the gels were fixed with 2 % (v/v) glutaraldehyde for 40 min and blocked with 1 % (w/v) bovine serum albumin (BSA) in phosphate-buffer saline (PBS) for 24 h at 4 °C. Subsequently, gels were incubated first for 72 h at 4 °C with primary antibodies, diluted 1:100 with 1 % (w/v) BSA in PBS, and then washed three times with PBS for 20 min respectively. Finally, the ECM gels were incubated for 48 h at 4 °C with secondary antibodies, diluted 1:200 with 1 % (w/v) BSA in PBS before images were obtained using a SP8 SMD confocal microscope (Leica, Wetzlar, Germany) and a 63x HC PL APO 1.2 NA water objective (Leica, Wetzlar, Germany). The thickness of the optical slices was 0.9 µm.

2.1.10 Scanning Electron Microscopy

To investigate the gel microarchitecture determined by all contributing proteins, scanning electron microscopy (SEM, JEOL-JSM-6060LV, Jeol, Germany) images were generated. Therefore, the ECMs were thawed on ice and diluted afterwards to a final protein concentration of 3.5 mg/mL with IMDM. 30 µL of ECM was pipetted onto a sample holder and incubated for 30 min at 37 °C to induce gelation. Each sample was fixated in 2.5 % (v/v) glutaraldehyde (in 50 mM 4-(2-hydroxyethyl)-1-piperazineethanesulfonic acid (HEPES), pH 7.4) for one hour and washed with ddH_2O for another hour. For dehydration, the samples were incubated in an increasing ethanol series of 50 %, 70 %, 80 % and 99.8 % (v/v) ethanol for 30 min, each. Then, the samples were critical point dried, sputtered with a conductive gold film (40 mA, 40 s) and imaged at 5 kV which allowed for obtaining a sufficient resolution without destroying the samples.

2.1.11 Rheological Characterization of ECM

To investigate the macroscopic viscoelastic properties of different ECMs, rheological measurements were performed on a commercial shear rheometer (MCR 302, Anton Paar GmbH, Graz, Austria). Gelation kinetics were obtained in stress-controlled mode. The applied oscillatory stress $\sigma = \sigma_0 \sin(ft)$ (with σ_0 being the stress amplitude, t the time and f the frequency) results

in an oscillatory strain, $\gamma = \gamma_0 \sin(ft + \delta)$, where δ denotes the phase shift between stress σ and strain γ. For a purely elastic material, the phase shift would be $\delta = 0°$ and for a purely viscous material $\delta = 90°$, whereas materials with a phase shift between $\delta = 0° - 90°$ are classified as viscoelastic materials. These can be subdivided further into viscoelastic gels and viscoelastic fluids with a phase shift $\delta = 0 - 45°$ and $\delta = 45 - 90°$ respectively. The storage modulus $G'(f)$ (2), which is a measure for the elastic properties, and the loss modulus $G''(f)$ (3), which is measure for the viscous properties of a material, can be calculated according to the following formulas:

$$G'(f) = \frac{\sigma_0}{\gamma_0}\cos(\delta) \quad \textbf{(2)}$$

$$G''(f) = \frac{\sigma_0}{\gamma_0}\sin(\delta) \quad \textbf{(3)}$$

with $\delta = \delta\,(f)$ (see **Figure 6**). For each experiment, 150 µL of ECM thawed on ice and afterwards diluted with IMDM to a final concentration of 3.5 mg/mL was pipetted onto a pre-cooled (5 °C) peltier plate using a 25 mm plate-plate geometry. After lowering the measuring head to 200 µm, a thin polydimethylsiloxane (PDMS, Dow Corning, Midland, USA) oil layer was applied to the outer rim of the sample to prevent sample dehydration. Gelation of the ECM samples were induced by a rapid change in temperature to 37 °C, and the response of the ECM to this shift in temperature was recorded for 30 min. This was achieved by applying a torque of 0.5 µNm at a frequency of 1 Hz. Afterwards, frequency spectra were obtained at 37 °C in strain-controlled mode form 0.1 – 10.0 Hz at constant strain, which was one and a half times the strain value obtained at the end of the gelation measurement to guarantee linear response during the frequency sweep.

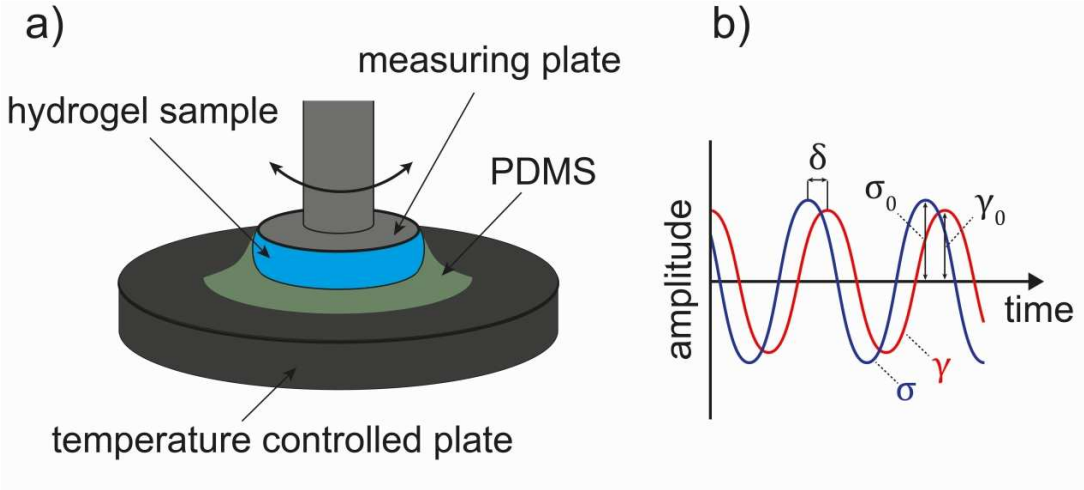

Figure 6 Rheological characterization of hydrogels. In (a) a schematic drawing of a measuring head and a temperature controlled plate of the rheometer, used for oscillatory measurements, is depicted. By oscillatory rotation, the measuring head induces shear stress on the hydrogel sample. (b) The deformation of the sample in response to the applied stress is recorded by the rheometer, where δ denotes the phase shift between the applied oscillatory stress, and the strain response which allows to calculate the viscoelastic moduli $G'(f)$ and $G''(f)$.

2.1.12 Fingerprint Mass Spectroscopy

ECM gels were thawed on ice and heated in Laemmli buffer supplemented with 250 mM dithiothreitol (DTT, Sigma-Aldrich) at 95 °C for 5 min. An amount of 30 µg of total protein was loaded on a 4 - 20 % gradient polyacrylamide gel (BIO-RAD, Munich, Germany) for each ECM sample. The proteins were separated by SDS-PAGE and stained with coomassie brilliant blue R-250 staining solution (Bio Rad, Munich, Germany). Even though the overall pattern of protein bands in the coomassie staining was similar in all four gels, some additional bands were detected in ECM1, which were further analyzed by means of fingerprint mass spectroscopy. The bands of interest were cut out and sent to the chemistry department (TUM, Garching) for trypsin digestion and subsequent matrix-assisted laser desorption/ionization time-of-flight/time-of-flight (MALDI TOF/TOF) fingerprint mass spectroscopy.

2.1.13 Life-Dead Assay

Since the migration behavior of dHL-60 cells differed, in part, remarkably between the four ECM gels, a life-dead assay was performed. Therefore, tissue-culture treated 96-well plates were loaded with 50 µL of the different ECM gels at a final concentration of 3.5 mg/mL containing 50 nM fMLP and $1x10^4$ dHL-60 cells as described in section 2.1.6. After gel formation for 30 min at 37 °C and 5 % CO_2 in a cell incubator, 100 µL fresh IMDM containing 15 % (v/v) FBS and 50 nM fMLP were added on top to avoid sample dehydration. After additional 24 h of incubation

in the cell incubator, a LIVE/DEAD Viability/Cytotoxicity Kit was used following the manufacturer's instructions (Life Technologies) to quantify the amount of live and dead cells. In short, 150 µL of a 4 µM calcein-AM/ethidium homodimer-1 mix in IMDM was added to each well. Calcein-AM is a fluorescent dye, which emits green light in its activated conformation in the cytoplasm of vital cells. Here, it is activated by intracellular esterases and, at the same time, becomes trapped after the acetoxymethyl (AM) group has been removed. The red fluorescent ethidium homodimer-1, on the other hand, binds to DNA in the cell nucleus of dead cells since these possess a damaged cell membrane. Accordingly, green vital cells can easily be distinguished from dead red cells and simply counted by using a fluorescence microscope. Image acquisition was performed after 1 h of incubation on an Axiovert 200M microscope (Zeiss) using a 10x objective (Zeiss) and analyzed using ImageJ 1.47d.

The following chapter follows in part the publication: "A Selective Mucin/Methylcellulose Hybrid Gel with Tailored Mechanical Properties" published 2016 in Macromolecular Bioscience.[108]

2.2 Bioactive Mucin Hydrogels as Wound Gels

Mucin glycoproteins combine a rich spectrum of medically interesting properties. They can reduce bacterial adhesion,[45, 46, 49] serve as a potent shielding layer reducing the infection rate of various viruses,[47] and would thus be ideal candidates for applications in infection prevention and wound management. However, aqueous solutions of mucins suffer from their unsatisfactory mechanical performance as they, by themselves, are only able to form a weak gel at acidic pH and low salt concentrations.[55] This issue has so far prevented their application in medical settings. Overcoming this long-standing problem was the motivation for the second part of this thesis. This issue was solved by combining purified mucin glycoproteins with the biopolymer methylcellulose serving as mechanical adjuvant, creating a temperature responsive hybrid gel.

2.2.1 Mucin Purification

Porcine gastric mucins (i.e. mainly mucin MUC5AC) were purified from scrapings of fresh porcine stomachs, essentially as described in [51] with several modifications to accelerate the purification process and increase the yield. Importantly, the high glycosylation of the protein, which can make up to 75 % of the weight of the mucin[48] and is essential for its properties, was conserved during the process.[4]

In the following three chapters to avoid fast protein degradation and bacterial growth, all solutions and the equipment used were precooled, and the individual purification steps were performed on ice or at 4 °C if not stated otherwise.

[4] I want to thank Konstantina Bidmon and Benjamin Käsdorf, who were the people mainly responsible for the purification of mucin.

2.2.1.1 Mucin extraction

Stomachs were opened to discard the food debris, and the lumen was gently rinsed with tap water before the thick mucus gel could be collected by scraping the mucosal surface. The mucus was subsequently diluted 1:4 with 10 mM PBS, before the pH was adjusted to pH 7.4 using 1 M sodium hydroxide (NaOH). Afterwards, 0.04 % (w/v) sodium azide (NaN_3) was added as a bacteriostatic agent. To prevent degradation, protease inhibitors were added as follows: 5 mM benzamidine-HCl, 1 mM 2,4‘-dibromoacetophenon, 1 mM phenylmethane sulfonyl fluoride (PMSF, stock solution 1 M in DMSO), 5 mM ethylenediaminetetraacetic acid (EDTA, stock solution 0,5 M, pH 7,4). To solubilize the mucus, the suspension was stirred gently overnight at 4 °C.

2.2.1.2 Ultracentrifugation and size exclusion chromatography

The overnight suspension was centrifuged for 30 min at 8300 x g, and the supernatant was collected. This step was repeated for 45 min at 15000 x g to remove all food debris and coarse impurities. Until further processing, the supernatant was stored at -80 °C. Due to the large molecular weight of mucin, which ranges from several hundred kDa up to ~15 MDa when multimers are formed,[109] it can easily be separated from smaller proteins by means of size exclusion chromatography (SEC). Therefore, the mucus solution was thawed over night at 4 °C and centrifuged a last time at 4 °C for 60 min at 149000 x g. Subsequently, 180 mL of the supernatant was injected into an ÄKTApurifier system (GE Healthcare, Freiburg, Germany) equipped with a sepharose 6FF XK50/100 column (GE Healthcare, column volume 1639.52 mL) which was connected to an Faco-950 autosampler (GE Healthcare). Separation parameters were as follows: running buffer: degassed PBS; flow rate: 9.5 mL/min; pressure limit: 0.35 MPa; temperature: 4 °C; fraction volume: 44 mL. During the separation process, the protein content was monitored at 280 nm, where the first peak of the flow-through was attributed to mucins. This assumption was later verified by a periodic acid-Schiff assay according to reference [110], which is a detection method for polysaccharides of glycoproteins like mucins. Thus, fractions corresponding to the mucin peak were pooled and stored at -80 °C.

2.2.1.3 Crossflow filtration

To concentrate the mucin solution by a factor of about three, the pooled mucin solution was thawed overnight at 4 °C and concentrated by means of crossflow filtration using a QuixStand Benchtop System (GE Healthcaere) equipped with an UFP-100-E-3MA ultrafiltration hollow fiber cartridge (100,000 MWCO; GE Healthcare). To optimize the mucin yield the trans-membrane pressure was kept at 0.78 bar while operating the pump with 100 rpm. Since mucins

are known to form a weak gel only at low pH and low ionic strength,[55] an additional diafiltration step of the mucin solution against ddH_2O was necessary to decrease the salt concentration. Desalting process was stopped when a conductivity value of 50 µS/cm² or lower was reached, which was determined using a FiveEasy Plus conductivity meter (METTLER TOLEDO, Gießen, Germany). Finally, the solution was concentrated to ~90 mL, before 4.5 mL aliquots were frozen at -80 °C and afterwards lyophilized. From this procedure, sufficient amounts of the mucin MUC5AC were obtained in lyophilized form and could be reconstituted at distinct pH conditions and ionic strengths by rehydration in tailored buffers.

2.2.2 Methylcellulose

Methylcellulose (MC) with an average number of 1.5 – 1.9 methoxide substituent groups attached to the ring hydroxyls (resulting in maximum water solubility) with an average molecular weight of approximately 88 kDa and 17 kDa, respectively, was obtained from Sigma-Aldrich. A 2 % (w/v) aqueous solution of the larger MC molecule exhibits a relatively high viscosity of 4000 mPa*s at 20 °C, whereas a 2 % (w/v) aqueous solution of the smaller MC molecule has a viscosity of only 25 mPa*s.[5]

2.2.3 Methylcellulose/Mucin Hybrid Gel Preparation

Lyophilized mucin was rehydrated over night at 4 °C under constant shaking. The final MC/mucin hybrid gel mixture was prepared by dilution from a stock solution which contained all additives except mucin. Unless stated otherwise, the final hybrid gel contained 10 % (w/v) 17 kDa-MC, 10 % (v/v) glycerol, 150 mM NaCl, 20 mM HEPES ([4-(2-hydroxyethyl)-piperazino]-ethanesulfonic acid) and 1 % (w/v) mucin at pH 7.0.

2.2.4 Rheological Characterization of Hybrid Gel Mixtures

The quantification of the viscoelastic properties as well as the gelation kinetics of the different hybrid gel mixtures were performed similarly as described in section 2.1.11 with the following exceptions: A plate separation of 150 µm, a torque of 10 µNm and 100µL sample volume were used. The samples were first kept at 4 °C for 10 min and then heated up to 37 °C. After 1 h at 37 °C (where the normal force was kept at zero during gelation to allow for temperature induced sample contraction) frequency spectra from 0.1 – 10.0 Hz were measured. In addition, a viscosity measurement was performed with a 25 mm cone-plate geometry (cone angle of 1°) at 4 °C using a shear rate ramp. The viscosity η was calculated according to Newton's Law (4) where the shear

[5] According to the manufacturer's information

stress τ is given through equation (5). Here, M denotes the torque and R_c the cone radius. The shear rate $\dot{\gamma}$ is given trough equation (6), where rpm denotes the speed of rotation and θ the cone angle.

$$\eta = \tau/\dot{\gamma} \tag{4}$$

$$\tau = \frac{M}{2/3 * \pi * R_c^3} \tag{5}$$

$$\dot{\gamma} = 2 * \frac{2 * \pi * rpm/60}{\sin\theta} \tag{6}$$

2.2.5 Gelation Experiments on a Tilted Model Tissue

To test the adhesion and gelation of the hybrid gel on an uneven wound naturally consisting of cellular tissue a model tissue surface was developed: Human NIH-3T3 fibroblasts were cultivated at 37 °C in 7.6 % CO_2 in IMDM supplemented with 15 % (v/v) heat-inactivated FBS (PAA Laboratories, Pasching, Austria). Cells were then harvested by trypsination and cultivated to confluency on two PDMS half-pipes with dimensions of approximately 8.3 cm x 1.2 cm x 0.4 cm. Each half-pipe was designed to open into a round cavity at one side. Subsequently, the medium was discharged and 300 µL of ice-cold biopolymer solution colored with 5 % (v/v) royal blue ink (Pelikan, Hannover, Germany) was added to those cavities. By adjusting the tilt angle α to 10° or 45°, respectively, the experiment was initiated, and the biopolymer solution started to flow along the cell-covered half-pipe channel (see **Figure 7**). To monitor flow/gelation at 37 °C, pictures were taken over a time period of 3 h using a Canon SX240 HS camera (Canon, Krefeld, Germany). The flow distance was then calculated from the digital pictures using the image processing software ImageJ, version 1.47d.

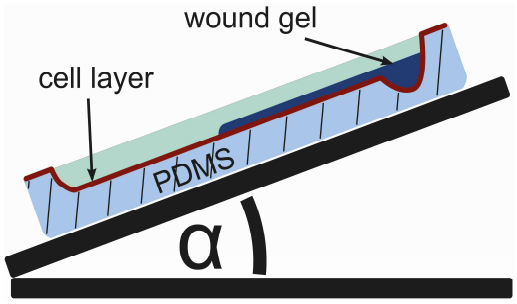

Figure 7 Schematic visualization of the gelation assay on a tilted model tissue surface. The scheme shows the half-pipe made from PDMS which is coated with fibroblasts and can be placed at defined tilt angles to model an uneven tissue surface.

2.2.6 Wound Healing Assay

HT-1080 fibroblasts were maintained following the same protocol as described for NIH-3T3 cells in section 2.2.5 and cultivated to confluency on tissue culture treated PET transwell plates with a pore size of 0.4 µm (Corning Life Science, Amsterdam, Netherlands). A straight scratch through the cell layer was applied with a 200 µL pipette tip to generate an artificial wound. Detached cells were removed by several washing steps with PBS before the artificial wound was covered with 300 µL of the MC/mucin hybrid solution. Image acquisition for the wound healing experiments was performed on an Axiovert 200M microscope (Zeiss) equipped with a 5x objective (Zeiss) in phase contrast mode. An incubation chamber mounted onto the microscope was used to control temperature and CO_2 concentration. Images of the artificial wound were recorded with an AxioCam digital camera (Zeiss) using the software AxioVision V.4.8.20 (Zeiss). To avoid artefacts arising from gel swelling, an initial adjustment time of 6 h was provided. Then, phase contrast images were acquired every 15 min for 24 h.

2.2.7 Fluorescence Microscopy and Particle Tracking

Fluorescence microscopy images of the hybrid gel were acquired on an Axioskop 2 MAT mot microscope (Zeiss) equipped with a 10x objective (Zeiss) and an Orca-R2 C10600 camera (Hamamatsu, Japan) and the image acquisition software HCImageLive (Hamamatsu) was used. Images were acquired 48 h after sample preparation to test for phase separation. Mucins were pre-stained using 10 µg/mL lectin-tetramethylrhodamine isothiocyanate (lectin-TRITC, Sigma-Aldrich) one day before final sample generation to allow for binding of the fluorescently labeled lectin to the sugar moieties of the mucin. 100 µg/mL of either negatively charged 4 kDa carboxymethyl (CM) dextrans or positively charged diethylaminoethyl (DEAE) dextrans fluorescently labeled with fluorescein isothiocyanate (FITC) were incorporated into the gel before taking pictures. The same procedure was performed to test the charge selective permeability of

the gel towards customized oligopeptides obtained from PEPperPRINT (Heidelberg, Germany) using either 10 µg/mL positively charged $(KKK)_8$ or negatively charged $(EEE)_8$ conjugated to a carboxytetramethylrhodamine (TAMRA) fluorophore. For this set of experiments, mucins were labeled with 20 µg/mL lectin-FITC instead of lectin-TRITC.

To verify the homogeneous distribution of mucin within the hybrid gel, sample preparation and acquisition were performed exactly the same way as for the permeability tests; however, neither dextrans nor peptides were added and only 20 µg/mL lectin-FITC (Sigma-Aldrich). For particle tracking experiments, mesoporous silica nanoparticles (MSNs) were mixed into the MC/mucin solution and incubated for 30 min at 37 °C prior to the measurements. MSNs were coated with amine- or carboxyl-groups on the outside, the former was fluorescently labeled with Atto 633 and the latter with Atto Rho6G. MSN synthesis was performed according to ref.[111] in the Functional Nanosystem research group of Prof. T. Bein by C. Hsin-Yi at the Ludwig Maximilians University of Munich. Dynamic light scattering was used to determine the particle size distribution and zeta-potential on a Nano ZS zetasizer (Malvern Instruments). The average size and the polydispersity index (PDI) were determined using the general purpose analysis mode and a backscatter angle of 173°. Data acquisition for particle tracking was performed as described in section 2.1.3.

2.2.8 Interleukin-8 Diffusion Measurements by PFG NMR Spectroscopy

^1H pulsed-field-gradient nuclear magnetic resonance (PFG-NMR) measurements were performed on a Bruker 600 Avance III NMR spectrometer (resonance frequency of 600.1 MHz for ^1H equipped with 5 mm TXI probe with a z-gradient) in cooperation with A. Penk from the group of Prof. D. Huster at the Institute of Medical Physics and Biophysics of the University of Leipzig. To quantify human Interleukin-8 (IL-8) diffusion within the MC/mucin gel at 37 °C, the double echo PGSTE-Watergate sequence was used.[112] Human IL-8 was expressed in *E. coli*, purified as described before [113] and added at 1 mM concentration to the biopolymer mixture. As a control, IL-8 diffusion was also measured in the hybrid gel buffer in the absence of mucin and MC. In order to obtain sufficient water suppression and minimize all resonances except the IL-8 signals, the number of ^1H atoms in the sample was reduced to a minimum by replacing hydrogen by deuterium wherever possible. To this end, D_2O and deuterated glycerol were used when preparing the hybrid gel buffer. Further, IL-8 and MC were dialyzed against D_2O prior to sample preparation exchanging ^1H atoms of hydroxyl groups against deuterium.

2.2.9 Thermoresponsive Liposomes for Doxorubicin Release

Doxorubicin (Dox) loaded multilamellar liposomes with a size of 1 µm were produced as described in Fritze *et al*.[114]. To generate thermoresponsive liposomes with a phase transition temperature of about 37 °C, the following lipid mixture was used: 84 mol% 1,2-dipalmitoy-*sn*-glycero-3-phosphocholine (DPPC) (Avanti Polar Lipids, Alabaster, USA) and 16 mol% DOTAP (Avanti Polar Lipids, Alabaster, USA),[115] according to section 2.1.4 using 1 µmol of lipids and 1 mL of 300 mM $(NH_4)_2HPO_4$ buffer (pH 7.2). Dox hydrochloride (Sigma-Aldrich) was added to the liposome solution in a drug to lipid ratio of 1:3 (mol/mol). The drug automatically accumulated in the liposomes by following an ion gradient which was established by extra-liposomal buffer exchange. This ion gradient and the ensuing pH difference between the liposome volume and the outside buffer prevented Dox release from intact liposome particles. The buffer exchange was performed using a PD MidiTrap G-25 column (GE Healthcare) equilibrated with a 10 mM HEPES buffer (pH 7.4) supplemented with 140 mM NaCl. To demonstrate temperature-induced drug release, 1 mg/mL thermoresponsive liposomes loaded with Dox were mixed into a MC/mucin hybrid gel and transferred into dialysis tubes (Carl Roth) with a cut-off of 6-8 kDa. After gelation at 37 °C, those dialysis tubes were immersed into dialysis buffer containing 10 mM HEPES at pH 7.4, supplemented with 140 mM NaCl. A 10-fold excess of the sample volume was used for dialysis, which was performed either at 37 °C or 4 °C. Samples (100 µL each) were taken in 30-60 min intervals in triplicates from the dialysis buffer, measured and passed back to the dialysis volume. Dox concentration in the dialysis samples was quantified using a Victor3 plate reader (Perkin Elmer, Rodgaum, Germany) at λ_{ex} = 485 nm and λ_{em} = 642 nm. The phase transition temperature of those liposomes was determined following Michel *et al*.[116] In short, changes in the scattering intensity of the liposomes in water were measured with a Nano ZS zetasizer (Malvern Instruments) during a temperature sweep from 25 °C to 40 °C at a backscatter angle of 173°. The minimum of the mean count rate (= average number of photons detected per second) indicated the gel-to-liquid crystalline phase transition temperature (see **Figure 29**).

2.2.10 Retarded Drug Release

To demonstrate charge selective retarded drug release, FITC labeled 4 kDa dextrans of either negative or positive charge were mixed into the hybrid gel with or without mucin as described in section 2.2.7. The mixtures were transferred into dialysis tubes (Carl Roth) with a cut-off of 12-14 kDa and immersed into dialysis buffer containing 20 mM HEPES, 10 % glycerol and 150 mM NaCl at pH 7. Dialysis was performed at 37 °C using a ten-fold excess of sample volume. Over a time span of 24 h, samples (100 µL each) were taken from the dialysis buffer and were

returned to the buffer reservoir after dextran concentrations were measured using a Victor3 plate reader at λ_{ex} = 485 nm and λ_{em} = 535 nm.

2.2.11 Bacterial Penetration

To test for bacterial penetration through the hybrid gel, either 50 µL or 25 µL of the gel with and without mucin were layered onto polyester membranes of HTS Transwell-96 Well Permeable Supports with 8.0 µm pore size (Sigma-Aldrich) and incubated for 20 min at 37 °C to allow for gel formation. Afterwards, 25 µL of a green fluorescent protein (GFP) expressing *E. coli* (BZB1011) overnight culture were added on top. The lower chamber of each well was filled with 235 µL of LB-media containing 0.2 % (w/v) L-arabinose. The same L-arabinose containing LB-media was used to grow the overnight culture at 37 °C in a shaking incubator where L-arabinose acted as a transcriptional activator inducing the expression of GFP. After 20 h of incubation at 37 °C, the fluorescent intensity was measured using a Victor3 plate reader at λ_{ex} = 485 nm and λ_{em} = 535 nm. The obtained value correlated with the concentration of green fluorescent *E. coli* which were able to penetrate the gel layer and proliferate in the lower chamber.

2.3 Orchestrated Drug/Nanoparticle Release from Hydrogels

So far a MC/mucin hybrid gel could be developed, which possesses the feature to control drug release kinetics to some extent. However, from a pharmaceutical point of view, there is a need for more ambitious fine-tuned release solutions, e.g. allowing for the sequential release of therapeutic agents from hydrogels in an orchestrated and controlled manner. This issue is addressed in the last part of this thesis, where I introduced osmotic pressure sensitive liposomes loaded with DNA to initiate disaggregation of gold nanoparticle clusters trapped within a hydrogel matrix.

2.3.1 Polynucleotide Design

Cross-linker DNA (crDNA) sequences with self-complementary regions were designed such that the constructs can form cross-links between gold nanoparticles (Au-NPs) onto which they are bound through gold-thiol interactions. As a consequence of this cross-linking process, the Au-NPs are supposed to build large aggregates which are then trapped in the gel due to geometric constraints. Au-NP disaggregation is supposed to occur only in the presence of a suitable displacement DNA (dDNA) with a higher affinity to the crDNA (**Figure 8**).

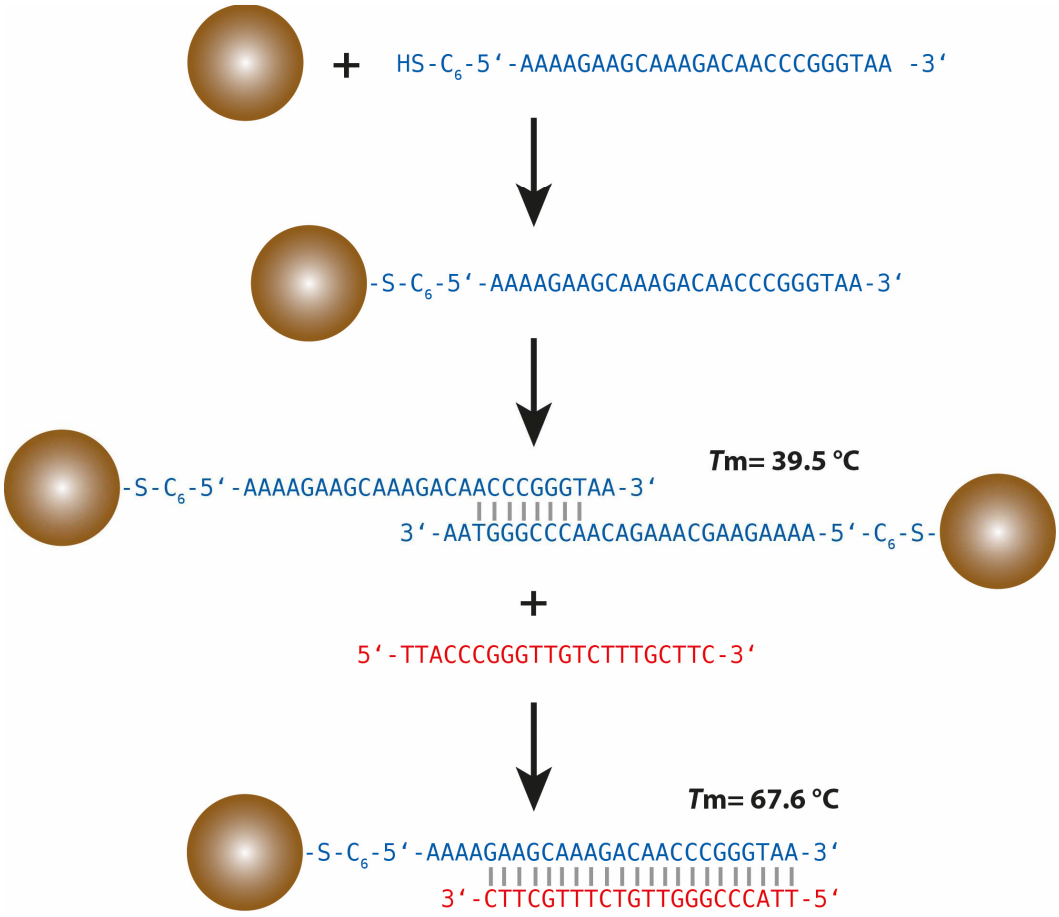

Figure 8 Molecular design of the cross-linking (crDNA) DNA sequence and the corresponding displacement (dDNA) DNA sequence. Two gold NPs, each functionalized with at least one crDNA sequence through a thiol-gold bond, are connected via a crDNA cross-link: a subsequence of the crDNA molecule is designed such that it can hybridize with another crDNA molecule forming a stable but weak 8 bp cross-link with a melting temperature of T_m = 39.5 °C. Displacement (dDNA) DNA molecules are designed to hybridize with a larger part of the crDNA molecule (22 bps) thus forming an energetically more favorable and more stable (T_m = 67.6 °C) double strand. For simplicity, only a single crDNA cross-link is depicted. In the experiments discussed in section 2.3, each gold NP is likely to carry several crDNA sequences on its surface and thus can form multiple cross-links with other gold NPs.

To enable covalent binding of the crDNA to the surface of Au-NPs, a thiol-C6 capped poly(A)-tail was integrated at the 5'-end of the sequence. The self-complementary region of the crDNA was chosen such that it had a melting temperature T_m above 37 °C so that the construct allows for the formation of stable cross-linked Au-NP aggregates at temperatures $\leq T_m$. In contrast, the dDNA sequence was designed to exhibit a higher affinity to the crDNA than two crDNA molecules have to each other. Thus, the crDNA/dDNA complex had a much higher (predicted) melting temperature than the crDNA/crDNA complex. As a control molecule, a polynucleotide sequence (coDNA) with the same number of nucleotides as the dDNA was chosen but designed such that it had only a negligible binding affinity to the crDNA sequence.

Two sets of polynucleotides pairs (crDNA and dDNA) with different T_m values and different sequences were designed as described, tested with the software OligoAnalyzer 3.1[117] (parameters: target type, DNA; oligo concentration: 0.25 µM; Na^+ concentration: 150 mM; Mg^{2+} concentration: 5 mM; deoxynucleoside triphosphate (dNTPs) concentration: 0 mM) to ensure that they fit the above mentioned requirements and then obtained from Integrated DNA Technologies (IDT, München, Germany). The detailed sequences and calculated melting temperatures of those constructs are listed in **Table 1**.

Table 1 Nucleotide sequence and melting temperature of both DNA sets (DNA1 and DNA2)

Abbreviation	Sequence from 5' to 3'	T_m [°C]	Secondary structure at 37 °C
crDNA1	AAAAAAGCGACGCTGACGCAACAGGCCTGTT	50.5	Yes
dDNA1	AACAGGCCTGTTGCGTCAGCGTCGCTTT	76.8	Yes
coDNA1	ATCCGCCGTGACCCGTCTGTGTGGATAT	N/A	Yes
crDNA2	AAAAGAAGCAAAGACAACCCGGGTAA	39.5	No
dDNA2	TTACCCGGGTTGTCTTTGCTTC	67.6	No
coDNA2	AATGAGCACAACAGAAACGAAG	N/A	No

Here, the self-complementary regions of the respective crDNA sequences responsible for establishing cross-links are highlighted in red, and the melting temperatures given in **Table 1** describe the stability of the formed crDNA/crDNA or dDNA/crDNA complex. The NUPACK web application was used to calculate the minimum free energy (MFE) structures of the designed DNA sequences. The free energy of a secondary structure was calculated using nearest-neighbor empirical parameters as outlined in ref. [118] for DNA at 37 °C in the presence of 150 mM Na^+ and 5 mM Mg^{2+}.[6]

2.3.2 PAGE Analysis of DNA-Hybridization Efficiency

To verify that the designed polynucleotide constructs only efficiently hybridize when DNA constructs with complementary sequences are mixed, a polyacrylamide gel electrophoresis (PAGE) analysis was performed. For the constructs, a high degree of complementarity is only expected for sequence combinations with a high calculated T_m (i.e. only for matching crDNA/dDNA sequences). As a control, synthetic DNA sequences (coDNA) with a length

[6] I want to thank Prof. Fritz Simmel for helpful discussions about how to design the DNA sequences to fulfill the needed requirements.

identical to the dDNA molecules but with a different sequence (and thus very low calculated T_m) was used. DNA sequences were mixed in 1:1 ratios at a concentration of 1 nmol each and were incubated at room temperature (RT) for 2 h in presence of 500 mM DTT and 0.5 mM tris-(2-carboxyethyl)-phosphin hydrochlorid (TCEP, Carl Roth) to prevent the formation of S-S-bonds. Subsequently, 6x sample loading buffer (Sigma-Aldrich) was added, and the samples were loaded into Mini-PROTEAN TBE Precast Gels (BIO-RAD). Electrophoresis was performed at 100 V in 0.5x Tris-Borat-EDTA (TBE) buffer (pH 8.0) containing 5 mM DTT, and pictures were recorded on a Molecular Imager Gel Doc XR System (BIO-RAD) after the gels were stained at RT for 1 h with SYBR Green I solution (Sigma-Aldrich) in 0.5x TBE buffer.

2.3.3 Gold Nanoparticle Functionalization and Aggregate Formation

Polyvalent DNA-functionalized gold nanoparticles were generated by coating colloidal gold with a monolayer of DNA. This coating approach makes use of the strong interaction between gold and thiols, the latter of which have been integrated at the terminus of the synthetic polynucleotides via a 5'-Thio-Modifier C6 S-S linker. Such thiol-modified crDNA sequences were obtained from IDT in their oxidized form, i.e. with the sulfur atoms protected by a S-S-bond. Thus, to enable thiol-gold interactions, those disulfide bridges had to be reduced. Lyophilized crDNA was therefore dissolved in 180 mM phosphate buffer (pH 8.0) containing 100 mM DTT and incubated at RT for 1 h. Deprotected crDNA was separated from the protection groups by means of SEC using a NAP-25 Sephadex G-25 column (GE Healthcare); in this step, also a buffer exchange was performed to 180 mM phosphate buffer (pH 8.0) without DTT. The crDNA concentration was then measured with a NanoDrop-1000 spectral photometer (Thermo Fischer Scientific, Ulm, Germany) and adjusted to 100 µM. To obtain a sufficiently high coating density of Au-NPs with crDNA while minimizing the required amount of crDNA, the following estimation[119] was used to determine the number of crDNA molecules needed:

$$Mol\ (crDNA) = A_{NP} * c_{NP} * D_{crDNA} * V_{NP} \quad (7)$$

Here, A_{NP} denotes the surface area of the Au-NP, c_{NP} the concentration of the Au-NP solution (in units of Au-NPs/L), D_{crDNA} the crDNA density on each Au-NP (estimated to be ~35 pmol crDNA/cm^2 according to ref. [120]) and V_{NP} the volume of Au-NP solution used (in L). For the Au-NPs, this estimation gave a value of ~1.5 nmol crDNA for 1 mL of Au-NP solution. A corresponding volume of crDNA was then incubated in the presence of 100 µM of the reducing agent TCEP at RT for 1 h before commercial Au-NPs (5 nm in diameter, stock solution of 5.5*10^{13} Au-NP/mL stabilized in a citrate buffer, Sigma-Aldrich) were added. After 12 h of

incubation, the NaCl concentration of the Au-NP/crDNA mixture was increased by 50 mM, followed by a 10 s sonication step and 20 min of incubation at RT. This process was repeated until a final NaCl concentration of 1 M was reached, a process which promotes aggregate formation. At this high ionic strength, the Au-NP/crDNA solution was then incubated at RT for 48 h and subsequently stored at 4 °C. For each experiment, equal volumes of this Au-NP solution were centrifuged at 10000 x g for 20 min to separate the crDNA cross-linked Au-NP aggregates from unreacted reagents, and three washing steps with the desired final buffer were performed for the same purpose.

2.3.4 Calcein- and DNA-Loaded Liposomes

Liposomes loaded with calcein were generated by means of lipid film hydration as described in section 2.1.4 using 0.5 µmol of DOPG (Avanti Polar Lipids, Alabaster, USA). Hydration was performed with 120 µL PBS containing 2 M sorbitol (PBS-2MS) and 1.5 mM calcein, before the lipid/calcein solution was thoroughly vortexed and sonicated. Free calcein (= calcein which was not enclosed into liposomes) was removed by SEC using a PCR Kleen Spin Column (BIO-RAD) following the manufacturer's instructions.

Liposomes loaded with dDNA were produced in the same way, but using 0.5 µmol of a lipid mixture consisting of L-α-phosphatidylcholine from egg yolk (Egg-PC), DOTAP and cholesterol in a molar ratio of 3:1:1. All lipids were obtained from Avanti Polar Lipids, (Alabaster, USA). After rehydration in 120 µL PBS-2MS and 600 µM dDNA, the solution was subjected to five freeze/thaw cycles (freezing in liquid nitrogen / thawing at 37 °C) to increase the DNA loading efficiency, before free DNA was removed. For testing the efficiency of dDNA release by osmotic pressure, 30 µL of liposomes were added either to 270 µL of PBS (thus inducing a strong osmotic pressure) or PBS-2MS (= osmotically balanced buffer, serving as a control). For DNA detection, SYTOX green (a membrane impermeable nucleic acid stain, Thermo Fischer Scientific, Ulm, Germany) was used as this dye shows very low autofluorescence (i.e. more than a 500x fluorescence enhancement upon binding to nucleic acids). For DNA staining, SYTOX green was added to a final concentration of 1 µM and incubated at 37 °C for 30 min. dDNA release was then quantified spectroscopically using a Victor3 plate reader (Perkin Elmer, Rodgaum, Germany) at λ_{ex} = 485 nm and λ_{em} = 535 nm.

2.3.5 Formulation of NP-Loaded Agar Gels

A 2 % (w/v) agarose solution (Type IX-A, ultra-low gelling temperature agarose, Sigma-Aldrich) was prepared in PBS-2MS and was allowed to cool down from 80 °C to RT. Au-NP aggregates (obtained from 0.5 mL of the crDNA cross-linked Au-NP solution from chapter 2.3.3 by centrifugation) were incorporated into 100 µL of this RT agarose solution, supplemented with buffer containing either 0.33 µM dDNA or coDNA to a final agarose concentration of 0.5 % (w/v) and incubated at 4 °C for 20 min to form a gel. Both gel preparations, the one containing dDNA and the control (containing coDNA), were then incubated at 37 °C. Au-NP disaggregation could visually be followed by the development of a red color in the gel which originates from released single Au-NPs. Pictures of this NP-loaded agar gels were acquired over a time period of 24 h using a Canon SX240 HS camera (Canon, Krefeld, Germany).

2.3.6 Quantification of Au-NP Disaggregation

To quantify the observed Au-NP disaggregation process and the subsequent release of individual Au-NPs (or small Au-NPs complexes) from the agar gels, NP-loaded gels were prepared as described in section 2.3.5. However, this time a larger amount of Au-NP aggregates (i.e. the amount obtained from 1 mL of the crDNA cross-linked Au-NP solution from chapter 2.3.3) was used. Also, instead of free DNA, now 20 µL of a DNA-loaded liposome solution was incorporated. The prepared mixtures were then transferred to cuvettes (UV-Cuvette semi-micro, Brand, Wertheim, Germany) which had already been filled with 75 µL of the respective liposome-loaded agar gel (but lacking Au-NP aggregates). This procedure allowed to prevent sedimentation of the relatively large Au-NP aggregates and to trap them on top of the pre-filled liposome loaded ager gel layer, i.e. in the middle of an agar gel with a total volume of 150 µL (**Figure 9**). Another benefit of this filling procedure was that the Au-NPs were surrounded by dDNA-containing liposomes from above and from below.

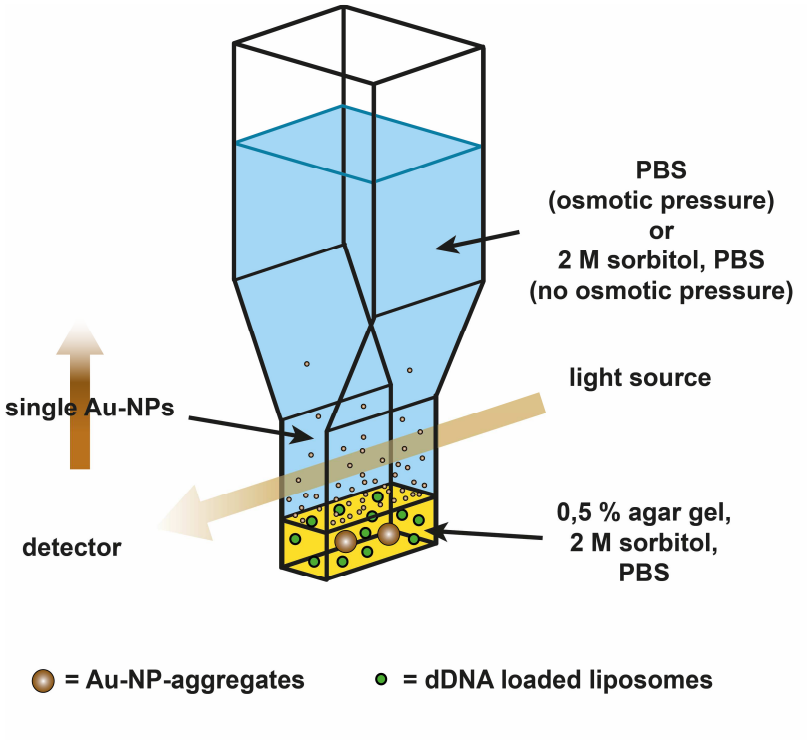

Figure 9 Schematic representation of the light absorption assay used for quantifying NP release from the gel. Individual Au-NPs (or small Au-NP complexes) are released from the agar gel and can be detected in the buffer supernatant spectroscopically.

After gel formation was concluded, the experiment was initiated by adding either 1350 µL of PBS (thus inducing a strong osmotic pressure) or PBS-2MS (= osmotically balanced buffer serving as a control). The cuvettes were sealed with PARAFILM M (Wagner & Munz, Munich, Germany) to prevent dehydration and were incubated at 37 °C. Release of single Au-NPs was monitored spectroscopically at 532 nm (see **Figure 9**) over a time period of several days using a specord 210 spectral photometer (Analytikjena, Jena, Germany). Samples were inverted carefully before each measurement to achieve homogeneous distribution of the released Au-NPs throughout the buffer phase of the cuvette to ensure accurate measurement signals.

To retard the triggered liberation of Au-NPs, positively charged polystyrene microparticles (amine-terminated, size 1 µm, fluorescent yellow green, stock solution $5*10^{10}$ particles/mL, Sigma-Aldrich, Schnelldorf, Germany) serving as charge traps for the negatively charged dDNA were added to the gel matrix. Therefore, polystyrene beads in dilutions ranging from 1:100 up to 1:10 were incorporated into the agar, Au-NP solution together with the DNA-loaded liposomes before gelation.

A similar setup was used to quantify the release of calcein from liposomes embedded into agar gels. Here, cuvettes were filled with 150 µL of agar containing calcein loaded liposomes, and the

gel was layered either with 1350 µL PBS or PBS-2MS to initiate the experiment. Samples of 200 µL each were taken from the supernatant, measured and returned to the cuvettes afterwards. The calcein concentration in the supernatant samples was quantified spectroscopically using a Victor3 plate reader (Perkin Elmer, Rodgaum, Germany) at λ_{ex} = 485 nm and λ_{em} = 535 nm.

3 Results and Discussion

The following chapter follows in part the publication of the same name: "The biophysical properties of basal lamina gels depend on the biochemical composition of the gel" published 2015 in Plos One.[102]

I want to thank Dr. Fabienna Arends and Dr. Kerstin Pflieger for contributing data discussed in this chapter of the presented thesis.

3.1 The Biophysical Properties of Basal Lamina Gels Depend on the Biochemical Composition of the Gel

Here, basal lamina gel preparations obtained from four different suppliers have been used as a platform to investigate how the biophysical properties of such gels depend on their biochemical composition. All four, commercially available, basal lamina variants originated from the same murine tissue, and were purified following the identical purification protocol established by Kleinman, [30, 31] and should therefore be very similar in their protein composition. Despite the similarity, minor differences in the protein composition between such basal lamina preparations can have large impact on the biophysical properties. Therefore, the biochemical constitution of these four basal lamina gels was analyzed and compared. The discovered variations in the composition were related to their microstructure, viscoelastic properties, permeability towards NPs, and results obtained from cell migration experiments of dHL-60 cells within these gels.

3.1.1 Molecular Gel Composition

The composition of the gels was examined by electrophoresis, loading each gel pocket with the same total amount of protein. As expected, the overall pattern of protein bands in the coomassie staining was similar in all four gels (**Figure 10a**), apart from minor differences in protein band intensities and some additional bands in the ECM1 (vendor: see Materials and Methods) lane. The intensity variations of the coomassie staining already hints towards quantitative differences in the ECM composition which were further analyzed by western blot. A comparison of the four main matrix constituents fibronectin, laminin, entactin, and collagen IV showed that all of them are more abundant in ECM2 (**Figure 10b, c**). Interestingly, the most prominent difference was observed for the cross-linker protein entactin, which was nearly absent in ECM1, ECM3 and ECM4. Entactin is responsible for the formation of connections between the collagen network and the laminin macromolecules.[26] Putative differences in the stiffness of ECM2 compared to the other three ECM gels are most likely to arise from variations in the entactin concentration. The stiffness of a biopolymer-based hydrogel is governed by several parameters: First, the

concentration of biopolymers determines the storage modulus, the more polymers the higher this value. However, the total protein concentration was adjusted to be equal. Western blots showed only a slight increase with respect to fibronectin, laminin and collagen IV concentrations in ECM2. Therefore, significant differences in stiffness caused by the concentration of these high molecular weight biopolymers are not expected. Second, the amount of cross-linking molecules determines the stiffness of a gel: the gel stiffness typically increases with the increasing concentrations of cross-linking molecules. In theory this should also be true for the cross-linker entactin, leading to a higher storage modulus of ECM2 compared to the other three gels. Third, parameters like temperature, pH and salt concentration can influence the mechanical properties of biopolymer-based hydrogels as well, however, those parameters were identical for all experiments and ECM variants. Therefore, ECM1, ECM3 and ECM4 were expected to have a similar elasticity to each other, but lower than ECM2.

Up to now, the additional bands from ECM1 have not been discussed yet. As it can be seen from the coomassie staining (**Figure 10a**) their concentration was quite low, making it unlikely that they contribute significantly to the gel stiffness if they were to represent biopolymers. However, in case that these bands were to represent cross-linkers, they could very well play a critical role regarding the gel stiffness. Therefore, it was necessary to further analyze these bands by a proteomics approach. From mass spectroscopy analysis, the laminin subunits alpha1 and beta1 were identified in one of the additional bands from ECM1 together with some proteins unrelated to the extracellular matrix (see **Table A1** of the appendix). However, there was no indication that one of the additional ECM1 bands originates from a cross-linker protein. The identified laminin subunit proteins are known from literature to have a molecular weight around 300 kDa and 200 kDa, respectively,[121] but were detected at approximately 50 kDa. An explanation for these fragments could be proteolytic breakdown during the purification process of ECM1.

Before, however, the viscoelastic properties of the four ECM gel variants are discussed, their microstructure is evaluated. This approach is reasonable since, in biopolymer networks, alterations in the microstructure very often affect the viscoelastic response of biopolymer hydrogels.

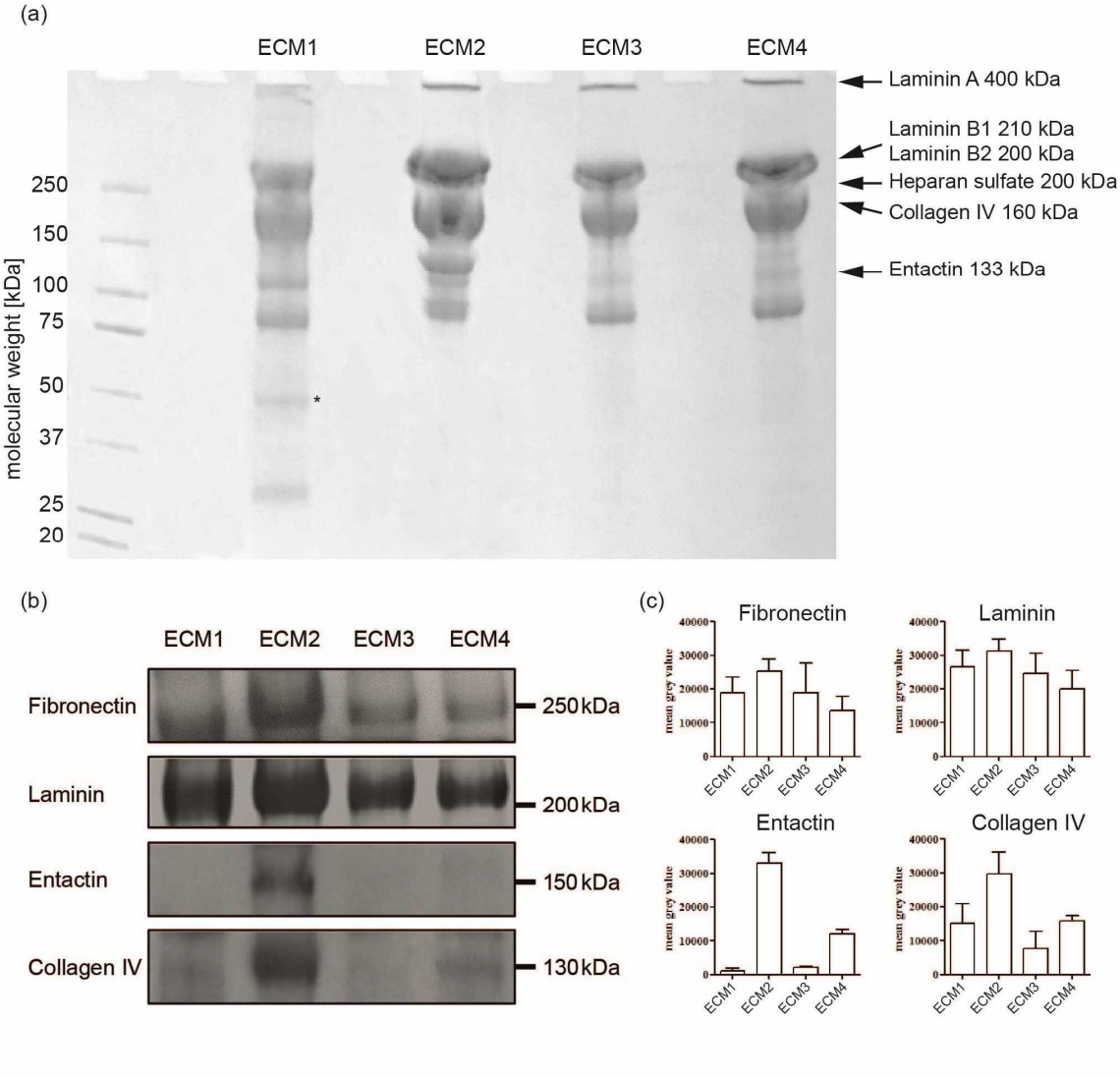

Figure 10 Content of selected ECM proteins in the four different ECM gel variants. (a) A coomassie staining of the four gel variants shows extra bands in ECM1 at low molecular weight. The star denotes the band which is further investigated by mass spectroscopy (see **Table A1** of the appendix for details). (b) The content of fibronectin, laminin, entactin and collagen type IV in the four different ECM gels is analyzed by western blot. (c) Densiometric analysis of fibronectin, laminin, entactin and collagen IV signals. The error bars denote the standard deviations as obtained from four independent gel runs.

3.1.2 Particle Diffusion and Gel Microarchitecture

The microscopic permeability properties and microarchitecture of the different gels were quantified. For this, 200 nm-sized fluorescently labeled polystyrene beads were chosen as tracer particles, and incorporated into the gels to investigate their Brownian motion. Two major gel properties can be obtained from such diffusion experiments of NPs within a gel: First, information about the gel microstructure can be obtained when inert NPs, that do not interact with the gel constituents, smaller or in the range of the mesh size are used. Second, selective properties of the gel matrix can be mapped when NPs identical in size (but smaller than the mesh size) but with

different surface modifications are compared [122]. Accordingly, the diffusion behavior of aminated, carboxylated or PEGylated polystyrene particles was compared. In a previous study with ECM1, it had been observed that only particles with neutral or weakly charged surfaces are able to diffuse within those gels – provided that their size is smaller than the mesh size, i.e. the average spacing between neighboring macromolecule strands of the gel. [105, 123] At a total protein concentration of 4.55 mg/mL for ECM1 the hydrogel mesh size is around 2-3 µm. [124] Therefore, considering that the final ECM concertation used, was 3.5 mg/mL instead of 4.55 mg/mL it can be assumed that for the utilized NPs with a diameter of 200 nm, which should be at least ten times smaller than the mesh size, geometrical constraints are minimal. However, this can only be said with certainty for ECM1 and needs to be verified for the other gel variants. It was expected that the diffusion behavior of the 200 nm polystyrene particles should only depend on their net charge, since buffer and temperature were the same for all experiments. From the previous study with ECM1 it was known that diffusion of strongly charged particles can be completely suppressed even for small particles. This behavior is most likely based on binding events of the particles to oppositely charged regions of the gel [105, 123]. Indeed, similar charge dependent diffusion behavior could be observed for the four gel variants. Aminated as well as carboxylated polystyrene particles were found to be immobilized within all gels. For PEGylated particles, on the other hand, two populations could be observed, a greater part of diffusing (80 ± 1 % in ECM1, 77 ± 3 % in ECM3 and 73 ± 4 % in ECM4) and a smaller part of immobilized particles. However, when monitoring PEGylated particles in ECM2, all of them were found to be immobilized. Exemplary particle trajectories from all gel variants are shown in **Figure 11a**. As particle PEGylation is well known to shield NPs from adhesive interactions established by both electrostatic and hydrophobic forces [125-127], this indicates that the microarchitecture of ECM2 might differ from that of the other three gel variants. A possible reason could be that the mesh size of ECM2 is even smaller than or at least comparable to the particle diameter (200 nm), thus obstructing the diffusion of the PEGylated particles by spatial hindrance. From this diffusion experiments it can be concluded that the microstructure should be different for ECM2 compared to the other three gel variants. Depending on whether this structural difference is large enough, it might be possible to directly visualize these differences in the gel architecture using fluorescence microscopy. To obtain a first impression of the micromorphology of the four gels, the main component collagen IV was stained with fluorophore-conjugated antibodies and imaged by means of confocal microscopy. The results shown in **Figure 11b** confirmed the previous notion based on the particle diffusion experiments: ECM2 showed a much more homogeneous micromorphology and an at least 10-fold smaller mesh size than the other ECMs - despite the fact that the same final protein concentration of 3.5 mg/mL was used. On the other hand, the collagen IV networks of ECM1, ECM3 and ECM4

appeared to be very similar, which agrees with the Brownian motion data. The advantage of fluorescence microscopy to visualize specific components of a complex material like ECM, is at the same time, the drawback of the method: it is very tedious and time consuming to get information of all components assembling such a network. In order to close this knowledge gap and to consolidate the findings obtained by fluorescence microscopy, the microarchitecture of the gels was also analyzed using scanning electron microscopy (SEM). **Figure 11c** shows the SEM images obtained for the four gels. Again, ECM1, ECM3 and ECM4 had a similar microarchitecture whereas ECM2 appeared to be more homogeneous with a smaller mesh size. There are two ways how a decreased pore size of a gel can be realized: First, by increasing the total protein concentration. However, in all experiments the ECM concentration for all four gels was adjusted to 3.5 mg/mL. Thus here, the second option, i.e. the formation of thinner strands might be responsible. Indeed, at high magnification SEM images suggest that, thinner fibers set up the local meshwork in ECM2 (**Figure 11c** lower row). Since ECM2 is very similar to the other gels with respect to the protein composition, and differs only significantly in the amount of entactin, the observed differences in mesh size and fiber thickness are most likely a result of the increased amount of entactin. This assumption is not self-evident, since higher concentrations of cross-linkers can in principle, lead to a decrease,[128] as well as to an increase in mesh size. The latter is, for example, known form actin networks, where increasing cross-linker concentrations may result in the formation of a bundle network.[129]

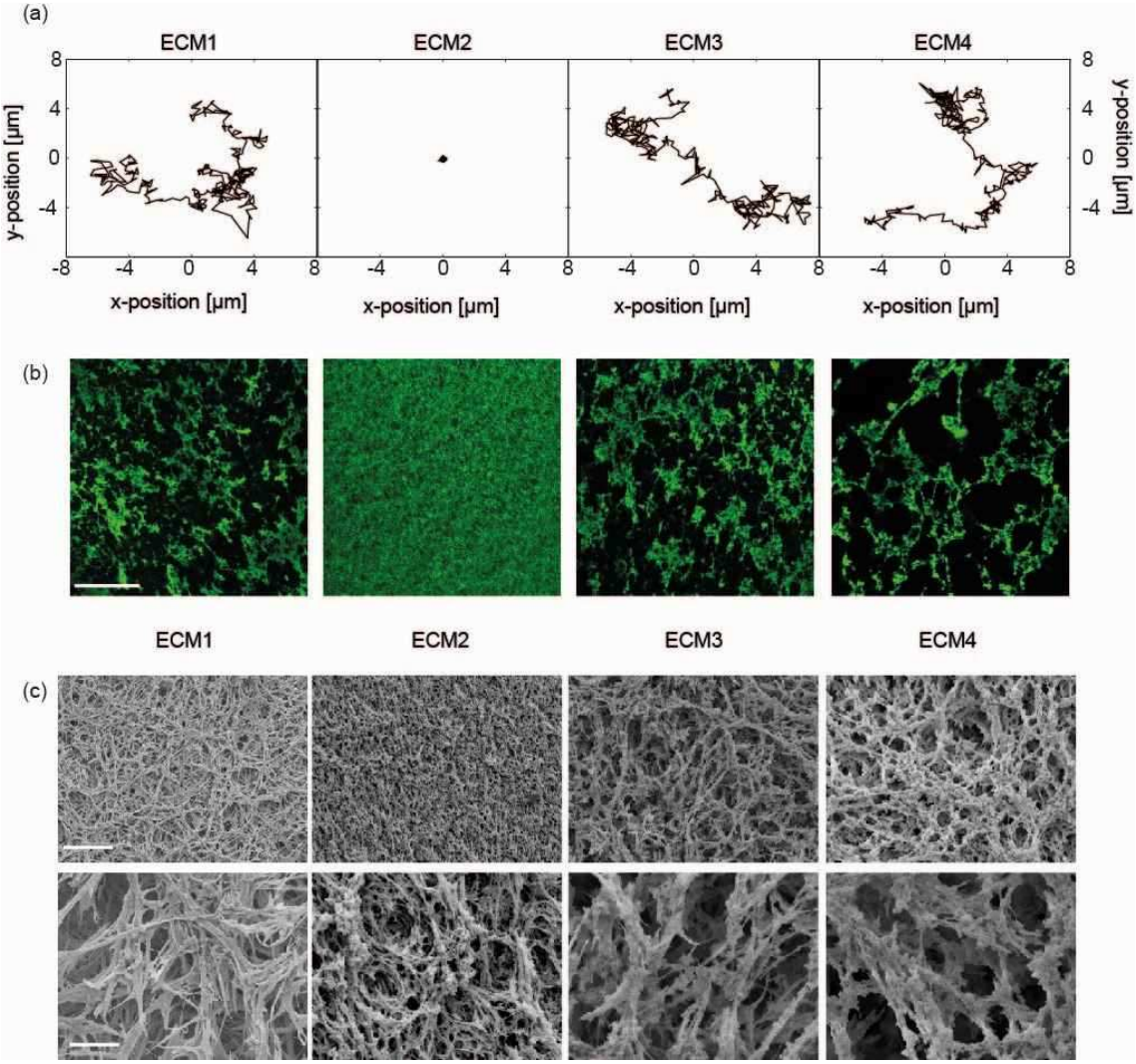

Figure 11 Micromorphology of the four gels determined by three different methods. (a) Exemplary trajectories of PEGylated particles with a diameter of 200 nm in the four different gels. (b) Micromorphology of the four different basal lamina gel variants as determined by confocal fluorescence microscopy. Representative staining of the matrix component collagen IV. The scale bar in the left image denotes 50 µm and applies to all images. (c) Micromorphology of the whole network of the four gel variants imaged by SEM. The scale bar in the upper row corresponds to 25 µm and in the lower row to 5 µm and applies to all images.

3.1.3 Viscoelastic Gel Properties

In the previous two sections it was shown, that the four ECM gels differ, in part, in their composition and in terms of their mesh size and microstructure. Therefore, it is reasonable to expect differences in their macroscopic viscoelastic properties. This expectation is based on the fact that macromechanical properties of hydrogels depend, despite from external factors, on the concentration and micromechanical properties of their macromolecules (stiffness, ability to form bundles and cross-links), and the microarchitecture of the gels. The latter can be described by the type of spatial configuration within the hydrogel – be it a homogeneous or heterogeneous

distribution of components – and the pore size.[129, 130] Thus in a next step, the impact of the altered microstructure observed for ECM2, which is probably caused by the entactin concentration, was investigated using a macrorheometer (see chapter 2.1.11). The ECM gels used here are typically stored at -20 °C, thawed slowly on ice and kept at temperatures of 5 °C or below until usage in the experiments. This is necessary since ECM is known to form a viscoelastic gel at RT. First, the gelation kinetics of the gels were examined at 37 °C. As before, the total protein concentration of the four gels was adjusted to 3.5 mg/mL to allow for experimental comparison. In accordance with the manufacturers' information, all ECM variants formed a gel within the first few minutes when heated to 37 °C. Significant differences in gelation kinetics between the four gel variants did not occur (**Figure 12**). Second, the final elasticity after complete gelation of the four basal lamina gels was compared. ECM1, ECM3 and ECM4 reached nearly identical final elasticities of $G' \sim 3$ Pa, whereas ECM2 showed a four-fold higher stiffness (**Figure 12**) which was independent of the measuring frequency (**Figure 13**). This agrees with the previous results obtained from fluorescence microscopy and SEM images and confirms the notion that differences in the gel mesh size should manifest themselves in the viscoelastic properties of the gel. At the same time, it strengthens the assumption made in chapter 3.1.1 that the additional bands in the coomassie staining of ECM1 do not originate from cross-linkers, but represent other protein fragments.

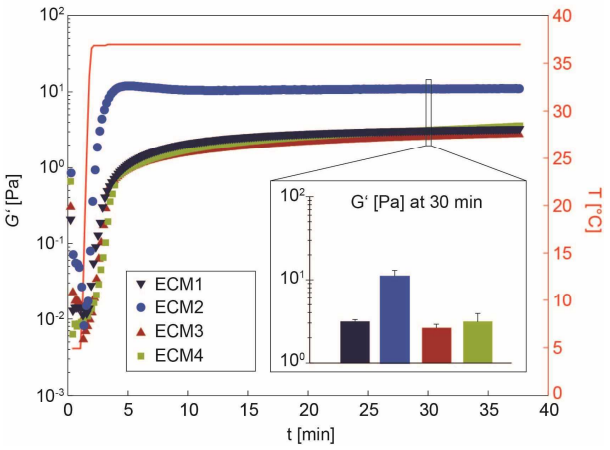

Figure 12 Gelation kinetics of the four different gels measured with a macrorheometer. The temperature is increased from 5 °C to 37 °C after one minute to induce gelation. The curves shown represent averages of three independent measurements. The inset shows the storage moduli *G'* of the four gels at 30 min. The error bars denote the error of the mean.

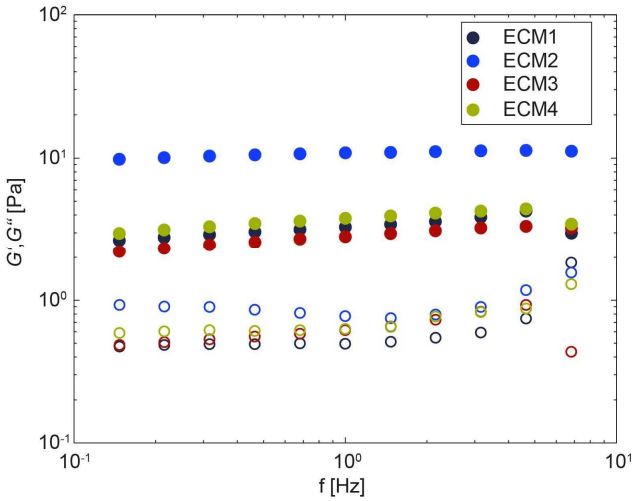

Figure 13 Viscoelastic frequency spectrum obtained for the basal lamina variants. The storage moduli *G'* (full circles) dominate over the loss moduli *G''* (empty circles) for all gel variants. Moreover, the storage moduli of all gels are nearly constant over two decades of frequency. The measurements were performed on a stress-controlled macrorheometer with a 25 mm plate-plate geometry at a plate separation of 200 µm after 30 min gelation time at 37 °C.

3.1.4 Cell Migration Studies

As a next step, the tested ECM gels were used for one of their classical applications: Reconstituted extracellular matrices such as basal lamina gels are mostly used for embedding cells and analyzing their migration behavior as a function of distinct knock-out mutations or external (bio)chemical stimuli. Such ECM gels offer a more *in vivo*-like 3D environment than, for example, fibronectin coated 2D systems [16-18]. In such cell migration experiments, the unaffected migration activity of the cells within the 3D environment of the gel is typically used as a reference. Cell migration can be influenced by two types of factors: First, external factors like pH, temperature or cytokines. And second, physical influences of the extracellular environment such as confinement, rigidity, surface topology and whether forces generated by the cells are transmitted to other cells, the ECM, or both.[131] However, all experiments described here were performed under identical external conditions. From the previous set of experiments on the gel composition and its effect on the microstructure and the macromechanical properties, comparable cell migration within ECM1, ECM3 and ECM4 but a decrease of cell migration activity in ECM2 was expected. The external environment for cells in respect to final elasticity and micromorphology are quite comparable within ECM1, ECM2 and ECM3 gels, and should therefore have an equal impact on cell migration. However, ECM2 has a much more homogeneous microstructure and smaller mesh size compared to the other gels, leaving cells no weak points to migrate through. In combination with the higher final shear stiffness of ECM2, this should force migrating cells to apply higher forces on the gel matrix or to weaken the gel locally by enzymes to be able to migrate within the gel,

slowing them down. In order to verify if this assumption was true, all cell migration experiments were conducted with the same concentration of dHL-60 cells embedded into the ECM. Experiments were performed on a microscope equipped with an incubation and CO_2 chamber to ensure constant temperature and pH. Constant temperature was not only crucial for the cells, but also for controlled and fast ECM gelation after the cells together with the chemoattractant fMLP were mixed with the liquid, precooled gels. **Figure 14** shows the trajectories of migrating dHL-60 cells obtained 4 hours after gelation of the basal lamina gels. This delayed observation time was necessary to exclude influences of gel swelling (as it occurs during the first hours of the experiment) during acquisition on the cell migration data. Each trajectory shown denotes the time-dependent x- and y-position of a cell for a time course of 2 hours. For clarity, the start point of all trajectories was shifted to the origin, and the end point after 2 hours of migration was marked by a dot. As shown in **Figure 14**, dHL-60 cells are able to efficiently migrate within ECM2, ECM3 and ECM4. Due to the uniform distribution of the chemoattractant fMLP, which was added to stimulate cell migration, random cell migration without any spatially oriented preference was observed. The area covered by the trajectories of the cells varied depending on the ECM used and is a measure for the migration activity. This area was comparable for ECM3 and ECM4 whereas it was significantly smaller for ECM2. For ECM1, no migratory activity could be detected, since the single trajectories and the area covered by them were on the order of the tracking error. Another measure for the migratory activity of cells is the Euclidean distance (*ED*) (the distance between the start and the end point) which was only $ED = (4 \pm 4)$ µm for cells embedded in ECM1 and $ED = (41 \pm 43)$ µm for ECM2. ECM3 and ECM4, on the other hand, gave significantly higher values: $ED = (112 \pm 90)$ µm for ECM3 and $ED = (132 \pm 92)$ µm for ECM4, which were again very similar to each other. A further analysis of this data revealed that only a fraction of $f = 10$ % of the migrating cells embedded within the ECM2 showed an Euclidean distance greater than 105.5 µm (depicted by a red circle in **Figure 14**). In contrast in ECM3 and ECM4, a fraction of $f = 44$ % and $f = 51$ % respectively was calculated. In ECM1, cell migration was basically absent and $f = 0$ %. To further quantify those differences in the migratory behavior of the dHL-60 cells in the four different gels, the cell migration speed was calculated from the individual trajectories. When this velocity data was pooled for each basal lamina gel and compared in a box plot (**Figure 14e**), the following differences between the distinct gel environments were observed: First, the migration speeds determined for cells in ECM1 was close to zero (although only living cells were included in the analysis) and the median velocity of cells within ECM3 and ECM4 was higher than in ECM2. These results corroborated the findings from the analysis of the total area explored by the migrating cells and the *ED* of the four gel variants. Second, the velocity distribution of migrating dHL-60 cells is quite broad, both in ECM3 and ECM4, but more

homogeneous in ECM2. Together, this data suggests that ECM3 and ECM4 offered the most favorable extracellular environment for dHL-60 migration, whereas ECM2 appeared to slow down the cellular migration activity and ECM1 suppressed dHL-60 cell migration completely. These findings correlate well with the results from the previous experiments on gel composition and its effect on the macromechanical properties and the microstructure, except for the suppressed cell migration within ECM1. The detected laminin fragments (see chapter 3.1.1), which might originate from proteolytic breakdown during the manufacturing procedure of ECM1, may be responsible for this observation, since they are known to be able to affect cells (e.g. via increased substrate adhesion). Already in 1991, cellular activities of proteolytic laminin fragments with exposed cryptic motifs have been described.[132] By now, this has been confirmed by several publications.[133, 134] However, a clear and systematic analysis of the different fragments and their biological effects is still missing.

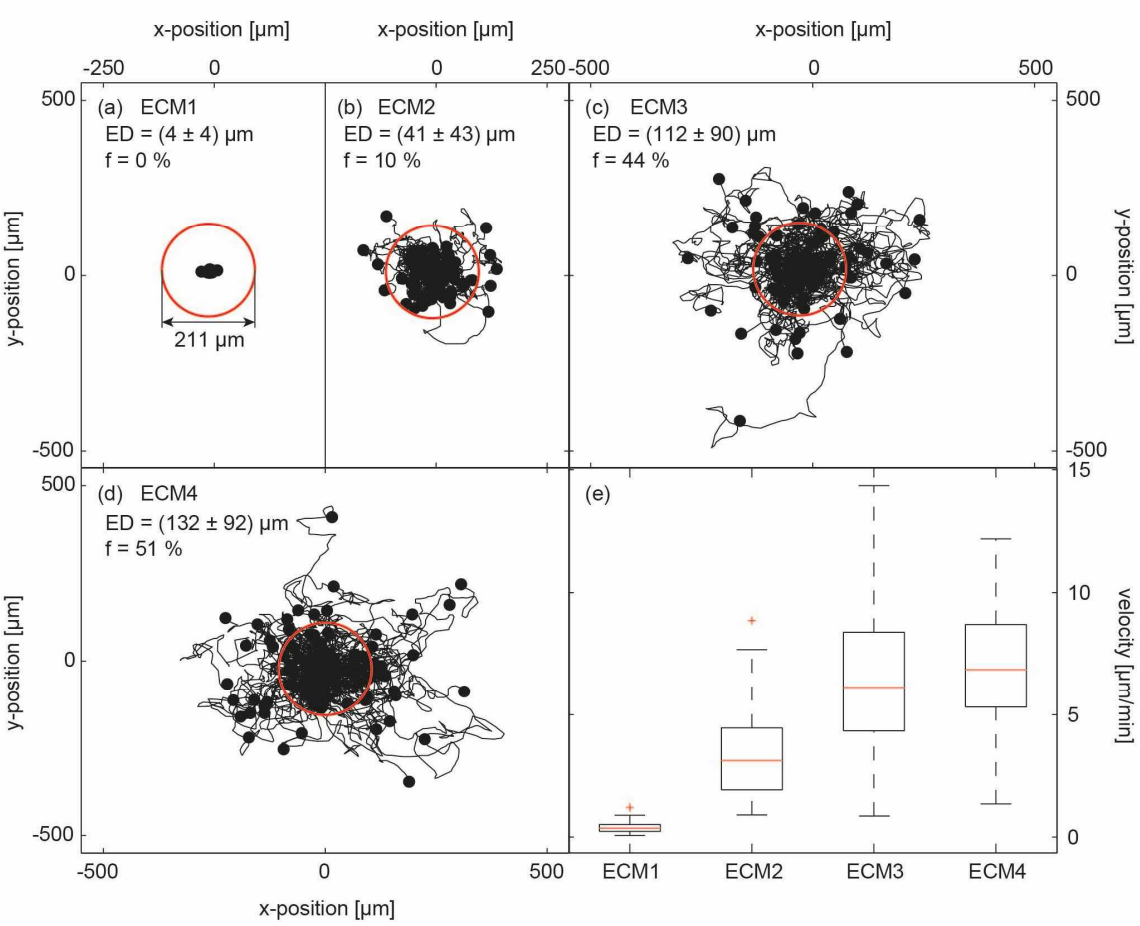

Figure 14 Migration trajectories of dHL-60 cells tracked from hours 4-6 after the cells are embedded into the four different basal lamina matrices. (a-d) The starting point of all trajectories is shifted to the origin for clarity, and the end point is marked by a dot. The average start-to-end distance (Euclidean distance) travelled by the cells and the respective standard deviation is denoted by *ED*. The fraction of cells with an *ED* greater than *ED* = 105.5 µm (red circle) is denoted by *f*. (e) Comparison of the migration velocity of dHL60 cells in different ECM gels. The red line denotes the median of the velocity distribution, the box includes 25 % of the observed velocities above and below this median, respectively. The remaining 25 % of slower as well as the 25 % of faster cells are indicated by the dashed lines. Outliers are denoted by a red cross.

In addition to the suppressed cell migration activity, more dead cells were observed in ECM1 than in any of the other ECMs. To quantify this observation, a live/dead assay staining dead cells fluorescently red and vital cells green was performed. In ECM2, ECM3 and ECM4 a comparable fraction of dead cells in the range of 5-10 % was detected, but at least twice as many, i.e. about 20 % dead cells, was observed for ECM1 (**Figure 15**). This could indicate a cytotoxic effect brought about by the laminin fragments.[132-134]

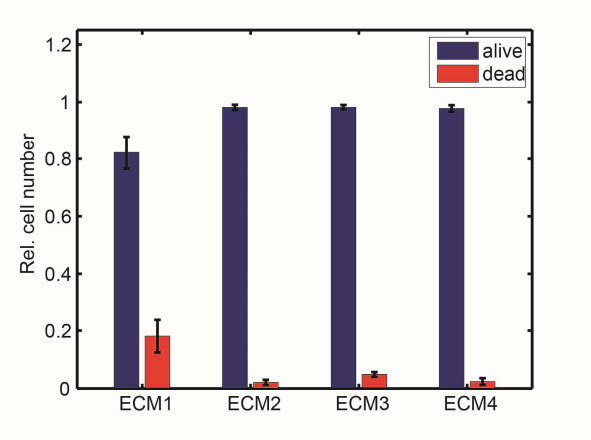

Figure 15 Life dead assay for dHL-60 cells embedded in the four basal lamina variants. Dead cells are obtained in all gels, but the amount differs significantly between ECM1 (about 20 % dead cells) and the other three variants (about 5-10 % of dead cells).

According to the presented results, all examined ECMs, except from ECM1, are well suited for cell experiments in a 3D-envirnonment. Therefore, in a final experiment, ECM2 gel was chosen in combination with liposomes to investigate if charged nanoparticles can influence the migration behavior of dHL-60 cells. This experiment is motivated by the fact that hydrogels are not only used for classical cell culture experiments, but more and more frequently also as medical products in combination with diverse nanoparticles to promote the healing process. Depending on the type of nanoparticle and the applied concentration, a considerable amount of neutral, positively or negatively charged nanoparticles can accumulate within hydrogels and may locally influence the cell migration behavior of cells. Such a phenomenon would be important for our immune system and could potentially compromise the healing process. Therefore, neutral DOPC (+/-), negatively charged DOPG (-) and positively charged DOTAP (+) liposomes with a zeta potential of -0.8 ± 0.5 mV, -36.4 ± 1.1 mV and 37.2 ± 0.9 mV respectively, were introduced at a final concentration of 10^{10} liposomes/µL into the ECM2, fMLP, dHL-60 hydrogel system. It could be shown, that, at least in an ECM2 matrix, the migration activity of dHL-60 cells seems not to be compromised by liposomes, regardless of the charge of the liposomes (see **Figure 16**). However, changing the kind of nanoparticle or the type of hydrogel may alter the outcome of this experiment, and has to be tested individually. Nevertheless, this result can serve as a first indication that charged nanoparticles do not drastically influence cell migration within hydrogels. The charge of nanoparticles should therefore most likely not restrict their application as drug carriers in hydrogels for medical applications, which is a topic that will be revisited later in this thesis.

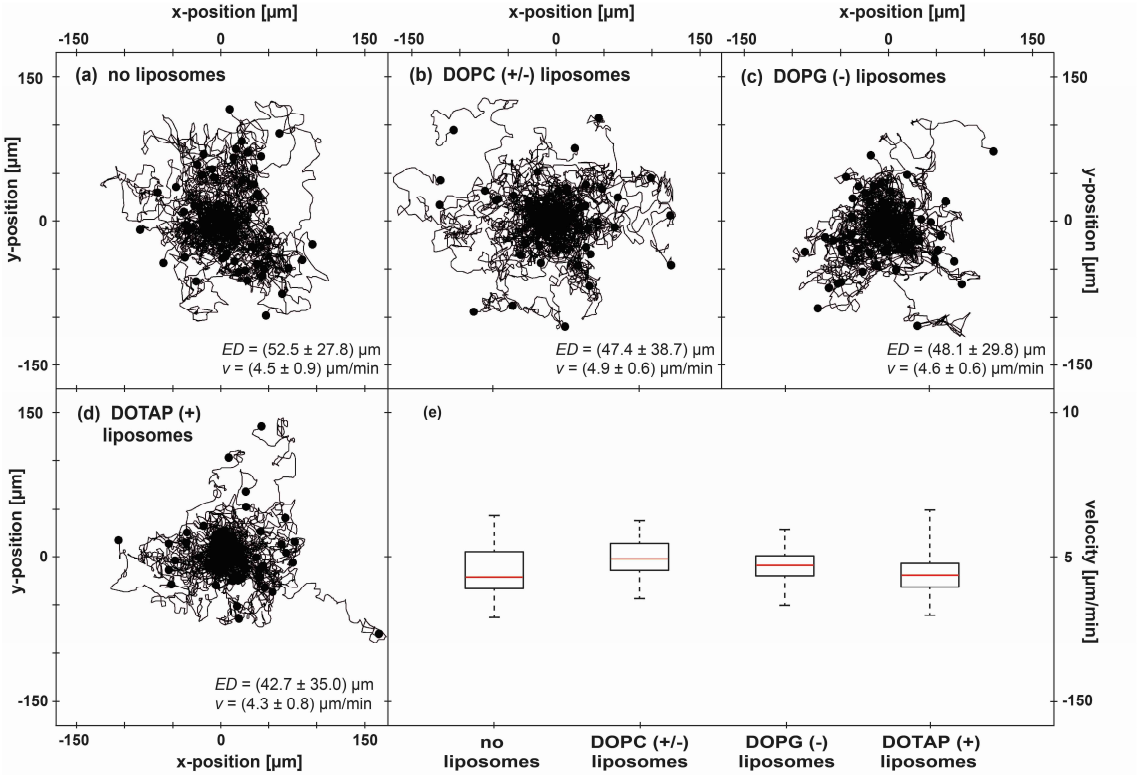

Figure 16 Migration trajectories of dHL-60 cells tracked from hours 4-6 after the cells are embedded into ECM2 in presence of liposomes of varying charge. (a-d) The starting point of all trajectories is shifted to the origin for clarity, and the end point is marked by a dot. The average start-to-end distance (Euclidean distance) travelled by the cells and the respective standard deviation is denoted by *ED*. (e) Comparison of the migration velocity of dHL60 cells in ECM2 gels in presence of different charged liposomes. The red line denotes the median of the velocity distribution, the box includes 25 % of the observed velocities above and below this median, respectively. The remaining 25 % of slower as well as the 25 % of faster cells are indicated by the dashed lines.

It should be mentioned, that all experiments except from the cell migration experiments were repeated with a second batch of the four ECMs, showing the same outcome. Therefore, it can be assumed that the discovered differences between the basal lamina gels are indeed very likely to arise from deviations in the manufacturing process of the four suppliers and do not represent batch-to-batch variations.

3.1.5 Conclusion to Chapter 3.1

By comparing the four different basal lamina gel variants, strong differences in the Brownian motion of NPs, the gel microarchitecture and the viscoelastic properties of the gel were observed. Those findings were surprising considering that all four gels were adjusted to the same total protein concentration. Furthermore, identical experimental conditions were chosen for each set of experiments to maximize comparability of the results. It could be shown, that the increased amount of the cross-linker protein entactin in ECM2 compared to the other ECMs leads to a

smaller pore size, and this altered mesh size is most likely responsible for those unexpected differences: the cell migration activity of dHL-60 cells within the gels, the final elasticity of the gels and differences in particle diffusion behavior, could all be attributed to those variations in the gel microarchitecture: small pore sizes cause higher gel stiffness and increased hindrance towards migrating cells and diffusion of NPs (ECM2), while larger pores facilitate cell migration and particle diffusion (ECM3, ECM4). The only discrepancy in this correlation appeared for ECM1. Although the microarchitecture (and therefore the pore size), particle diffusion and final gel elasticity are comparable with those of ECM3 and ECM4, cell migration activity deviated dramatically in comparison to the other gels. A possible explanation is that the proteins detected as additional bands by coomassie staining of ECM1 are somehow responsible for this difference. In addition, using ECM2 as a 3D scaffold for cell migration experiments, it could be shown that NPs of either charge have no strong influence on cell migration activity within ECM hydrogels.

The following chapter follows in part the publication of the same name: "A Selective Mucin/Methylcellulose Hybrid Gel with Tailored Mechanical Properties" published 2016 in Macromolecular Bioscience.[108]

3.2 A Selective Methylcellulose/Mucin Hybrid Gel with Tailored Mechanical Properties

The structure and therefore the mechanics of ECM mostly depends on the amount of the cross-linker entactin which serves as a bridge between type IV collagen and laminin.[135] There are more examples of naturally occurring cross-linked biopolymer hydrogels such as F-actin and microtubule gels.[136, 137] However, if searching for a base material to design a wound gel, these cross-linkable biopolymers are not necessarily the optimal choice since they are quite expensive and the mechanical properties of gels assembled from them may fluctuate significantly from batch to batch. Alternatively, chemically cross-linked hydrogels could be used. Most of them are cheap to manufacture, their mechanical stiffness can be adjusted as desired, and the resulting material qualities are very reproducible. The major disadvantage of such chemically cross-linked hydrogels arises from chemicals which have not reacted. These unreacted chemicals are often toxic, and it takes great effort to remove them. Moreover, in most cases neither biopolymers cross-linked by proteins nor chemically cross-linkable polymers provide the possibility to undergo gelation upon contact with a wound. Physical triggered cross-linking by to the unique ionic strength/pH/temperature of the human body would be an ideal mechanism if gelation should be achieved upon contact with a wound.[138] From these three options, temperature is most likely the most promising trigger for designing a wound gel since materials possessing sol/gel transitions on the basis of small changes in pH or ionic strength (those changes have to be small to avoid tissue damage) are rare. For a wound gel that can undergo a thermally activated gelation process upon contact with the wound and its physiological temperature, deacetylated chitosan and methylcellulose (MC) could be well-suited, since solutions of either biopolymer can form a gel at higher temperature.[61, 139] The driving force behind the sol/gel transition of those two biopolymer systems is the hydrophobic effect, which triggers a phase separation in aqueous solutions. This mechanism, which does not require any additional (potentially toxic) chemicals, constitutes a highly promising candidate for *in situ* gelation on wounds. Furthermore, both MC and chitosan are commercially available, relatively cheap and have been proven to be nontoxic and biocompatible.[62, 140] One critical advantage of MC over chitosan, however, is that MC can reduce the formation of scars, and this is especially important after

surgery.[141] Therefore, MC was chosen here as base material to design a thermoresponsive wound gel. The ability of such a MC solution to form a gel at physiological temperature makes it especially attractive for internal surgery, since there is no need of postoperative activation from the outside. Furthermore, due to the good biocompatibility the closed and partially healed wound does not have to be opened again to remove the old MC wound gel.[142]

Once a solid foundation for a wound gel is laid, i.e. a system providing the mechanical properties and gelation kinetics to quickly form a stiff gel of a few kilo Pascal on a wound, this platform can be used to incorporate biologically active materials which contribute beneficial qualities for wound care. Mucin, the main biopolymer of mucus, is such a bio-active material. It is known to prevent bacterial adhesion, [45, 46] and can trap different kinds of viruses, [47] thereby shielding the wound against microbial attacks. Unfortunately, reconstituted mucin solutions are only able to form a weak gel with a shear stiffness on the order of a few Pascal, and only at acidic pH and at low ionic strength.[55] Both conditions are not compatible with the physiological environment of a wound. Thus, due to their unsatisfactory mechanical performance reconstituted mucin solutions are not suitable for a direct application as a wound gel. However, to harness the valuable anti-microbial properties of mucins, mucins were incorporated into the MC based hydrogel. The rationale behind this was that the MC component should compensate for the weak mechanical properties of the mucin without diminishing its anti-microbial features. However, the performance of hybrid materials comprising two or more components are by no means easy to predict and often not just a combination of the individual characteristics. Unwanted effects such as phase separation or intermolecular interaction need to be tested and – if possible – prevented.

3.2.1 Adjusting the Gelation Properties of a Methylcellulose Solution

In initial experiments, the gelation behavior of a MC variant with a large average molecular weight of 88 kDa was tested. However, when a 3 % (w/v) solution of this MC variant was hydrated in 20 mM HEPES buffer with a physiological concentration of 150 mM NaCl at pH 7.0, the mixture remained a viscoelastic fluid at 37 °C and no gelation occurred (**Figure 17a**). This is in line with previous reports on the gelation properties of MC solutions which determined the gelation temperature for MC to be above 40 °C.[143] A simple strategy to reduce the gelation temperature is to increase the ion concertation of such MC solutions,[144] yet such an approach would not be well suited developing a wound gel where physiological conditions are required. As a consequence, an alternative method

was needed to induce gelation at a physiological temperature of 37 °C. Since glycerol is reported to enhance the aggregation mechanism responsible for MC gelation, the addition of glycerol was expected to lower the gelation temperature of the MC solution.[145] Indeed, when 10 % (v/v) of glycerol was added to the 3 % (w/v) MC solution with physiological salt and pH, gelation was achieved at 37 °C, and the 88 kDa-MC solution reached a shear stiffness of ~200 Pa after ~60 min of heating. Moreover, glycerol is not only able to enhance the gelation of MC mixtures, but it is also known for stabilizing proteins in aqueous solutions,[146] which could be an advantage for the incorporation of mucin. However, the so far realized gelation kinetics were to slow, and therefore not sufficient for applying the mixture as a wound gel. To accelerate the gelation process, a MC with a smaller molecular weight of 17 kDa was chosen next. The rationale was that, for the shorter MC macromolecules, the thermally driven process of aggregation should occur considerably faster and, accordingly, gelation of the solution should be significantly enhanced. This assumption turned out to be correct, and a strong increase in the gelation kinetics for a 3 % (w/v) 17 kDa-MC solution could be observed: the MC/glycerol mixture was now able to form a gel within a few minutes (**Figure 17b**).

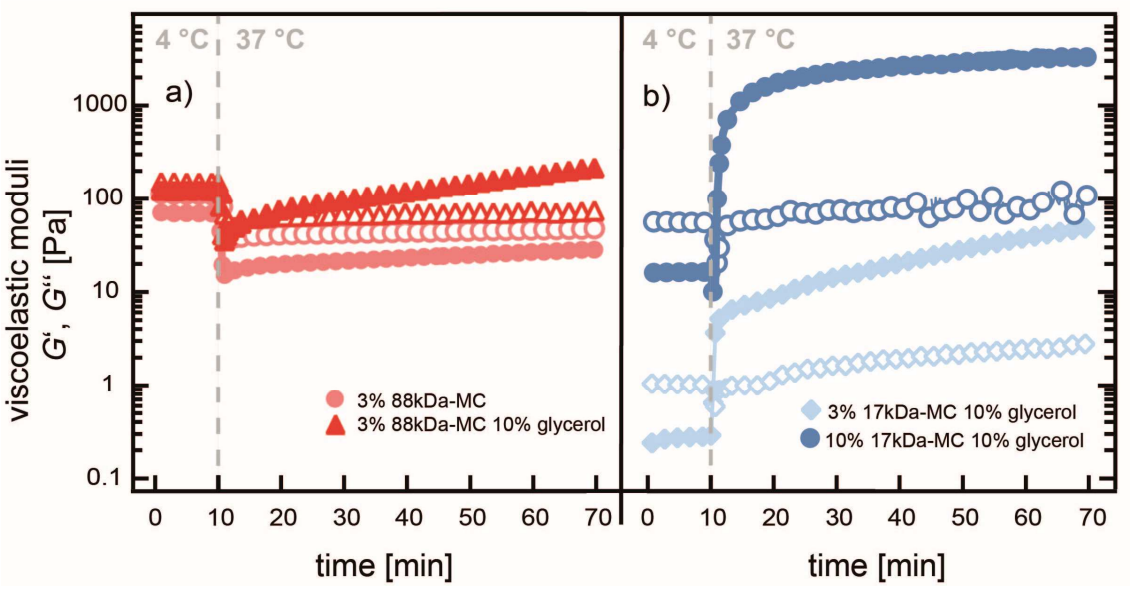

Figure 17 Thermal gelation behavior of different MC solutions. (a, b) By tuning the molecular weight and concentration of MC and the addition of glycerol, rapid gelation behavior is obtained. Closed symbols represent the storage modulus G′ and open symbols denote the loss modulus G″. Both moduli are shown for a probing frequency of 1 Hz. In addition, the final shear stiffness of the gel can be adjusted so that the elasticity of soft native tissue (i.e., connective tissue) is approximated. All symbols represent the mean of at least three measurements.

However, the maximal stiffness of the gel was now reduced compared to when the longer MC species were used. This called for further adjustment. Ideally, a wound gel should exhibit a final shear stiffness that is on the order of the wound stiffness itself and therefore of the stiffness of cells and soft tissues, i.e. in the range of a few to tens of kPa.[56] The final shear stiffness of MC solutions depends on the concentration of MC macromolecules.[145] Therefore, the gel stiffness was adjusted by increasing the 17 kDa-MC biopolymer concentration to 10 % (w/v). As a side effect, this higher amount of MC led to an increase in viscosity. However, the viscosity was still relatively low (15.8 ± 0.4 Pa·s at 4 °C and a shear rate of 1/s, see **Figure 21b**) and should enable a refrigerated MC solution to readily wet and cover the entire area of an uneven wound. Now, the MC/glycerol mixture exhibited both rapid gelation kinetics (which is important for the polymer material to remain in place after application) and a suitable final shear stiffness of about 3-4 kPa (**Figure 17b**).

Virtually the same final gel stiffness was obtained for the MC solution when the gelation was performed outside of the rheometer, i.e. inside an incubation chamber set to 37 °C, and the resulting gel exhibited viscoelastic moduli that were almost independent of frequency (**Figure 18**).

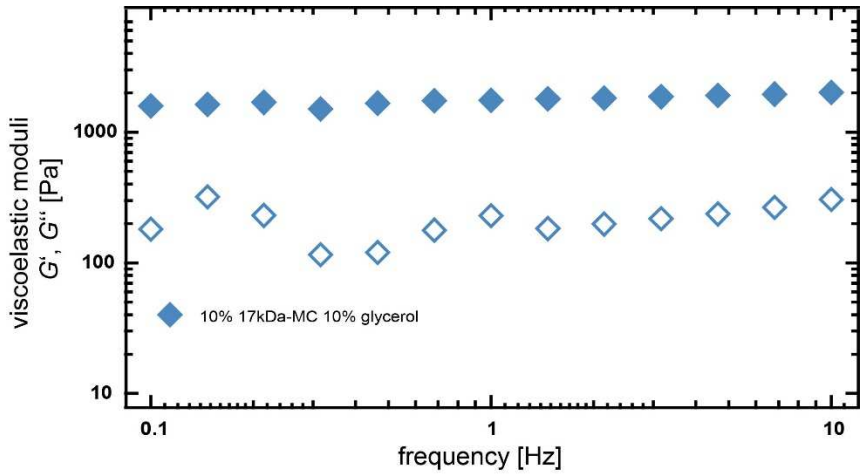

Figure 18 Frequency-independent viscoelastic behavior of the methylcellulose-based gel. Closed symbols denote the storage modulus *G'* and open symbols denote the loss modulus *G''* as measured at 37 °C. All symbols represent the mean of at least 3 measurements.

Furthermore, it was tested, if the gelation kinetics of the designed MC solution could be further improved by substituting 130 mM of NaCl with the slightly more kosmotropic salt KCl. Kosmotropic ions like KCl are known to strengthen hydrophobic interactions[147] and might

therefore accelerate the gelation process. Nevertheless, no sign of improvements of the gelation kinetics could be observed (**Figure 19**). Of course, one could argue that the use of even stronger kosmotropic ions would provide a stronger acceleration of the gelation kinetics. However, strong kosmotropic ions such as Rb^+ or NH_4^+[148] are not compatible with the physiological context of a wound. As a consequence, the physiological NaCl was used for the remainder of this study, as this salt variant possesses the advantage to cause no cell signalling as e.g. calcium ions do.[149]

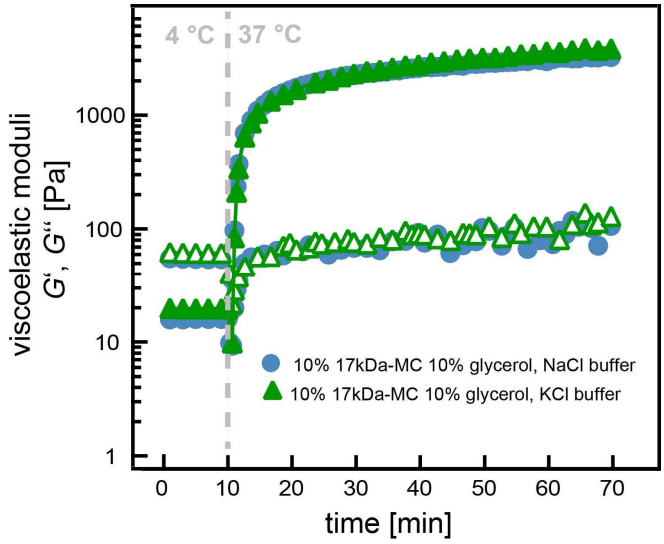

Figure 19 The kinetics of the thermal autogelation of the MC mixture are robust towards minor changes in the ion composition. When the ion composition of the buffer is changed from 150 mM NaCl to 130 mM KCl + 20 mM NaCl, i.e. when a slightly stronger kosmotropic ion is used, the virtually identical gelation behavior of the biopolymer mixture is observed. Closed symbols represent the storage modulus *G'* and open symbols denote the loss modulus *G''*. Both moduli are shown for a probing frequency of 1 Hz. All symbols represent the mean of at least 3 measurements.

3.2.2 Mucin Glycoproteins can be Integrated into the Methylcellulose Matrix without Disturbing Gel Formation

So far, the type and concentration of the MC macromolecule and the buffer system to adjust the viscoelastic properties required for a thermoresponsive wound gel have been tuned. The next aim was to integrate the medically active mucin glycoprotein into this base material, without disturbing the gelation properties of the system. From previous experiments with purified gastric mucins it was known that high antiviral activity of the mucins is already achieved at a concentration of 1 % (w/v).[47] This value is also a good approximation for the concentration of mucins in native mucus gels.[58-60] Thus, a concentration of 1 % (w/v) mucin was chosen for a first formulation of a hybrid gel mixture. For such a polymer blend, a homogeneous distribution of mucins throughout the MC matrix is mandatory so that the final hybrid gel can perform its protecting abilities without presenting any open voids for pathogens. To check the spatial

distribution of mucins within the MC matrix, mucin glycoproteins were selectively stained with fluorescently labeled lectins which could afterwards be localized within the gel by means of fluorescent microscopy. On a microscopic scale, the spatial distribution of 1 % (w/v) mucin in a 10 % (w/v) MC mixture strongly depended on how the blend was generated. When both biopolymers, mucin and MC, are mixed in their lyophilized form and afterwards simultaneously co-hydrated in 20 mM HEPES containing 10 % glycerol and 150 mM NaCl at pH7.0, strong heterogeneities in the spatial mucin distribution were observed (**Figure 20a**). However, those heterogeneities could be eliminated to a large extent when the hydrated MC/mucin solution was thoroughly mixed on a magnetic stirring table for 20 min (**Figure 20b**). The achieved sample homogeneity was no temporary effect, but stable over time, and no spontaneous phase separation could be detected within a time span of 24 h.

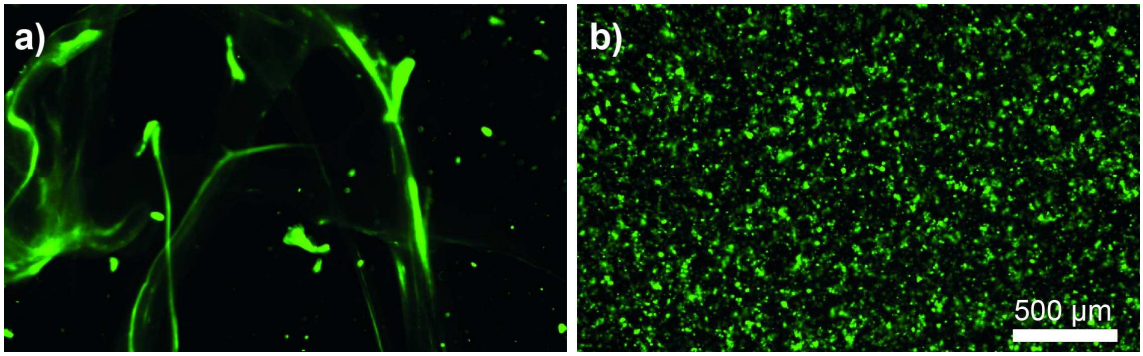

Figure 20 Mucins can be successfully integrated into the MC matrix if the blend is thoroughly mixed. Fluorescence microscopy images demonstrate the spatial distribution of mucins in a MC/mucin hybrid gel which has been generated by (b) simple co-hydration and (c) by additional mechanical mixing**.**

Having demonstrated that the medically active mucin component can be distributed reasonably well within the MC matrix, it was confirmed that the viscoelastic properties of this hybrid mixture are not compromised by the integration of the glycoprotein. Therefore, the *in situ* gelation experiment with the mucin/17 kDa-MC/glycerol solution was repeated, which showed that the hybrid solution exhibits nearly identical gelation kinetics and frequency-independent viscoelastic behaviour as the pure 17 kDa-MC/glycerol solution (**Figure 21a, b, c**).

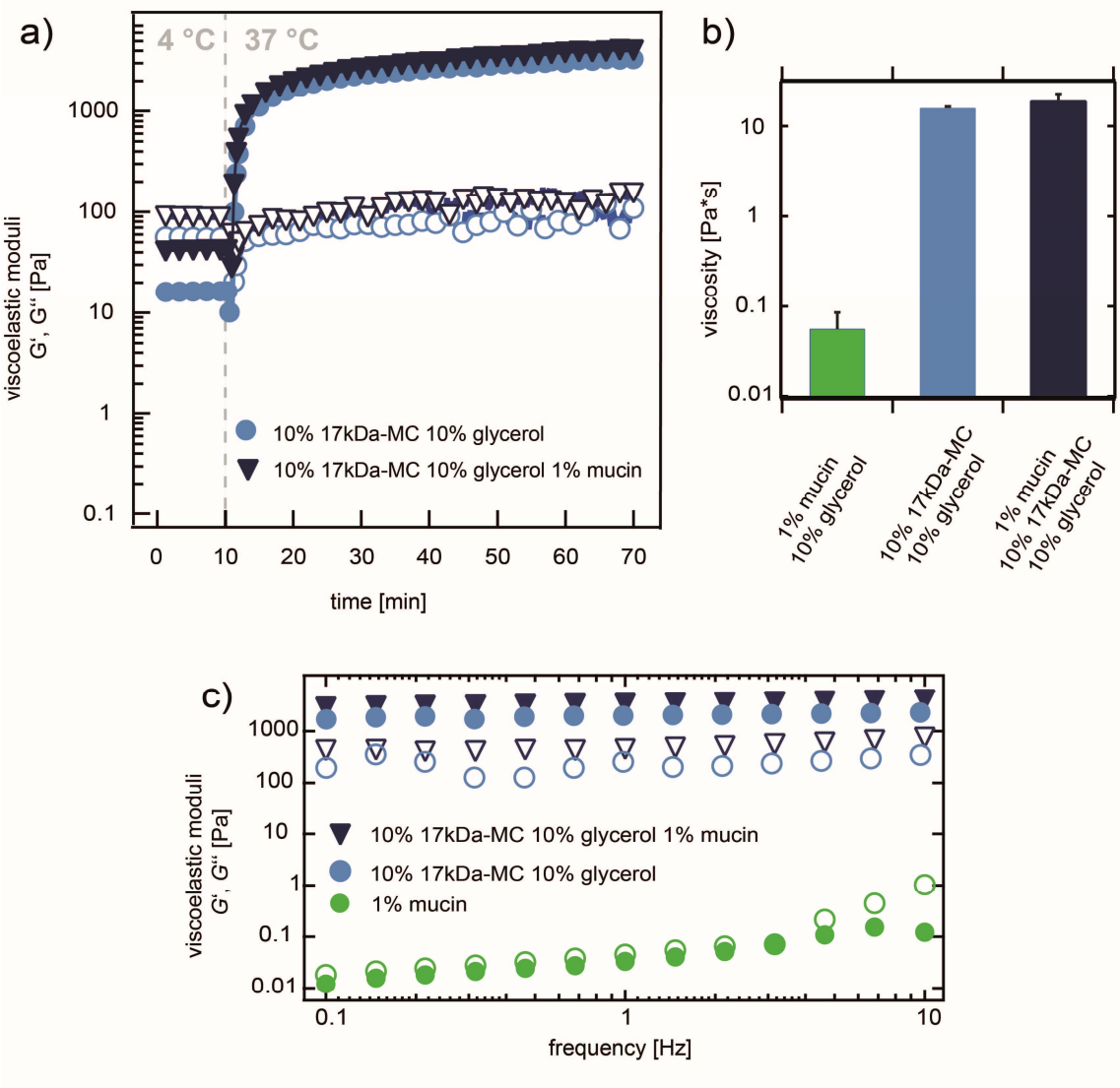

Figure 21 Mucins can be successfully integrated into the MC matrix without compromising the viscoelastic properties. (a) The addition of 1 % (w/v) mucin to the MC solution does not interfere with this thermal gelation process. And the addition of the mucin component does not significantly affect the viscosity (b) or the frequency-independent viscoelastic behavior (c) of the methylcellulose-based gel. Closed symbols denote the storage modulus *G'* and open symbols denote the loss modulus *G''* as measured at 37 °C. All symbols represent the mean of at least 3 measurements. Viscosity values were determined at 4 °C and a shear rate of 1/s. Error bars denote the standard deviation as obtained from at least three independent measurements

The same was true when the concentration of the mucin component was increased up to 3 % (w/v) (**Figure 22**). These results supported the assumption that the viscoelastic properties of the MC/mucin blend will be mostly determined by the mechanical adjuvant, MC.

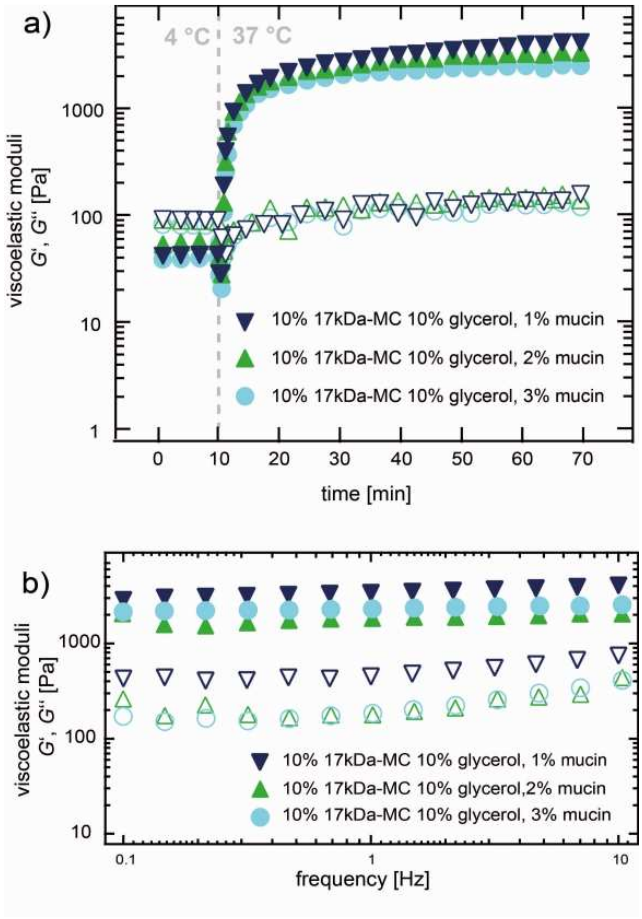

Figure 22 The viscoelastic properties of MC mixtures are robust towards increasing amounts of mucins. Increasing the concentration of the mucin component does not significantly affect the thermal gelation behavior (a) or the frequency-independent viscoelastic behavior (b) of the biopolymer mixture. Closed symbols represent the storage modulus *G'* and open symbols denote the loss modulus *G''*. Both moduli of the gelation curve are shown for a probing frequency of 1 Hz. All symbols represent the mean of at least 3 measurements.

3.2.3 Gelation on a Model Tissue Surface

So far, the gelation properties of the MC/mucin biopolymer solution have been probed on a plane metallic surface, which was part of the rheometer setup. However, eventually, the hybrid mixture is supposed to be applied on wound tissue surface covered by cells. Another challenge in this context will be that any wound in the human body will possess an intrinsic curvature and thus will be locally tilted. For a more realistic setup mimicking this challenging conditions, the gelation experiment was repeated on a tilted model tissue surface consisting of elongated PDMS wells that had been coated with a confluent monolayer of fibroblasts (see **Figure 23a** and methods). For this purposes, such a model tissue surface with a well-defined geometry provided a reasonable approximation of a cell-

covered tissue surface. The device was placed onto an adjustable ramp, which granted the opportunity to probe *in situ* gelation on the biological surface with well-defined tilt angles.

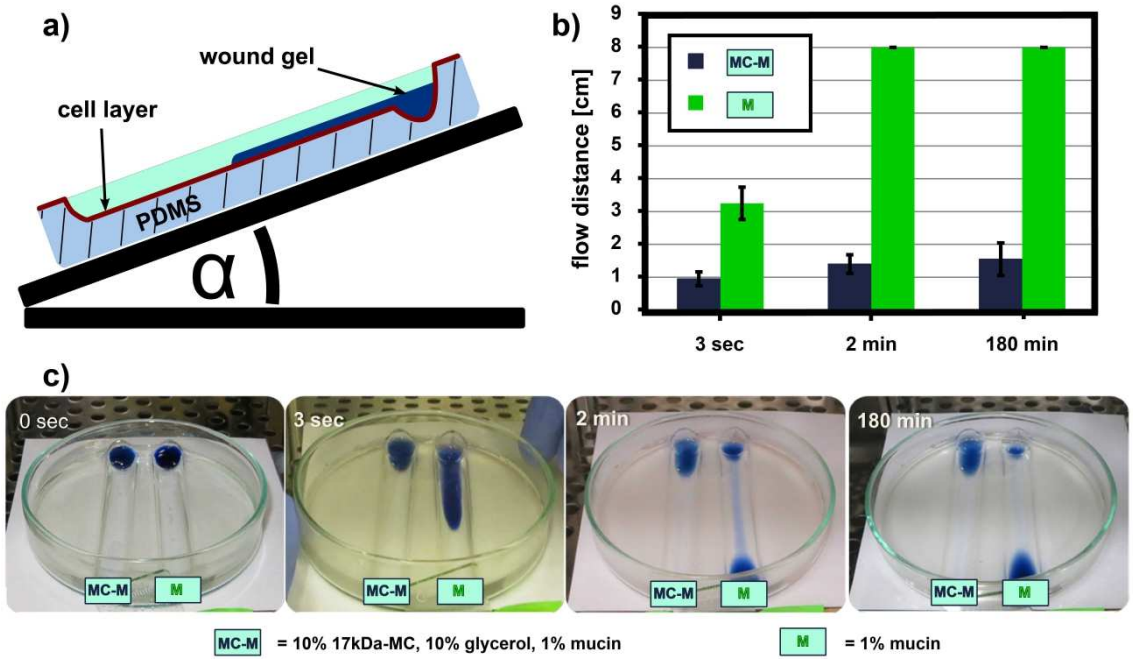

Figure 23 Thermal autogelation of MC/mucin solutions on tilted model tissue surfaces. A scheme of the gelation assay is depicted in (a). A half-pipe made from PDMS is coated with fibroblasts and placed at a defined tilt angle of 10° and stored in an incubator at 37 °C to model a tissue surface. (b, c) In contrast to pure mucin solutions (M), the MC/mucin mixture (MC-M) does not flow along the PDMS channel due to its thermal autogelation properties. The bar chart in (b) shows the mean value and standard deviation as obtained from two independent experiments.

First, the gelation efficiency of the MC/mucin (MC-M) solution was examined at a tilt angle of 10 ° and a temperature of 37 °C. For better visualization of the otherwise almost transparent solution, a few drops of ink were added to the biopolymer mixture. As control, a pure mucin solution (M) lacking the mechanical adjuvant MC was added to a neighboring well (**Figure 23c**). When this model tissue surface was tilted at the start of the experiment, the control solution (M) instantly started to flow due to its low viscosity (0.24 ± 0.02 Pa·s at 4 °C and a shear rate of 1/s, see **Figure 21b**), and after only 5 seconds the majority of the liquid had already reached the bottom of the ~8 cm long cell-covered channel. The MC/mucin solution, on the other hand, exhibited significantly less flow due to its higher viscosity (19.0 ± 3.7 Pa·s at 4 °C and a shear rate of 1/s, see **Figure 21b**) and its thermal auto-gelation properties. Thus, the hybrid mixture formed quickly a stiff gel *in situ* and remained at the site of application even after extended time periods, i.e. up to 3 h (**Figure 23b, c**). A very similar result was obtained at a large tilt angle of 45 ° (**Figure 24**).

This findings emphasizes the rapid and efficient auto-gelation properties of the MC/mucin mixture and agrees well with the results obtained using the rheometer setup.

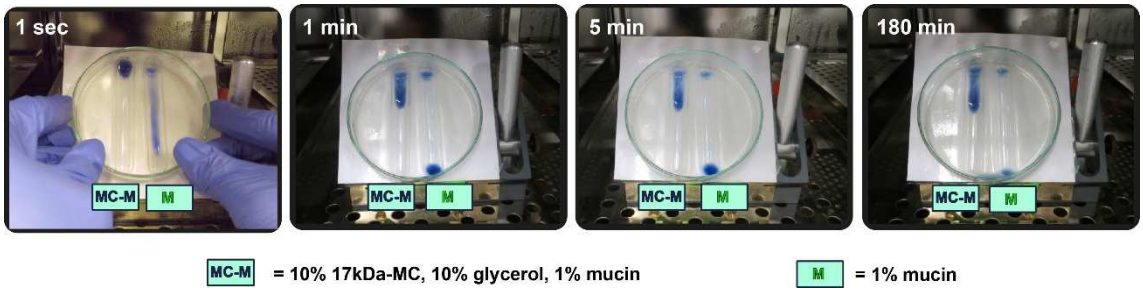

Figure 24 Thermal auto-gelation of MC/mucin solutions on tilted model tissue surfaces. A PDMS half-pipe is coated with a monolayer of fibroblasts and placed at a defined tilt angle of 45 ° and stored in an incubator at 37 °C to model a tissue surface. In contrast to pure mucin solutions, the MC/mucin mixture does not flow far along the PDMS-channel due to its thermal autogelation properties.

3.2.4 The Integrated Mucins Establish Selective Permeability in the Hybrid Gel

Naturally occurring mucin based gels possess selective permeability properties. This selectivity is caused by charge patterns along the mucin backbone and are mainly brought about by the sugar residues. Therefore, the net charge of particles and molecules is an important parameter, which dictates how efficiently those objects can penetrate a mucin gel.[52, 150] Thus, in a next step it was tested if the integrated mucin glycoproteins establish such charge selective permeability in the hybrid gel. First, the behaviour of two variants of fluorescent dextran molecules in the MC/mucin gel were compared: positively charged DEAE-dextran and negatively charged CM-dextran. Although those two dextran variants have almost identical molecular weight (≈ 4 kDa), it is expected that their distribution in the gel matrix will differ. The rationale for this notion is that the mucin glycoproteins carry a significant amount of negatively charged groups as a consequence of the high glycosylation density by e.g. sialic acid. Those negatively charged groups should selectively attract the positively charged DEAE-dextrans whereas the negatively charged CM-dextrans should remain unaffected. Indeed, when performing co-localization experiments by again using fluorescent lectins as a stain for mucins, a clear co-localization of DEAE-dextrans with the mucin domains of the hybrid gel was observed (**Figure 25a**). In contrast, the spatial distribution of the CM-dextrans was not influenced by the mucin macromolecules. As expected, pure MC-gels do not exhibit this charge-selective local accumulation of dextrans (**Figure 25b**), which underscores that the selective permeability properties of the hybrid gel are brought about by the integrated mucins.

Of course, this selective trapping of positively charged molecules should also occur for other molecules. Whereas dextrans are a convenient model system for probing the molecular distribution through hydrogels[151, 152] many molecules which are relevant in the context of wound healing applications are based on peptides.[153] Indeed, when the spatial distribution of positively charged $(KKK)_8$ oligopeptides is compared with that of negatively charged $(EEE)_8$ oligopeptides in the hybrid gel, the results agree with those obtained with the two dextran variants: the positively charged peptides co-localize with mucin whereas the negatively charged peptides do not (**Figure 25c**).

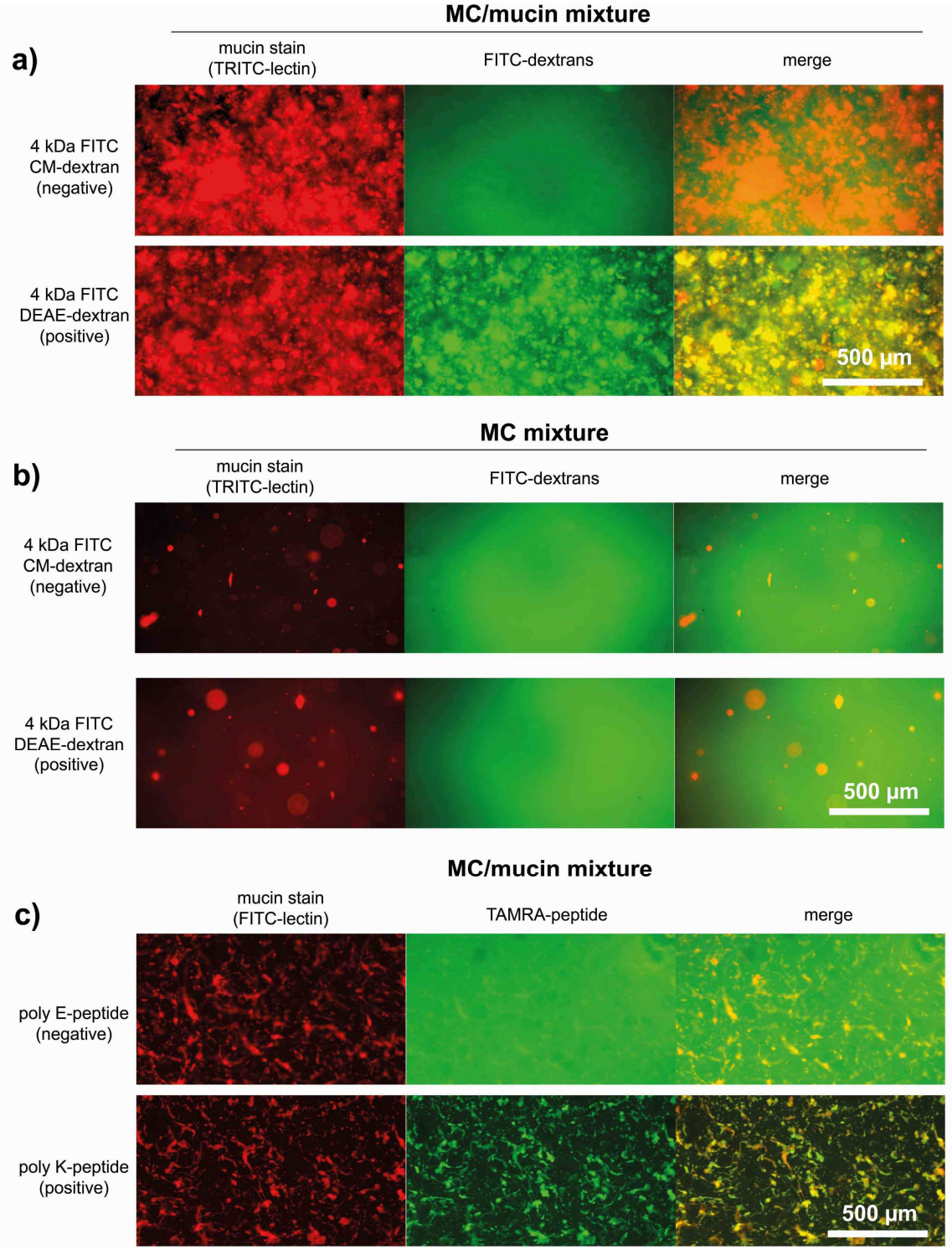

Figure 25 Mucins establish charge selective permeability in the hybrid gel. (a, c) Positively charged DEAE-dextrans (FITC labeled) as well as positively charged $(KKK)_8$ oligopeptides (TAMRA labeled) co-localize with mucin (labeled via a TRITC-lectin stain) in the MC/mucin gel. In contrast, negatively charged CM-dextrans as well as negatively charged $(EEE)_8$ oligopeptides do not co-localize with mucin but are distributed homogeneously throughout the hybrid gel. (b) In pure methylcellulose gels, negatively and positively charged fluorescently labeled dextrans are distributed homogeneously and no co-localization is observed.

Since the integrated mucins can selectively trap positively charged molecules in the matrix of the hybrid gel, the release of those molecules from the gel should also be selectively retarded. Indeed, for covalently cross-linked hydrogels comprising bovine salivary mucins such a behavior has recently been described.[57] Here, a similar release experiment with DEAE-dextrans and CM-dextrans from the MC/mucin hybrid gel was performed. In pure MC gels, the release kinetics of both positively and negatively charged dextrans, was virtually identical (**Figure 26a**). However, the MC/mucin hybrid gel selectively retarded the release of the positively charged DEAE-dextran, which underscores the previous notion that integrating the mucin glycoproteins into the gel conveys selective permeability properties similar to those of pure mucin gels.

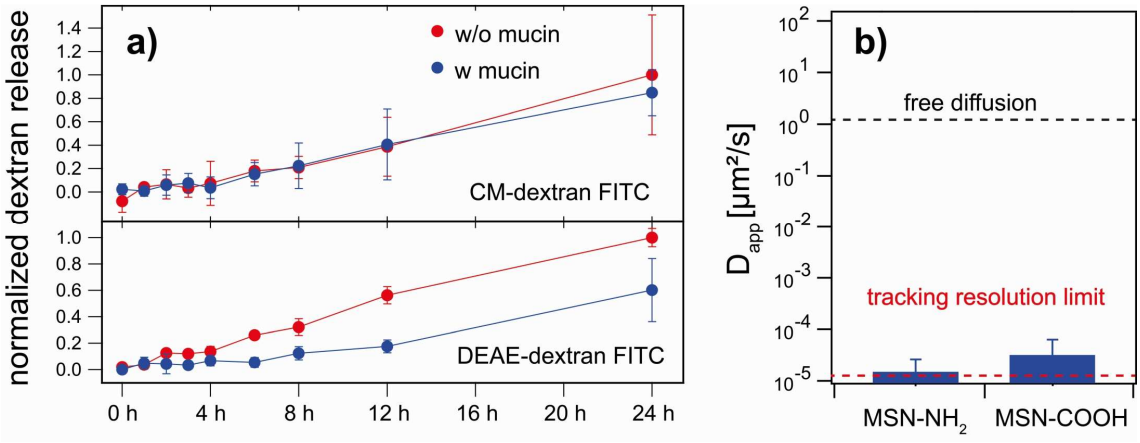

Figure 26 The MC/mucin hybrid gel selectively retards the release of positively charged dextrans, while trapping nanoparticles of either net charge. (a) The release of FITC labeled DEAE-dextrans form MC/mucin hybrid gels is significantly retarded compared to FITC labeled CM-dextrans. (b) On the length scale of drug delivery nanoparticles, the hybrid gel efficiently traps objects regardless of their net charge, i.e., both amine-terminated and carboxyl-terminated nanoparticles.

Finally, it was tested if the selective permeability properties of the hybrid gel as brought about by the mucin component are also present on the length scale of nanoparticles. For this purpose, two variants of porous nanoparticles which have been envisioned as potential carriers for drug delivery applications were incorporated into the hybrid gel:[154] silica particles coated with amine- and carboxyl-groups. Both nanoparticles have similar size distributions which are centered around 150 nm in diameter, yet the particles significantly differ in their zeta-potentials (see **Table 2**). When the diffusive mobility of these particles in the MC/mucin hybrid gel was determined, it was observed that both particle variants are efficiently immobilized in the gel. In contrast to the previous diffusion experiments with dextrans and peptides, even the negatively charged carboxyl-particles were

immobilized (**Figure 26b**). This effect is most likely due to steric confinement as imposed by the hydrogel microarchitecture, especially since the theoretical mesh size of a 0.4 - 1.0 % (w/v) MC gel ranges from 48 - 20 nm, suggesting that the mesh size of our hydrogel is even lower.[155] More importantly, this result shows the potential to firmly embed nanoparticles of either surface charge into the gel to allow for prolonged drug release from the gel matrix while avoiding nanoparticle depletion from the gel. Such an enrichment of the gel with NPs should have no strong impact on cell migration activity, at least previous experiments with liposomes of either net charge embedded into ECM gels did suggest so (see chapter 3.1.4).

Table 2 Size distribution and zeta-potential data from dynamic light scattering experiments.

	diameter [nm]	**polydispersity index**	**zeta-potential [mV]**
MSN-NH_2	155.1 ± 41.4	0.08	16.0 ± 0.7
MSN-COOH	140.8 ± 35.9	0.07	-35.3 ± 1.6

3.2.5 Methylcellulose/Mucin Hybrid Gels can Support Wound Healing Processes

When applied as a gel to support wound healing, the biopolymer mixture should provide three additional features in addition to possessing appropriate gelation properties and selective permeability: first, a damaged cell layer must be able to close when covered with the gel, i.e. the adhesion strength between the cells and the gel may not be too strong. Second, added substances that promote the wound healing process must be able to diffuse through the gel so that they can be released after application on a wound. Third, the release of embedded drugs from the gel should occur slowly, which is typically achieved by enclosing the drugs into nanoparticles. Ideally, the drug release from such nanoparticles would only occur after the gel has been applied onto a wound.

To verify if the first desired feature is met by the hybrid gel, an *in vitro* wound healing assay with a fibroblast monolayer was performed (see Methods). Indeed, the fibroblasts could successfully close the artificial wound within a time span of ~24 h even if they were covered with the MC/mucin gel. In the absence of mucin, i.e. when pure MC gels are used, the artificial wound closed within 24 h as well (**Figure 27**). This absence of cell-adhesive behavior of MC gels agrees well with our previous notion that the MC component should aid in reducing scar formation of the damaged tissue as described in ref.[141] It should be mentioned that a gel lacking significant cell-adhesion behavior but possessing a too high shear stiffness would probably also prevent the closure of a damaged cell layer - unless

the cells are able to soften the gel locally by enzymes. However, since the hybrid gel was adjusted to match the shear stiffness of soft tissue, this should not be an issue. Thus, being capable to close a damaged cell layer while preventing scar formation, the hybrid mixture constitutes a promising wound gel candidate, especially for damage tissue arising from burns. Here, the high water content of hydrogels such as the hybrid gel developed here conveys a soothing, cooling effect,[156] which leads to a faster healing process of the wound.

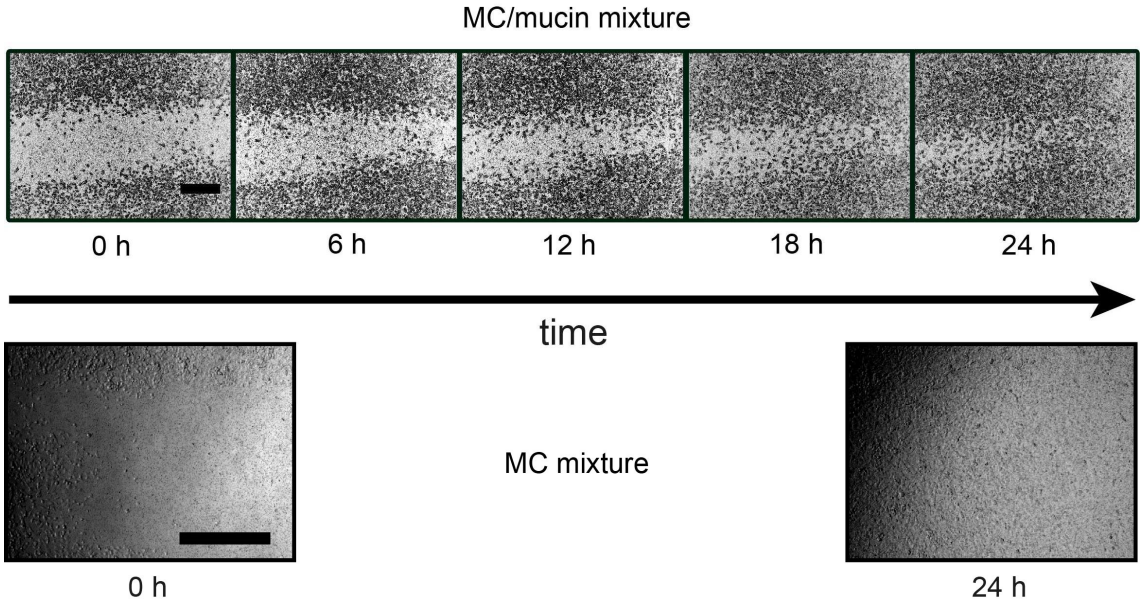

Figure 27 Healing of an artificial wound covered with the MC gel mixture with and without mucin. A monolayer of HT-1080 cells was damaged by performing a micro scratch and was then covered with the MC/mucin mixture or the MC mixture lacking mucin. Even though both mixtures form a viscoelastic gel with a stiffness of several kPa, the underlying cells are still able to close the wound by a combination of proliferation and migration. The scale bars represents 500 µm.

For testing the second gel property, the gel was enriched with molecules that are helpful for the natural wound healing response of the human body. Therefore, interleukin-8 (IL-8) was chosen as an example of cytokines, which play important roles in the inflammatory response of native tissues. IL-8 exhibits an isoelectric point of about 9.2 and is therefore positively charged at physiological pH.[157] Thus, it is possible that, similar to the positively charged DEAE-dextrans and peptides tested before, this molecule might get trapped in the gel matrix by the negatively charged mucins. As an experimental platform to test the diffusion behaviour of IL-8 in MC/mucin gels, ^{1}H PFG NMR spectroscopy was used (this was done in cooperation with A. Penk from the group of Prof. D. Huster at the Institute of Medical Physics and Biophysics of the University of Leipzig) as this technique does not

require any labeling of the IL-8 molecule. This is important as such a (for instance, fluorescent) label might drastically alter the diffusion behaviour of such a small protein in the complex environment of a multi-component biopolymer gel by e.g. introducing muco-adhesive interactions. However, due to the complex composition of MC/mucin hybrid gels, special care needs to be applied when selecting the signals for the diffusion analysis. In **Figure 28a** and **Figure 28b**, the IL-8 NMR signal used to directly measure its diffusion behaviour is marked with an asterisk. The signal attenuation for the relevant spectral range as a function of the applied gradient strength is shown in panel b for IL-8 in buffer (black) and in buffer with MC/mucin (red). From this decay, the apparent diffusion constant (D) can be calculated (**Figure 28c**). The value obtained in the hybrid gel, $D_{\text{IL-8 in MC/mucin}} = 69\ \mu m^2/s$, was only ~20 % smaller than its corresponding value in buffer, $D_{\text{IL-8 in buffer}} = 89\ \mu m^2/s$.

Thus, it could be shown that the diffusive mobility of IL-8 is not significantly restricted by the MC/mucin gel matrix. As a consequence, the protein of interest (here IL-8) would be efficiently released from the gel after its application onto the wound, where it should boost the healing process.

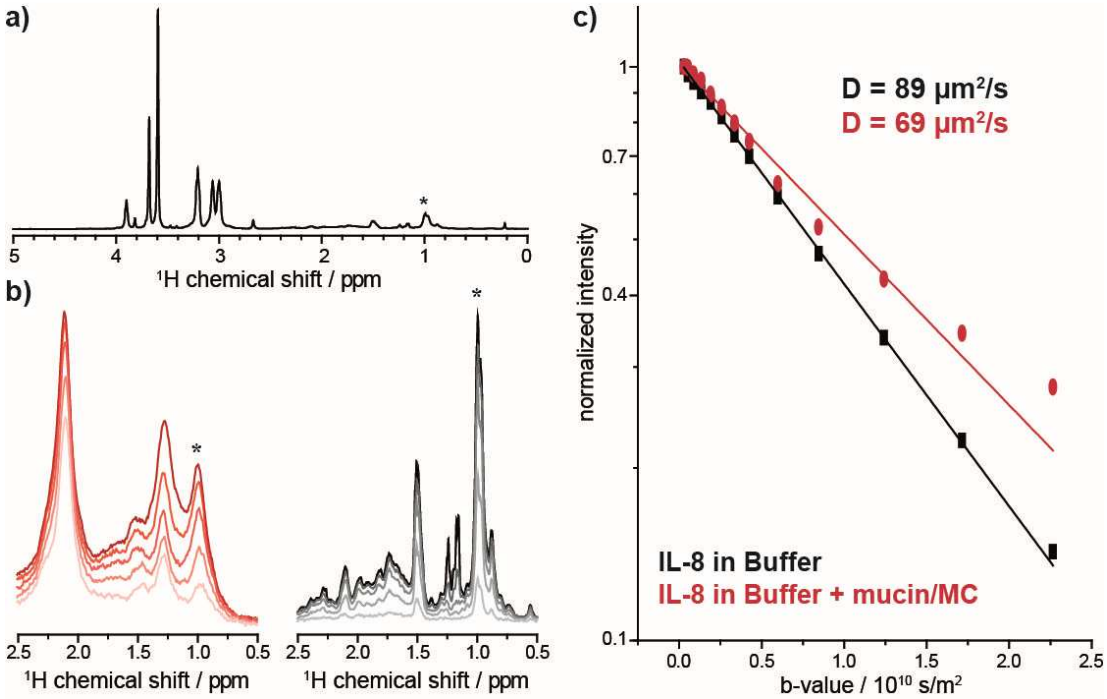

Figure 28 Interleukin-8 can diffuse in the hybrid gel. The signal of IL-8 used for data analysis (asterisk) is shown in panel (a), the enlarged relevant spectral region in (b) for IL-8 in buffer (black) and for IL-8 in the MC/mucin gel (red). Furthermore, the intensity decays of the spectra (from dark to light color) corresponding to the higher effective applied gradients are shown. In (c) the normalized intensity decays (I/I_0) of the IL-8 resonance with and without MC/mucin are plotted versus the b-value according to $I/I_0 = \exp(-D*b)$. The b-value is a function of the applied gradient strength and timing used to generate diffusion-weighted images and allows for the calculation of the apparent diffusion constant using linear regression in a semi-logarithmic plot. The IL-8 exhibits only a slightly weaker decay within the MC/mucin, which demonstrates that IL-8 diffusion is virtually unrestricted in the gel.

To achieve the third property, i.e. prolonged drug release from the gel, it was already demonstrated that choosing positively charged drug molecules can be a successful strategy as the release of these charged molecules is retarded by the integrated mucins. If this is not possible or when drug release over even longer time spans is needed, embedding drug-loaded nanoparticles into the gel is a good alternative. The results from the diffusion experiments with porous silica-nanoparticles suggest that any nanoparticles with diameters of 150 nm and larger could be used for this purpose since they will be trapped in the gel matrix independent of their net charge. Here, liposomes were chosen, which are already commonly employed for drug encapsulation and delivery since they are easy to produce, nontoxic and allow for prolonged drug release when the appropriate lipid composition is chosen.[158] In addition, the previous results from the cell migration experiments of dHL-60 cells within basal lamina gels in presence of liposomes suggest, that liposomes embedded into the hybrid gel will have no strong effect on cell migration activity (see chapter 3.1.4).

Several methods exist to load liposomes with drugs,[159] but achieving a triggered drug release is much more difficult. For the developed thermoresponsive gel system, it would be ideal to also use the gelation-inducing temperature shift as a trigger for drug release. Therefore, thermoresponsive liposomes were generated consisting of 84 mol% DPPC and 16 mol% DOTAP, as this particular lipid composition yields lipid bilayers with a phase transition temperature of about 37 °C (**Figure 29b**). Liposomes with an average size of 1 µm were chosen to guarantee efficient particle arrest in the gel and to provide sufficient particle volume for drug loading. During the heating-induced phase transition, the permeability of the lipid bilayer is strongly increased,[160] which offers a microscopic mechanism that should be sufficient to trigger drug liberation from the liposome particles. When the DPPC/DOTAP liposomes were loaded with doxorubicin (Dox), a fluorescent drug used in cancer chemotherapy,[161] a temperature-induced drug release of the uncharged Dox molecule at 37 °C was expected (**Figure 29a**).[114] In contrast, at 4 °C, i.e. when the phase transition is not triggered, the amount of released drug should remain low and constant over time. Indeed this temperature-dependent drug liberation occurs when the Dox-loaded liposome particles are embedded in the hybrid gel (**Figure 29c**). This demonstrates that the chosen trigger mechanism is also efficient in the complex environment of a multi-component biopolymer gel.

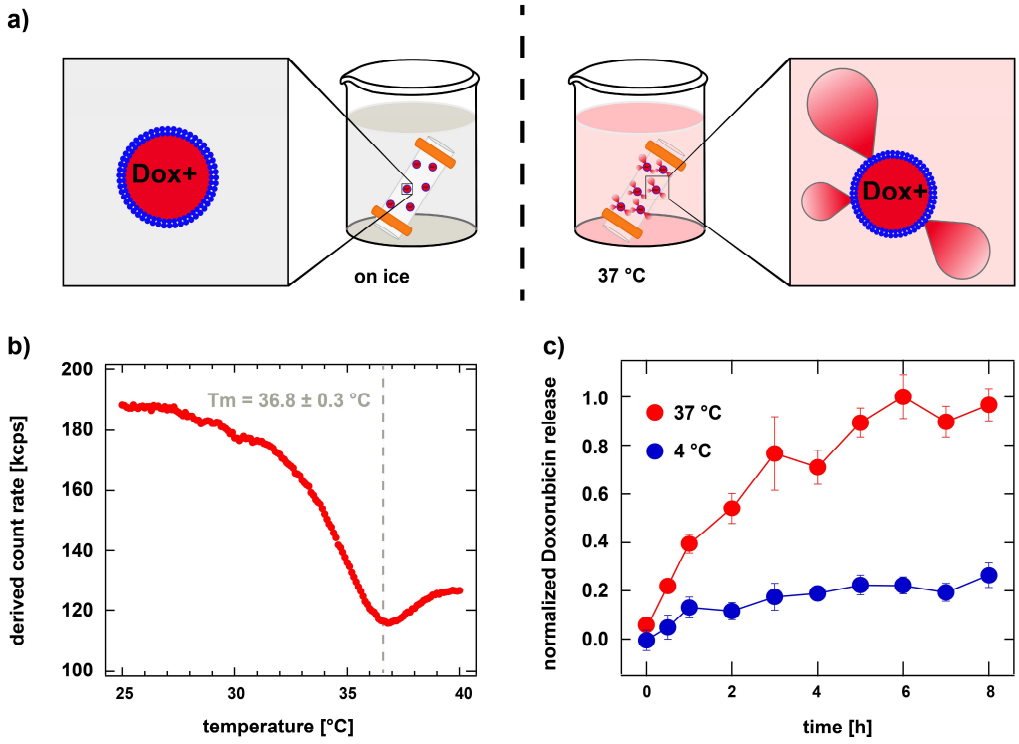

Figure 29 Drug release from the MC/mucin gel can be induced simultaneously with gelation due to gel-to-liquid crystalline phase transition of liposomes. A scheme of temperature-dependent drug release from thermoresponsive liposomes loaded with Dox is depicted in (a). Liposomes consisting of 84 mol% DPPC and 16 mol% DOTAP were produced in water to determine the phase transition temperature (T_m) at which the membrane gets leaky for small molecules. This transition temperature can be determined by changes in the scattering intensity observed during dynamic light scattering as shown in (b). The symbols represent the mean of four measurements. For the drug release data shown in (c), these thermoresponsive liposomes were embedded into the MC/mucin mixture. Dox release from the biopolymer mixture is significantly higher at 37 °C, i.e., when the MC/mucin mix has formed a gel, compared to 4 °C, i.e., when the MC/mucin mix remains a viscous solution. The highest Dox concentration measured during release is set to 1. The symbols in (c) represent the mean of three measurements and the error bars denote the standard deviation.

3.2.6 Anti-Microbial Properties of Methylcellulose/Mucin Hybrid Gels

An additional gel property, beneficial for any kind of wound treatment, would be to shield the injured tissue from viral and bacterial infections. The MC/mucin hybrid gel combines several anti-microbial properties to achieve this goal: Purified porcine gastric mucins show broad-range anti-viral activity at concentrations of 0.5 – 1 % (w/v) since the glycoproteins can trap different virus particles in the biopolymer matrix.[47, 162] The finely reticulated gel meshwork presented here traps nanoparticles with sizes of 150 nm and thus will also pose a significant barrier towards bacterial penetration as those microbes are considerably larger than those nanoparticles. This is exemplarily shown for *E. coli* (**Figure 30**). Of course, bacteria may be able to actively penetrate the gel layer if they manage to adhere to the gel;

however, the incorporated mucins should be able to prevent this initial adhesion step.[45, 163]

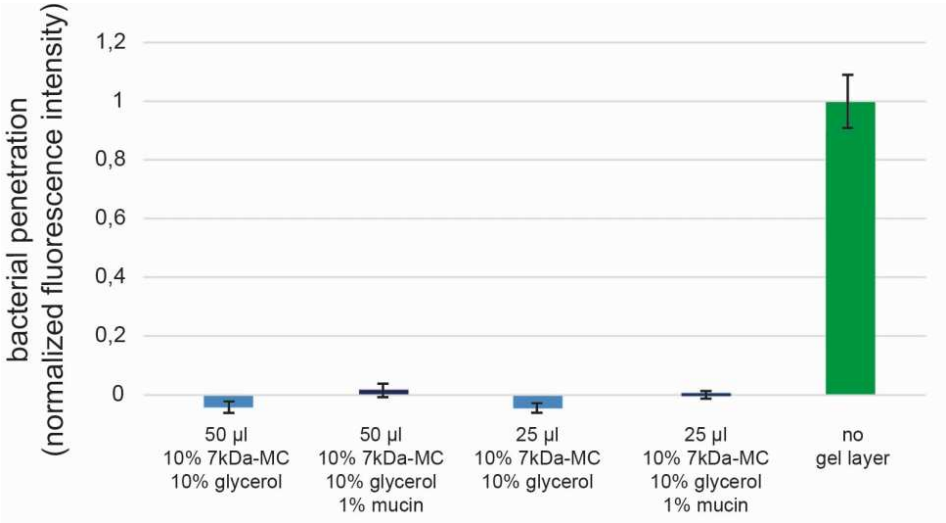

Figure 30 Owing to their small mesh size, both MC/mucin hybrid gels as well as MC gel mixtures without mucin prevent penetration of *E. coli* trough the gels. 50 µL and even 25 µL of wound gel, corresponding to 3.57 mm and 1.79 mm of layer thickness respectively, were sufficient to prevent migration of GFP expressing *E. coli* from the upper to the lower chamber of 96 transwell plates with a pore size of 8 µm. The highest fluorescence intensity measured in the wells where no gel layer was applied (= positive control) is set to one. The bars represent the mean of 3 measurements and the error bars denote the standard deviation.

In addition, the MC/mucin mixture can be enriched with further medically active anti-bacterial components other than mucin glycoproteins. As additional supplements, silver nanoparticles (Ag-NPs) could be interesting candidates as silver ions are known for their anti-bacterial properties and thus are already used as components in wound dressings.[164] To have an inhibitory effect on bacterial growth, the silver nanoparticles should be used in concentrations of at least 20 - 200 µg/mL depending on their size.[165] At those high concentrations, the nanoparticles might interfere with the gelation properties of the biopolymer mixture. Yet, when 200 µg/mL of 100 nm silver nanoparticles were added to the MC/mucin mixture, it was observed that the gelation behavior and the frequency-independent viscoelastic behavior of the biopolymer solution remains basically the same (**Figure 31a, b**). This robustness of the thermoresponsive auto-gelation system might prove to be a striking advantage over other gel-inducing methods.

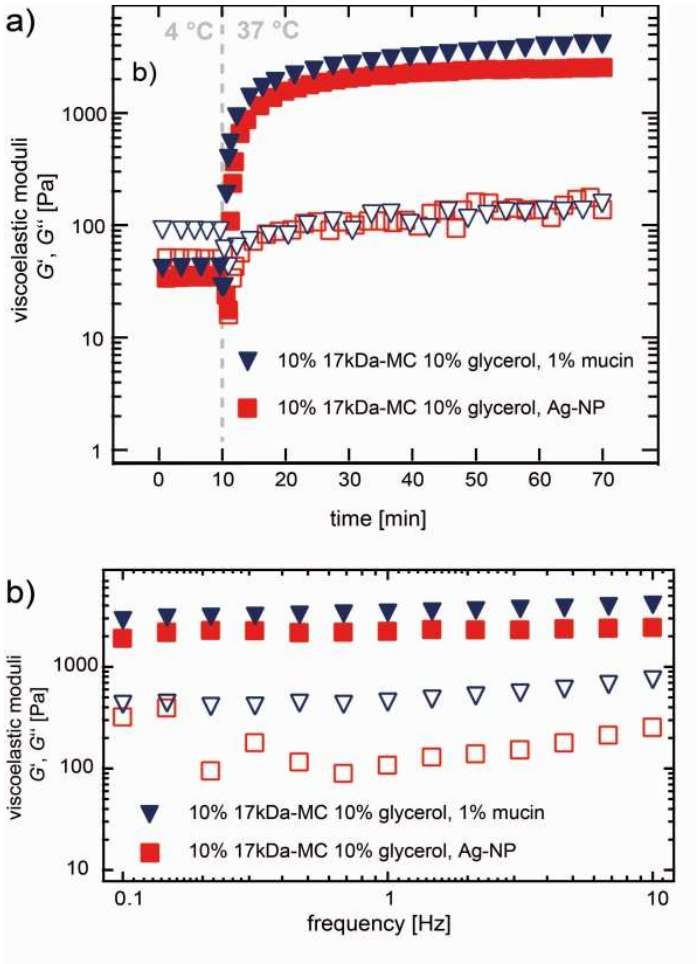

Figure 31 The viscoelastic properties of MC/mucin mixtures are robust towards incorporation of silver nanoparticles (Ag-NPs). (a) The virtually identical gelation behavior of the biopolymer mixture is observed when 200 µg/mL of silver nanoparticles are added to the hybrid gel. (b) The same is true for the frequency-independent behavior of the viscoelastic moduli of the biopolymer mixture. Closed symbols represent the storage modulus *G'* and open symbols denote the loss modulus *G''*. Both moduli of the gelation curve are shown for a probing frequency of 1 Hz. All symbols represent the mean of at least 3 measurements.

3.2.7 Long Term Storage of Methylcellulose/Mucin Hybrid Gels

Another key feature that makes the hybrid gel system very interesting for medical applications is the property that the MC/mucin solution can be frozen, stored at -20 °C and thawed again without losing its autogelation properties (**Figure 32a**) or its frequency-independent viscoelastic behavior (**Figure 32b**). This finding underscores again the robustness of the thermoresponsive auto-gelation system, probably lowering costs due to longer durability.

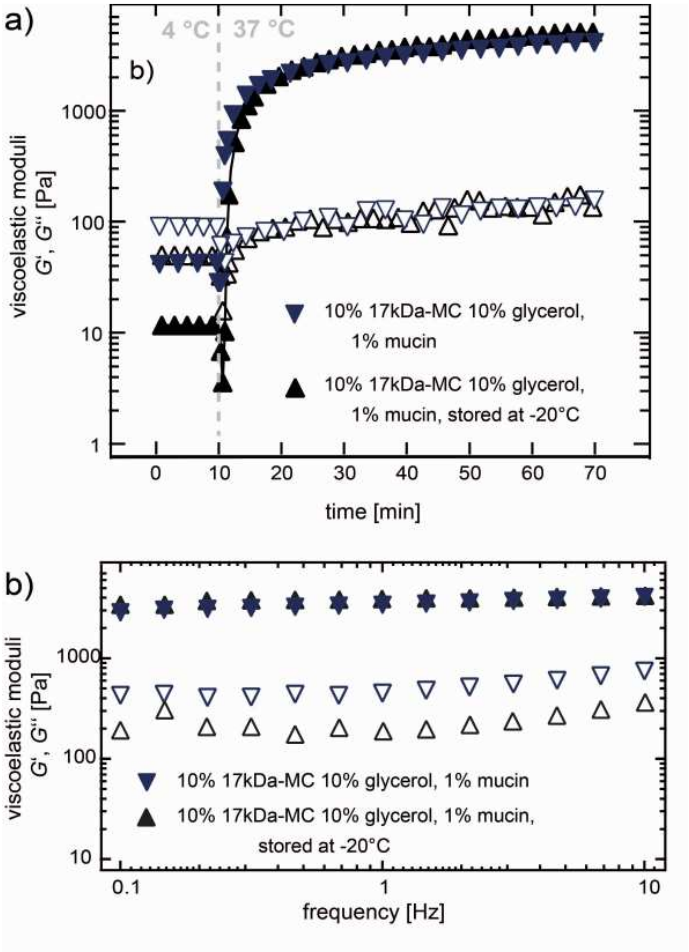

Figure 32 The viscoelastic properties of MC/mucin mixtures are robust towards storage at -20 °C. (a) When the biopolymer mixture is stored in a frozen state at -20 °C for several days, its thermal autogelation properties remain unaffected. (b) The same is true for the frequency-independent behavior of the viscoelastic moduli of the biopolymer mixture. Closed symbols represent the storage modulus *G*' and open symbols denote the loss modulus *G*''. Both moduli of the gelation curve are shown for a probing frequency of 1 Hz. All symbols represent the mean of at least 3 measurements.

3.2.8 Conclusion to Chapter 3.2

By developing and characterizing a MC/mucin hybrid gel, it could be demonstrated that the antimicrobial properties brought about by the glycoprotein mucin can be combined with a mechanical adjuvant such as MC. The generated biopolymer hybrid system possesses thermal autogelation properties at physiological pH and selective permeability properties. The relatively low viscosity of this MC/mucin hybrid solution should allow for wetting the entire area of an uneven wound. The mixture also quickly forms a viscoelastic gel upon contact with warm body surfaces, thereby the hybrid material remains in place even at steep tilt angles. The final shear stiffness resembles that of soft tissue, but nevertheless, allowed the closure of a damaged cell layer covered by the hybrid gel due to its low cell adhesive behavior. All additives used here, i.e.

MC, glycerol, and NaCl, are cheap and Food and Drug Administration (FDA) approved, and the ready-to-use hybrid mixture with all its additives can be frozen at -20 °C for long term storage without losing its autogelation properties. In addition the MC/mucin hybrid system can be enriched with diverse medically active components such as interleukin-8 thus further tuning its properties. The selective properties of the gel can be harnessed to control the diffusive release of certain molecules – in dependence on the size and the charge of the molecules. However, by integrating thermoresponsive liposomes into the gel matrix, it was possible to use an increase in temperature, which triggers the gelation process, to induce at the same time delayed and prolonged drug release from the gel. With this mechanism a better control over drug release is achived. Provided that functional mucin with antimicrobial activity can be made available in sufficient quantities, the MC/mucin hybrid gel developed here may provide a powerful and versatile platform for the efficient treatment of different types of wounds, ranging from cuts and bruises to large open wounds occurring during surgery.

3.3 Orchestrated Nanoparticles for Tailored and/or Prolonged Drug Release

The incorporation of temperature sensitive liposomes into the developed MC/mucin hybrid gel system allows to control drug release kinetics to some extent. However, for many pharmaceutical applications an orchestrated drug release at distinct time points, where different kind of therapeutic agents can be released, is necessary. A promising approach to achieve this goal is the liberation of molecules from NPs, which are embedded into a hydrogel matrix. Here, in a given hydrogel environment, the architecture of the NP determines the release kinetics of the encapsulated drug.[83] A further approach is to tune the chemical composition of the gel matrix to achieve control over the drug release kinetics. However, this would require tailoring the gel matrix for each drug separately. When several drugs are incorporated into one and the same gel matrix it is probably very difficult to find a gel composition which affects the release kinetics of all therapeutic agents as desired. Here, an inert agarose gel matrix was chosen, which does not influence the diffusion of molecules and small NPs. This agarose gel was then used to develop a complex drug release mechanism able to master the challenging task of tailored drug release. This drug release mechanism combines two different kind of NPs, which are incorporated into the agarose gel, where the release kinetics of one NP species directly influences the liberation of the other.

3.3.1 Gold-Nanoparticle Release from Hydrogels

The first step was to achieve a controlled release of NPs from a gel by triggering NP disaggregation (see **Figure 33**). NPs can not only be used to release drugs from their interior or exterior while trapped within a gel, but serve as potential drug carriers if they are mobile, i.e. be released from the gel over time. To accomplish this goal, it is necessary to use NPs, which are small enough so they can leave the gel by diffusion, but to generate relatively large NP-aggregates, which are trapped in the gel matrix according to their increased size.

In this thesis Gold-NPs (Au-NPs) were selected due to their unique physical, chemical, optical and electronic properties.[166] As a strategy for NP-aggregation, cross-linking by complementary DNA sequences was employed: such DNA-mediated NP-aggregates can be disassembled by adding complementary DNA sequences to the gel, which open the NP-cross-links through competitive binding.

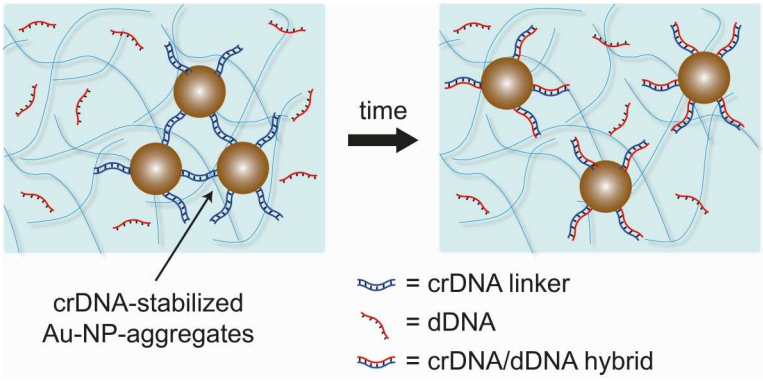

Figure 33 Schematic illustration of the NP release mechanism from a gel. Gold nanoparticle aggregates are embedded into the gel environment and are stabilized by DNA cross-links, each formed by the hybridization of two cross-linking DNA sequences (crDNAs). In presence of displacement DNA (dDNA) the dDNA starts to bind to complementary crDNA sequences and thus dissolves the crDNA-mediated cross-links. As a consequence, individual gold nanoparticles are removed from the aggregate, become mobile, and can leave the gel by diffusion.

For the formation of DNA-mediated Au-NP-aggregates, two sets of DNA sequences (DNA1 and DNA2) were designed, each consisting of a cross-linking DNA sequence (crDNA), the corresponding displacement DNA (dDNA) and a non-complimentary sequence of the same length then the dDNA serving as a control (coDNA). After attaching the crDNA molecules to the surface of 5 nm Au-NPs through a thiol linker present at the 5'-end of the polynucleotide, the crDNA molecules are supposed to form cross-links between Au-NPs by hybridizing with complementary parts of other crDNA molecules attached to the surface of neighboring Au-NPs. To ensure sufficient stability of this hybridized DNA strands at physiological conditions, the sequences were designed such that they possesed a calculated melting temperature T_m > 37 °C (**Table 1**). Indeed, when those crDNA sequences were loaded onto a PAGE gel, a band at higher molecular weight was detected (indicating successful hybridization) – but not for coDNA (**Figure 34**).

To meet the second requirement for the DNA-mediated (de)aggregation process, the dDNA sequences are designed to have a considerably higher affinity to the crDNA than the crDNA molecule to itself – which is indicated by the higher T_m values for the dDNA/crDNA polynucleotide hybrids (see **Table 1**). If this requirement is met, then the dDNA molecules should be able to displace one crDNA molecule from the crDNA/crDNA cross-link established between Au-NPs, thus inducing NP disaggregation. Consistently, also for dDNA, a band at higher molecular weight was found in the PAGE gel, which reflects both the ability of this polynucleotide sequence to hybridize with itself and the successful formation of a dDNA/crDNA complex at physiological conditions. In contrast, the coDNA constructs are designed to have only negligible affinity to the crDNA molecules and thus should be unable to hybridize, neither with

themselves nor with crDNA or dDNA polynucleotide sequences. Indeed, for the coDNA constructs, bands at higher molecular weight could not be detected.

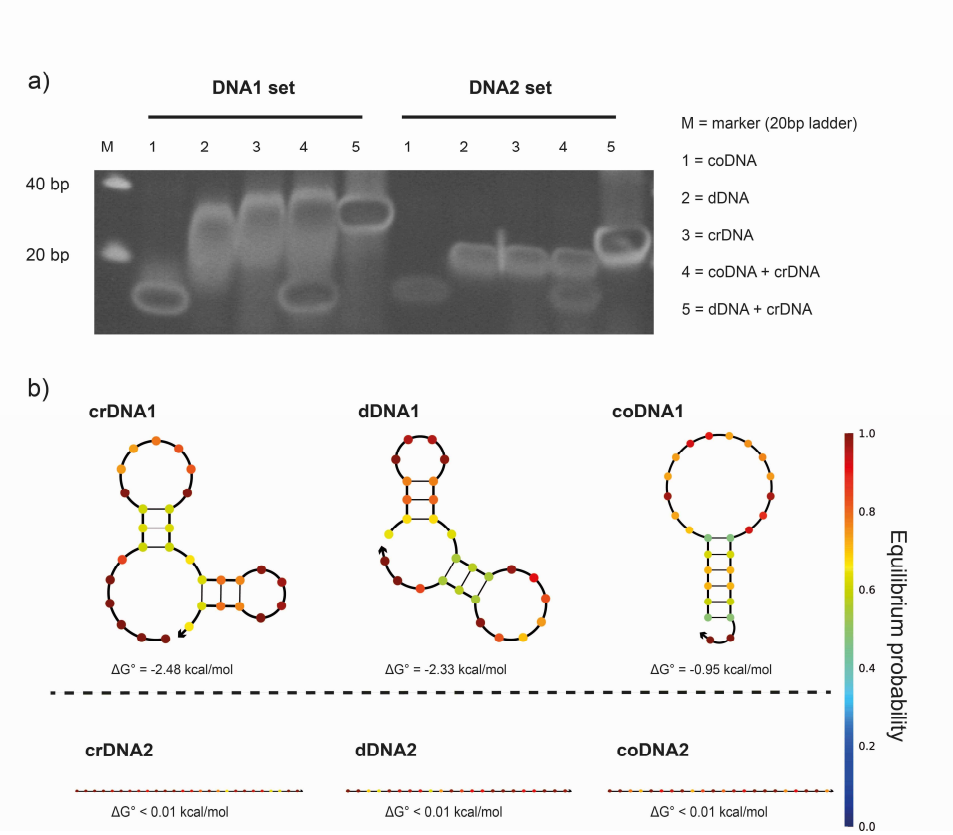

Figure 34 Properties of the designed DNA molecules. (a) Electrophoretic separation of SYBR Green I stained DNA mixtures indicates the hybridization efficiency of the different DNA mixtures. (b) Estimated minimum free energy secondary structures for the designed polynucleotide sequences at 37 °C. Each base is colored according to the probability at which it will assume the depicted paired or unpaired state at equilibrium.

In a next step, it was tested whether the dDNA sequences can indeed dissolve crDNA-cross-linked Au-NP-aggregates when they are incorporated into agarose gels. Successful NP disaggregation could be followed visually as single Au-NPs and aggregates consisting of only a very few Au-NPs released from lager aggregates introduce red color into the gel (**Figure 35**) – similar to individual Au-NPs in solution before aggregation is induced.

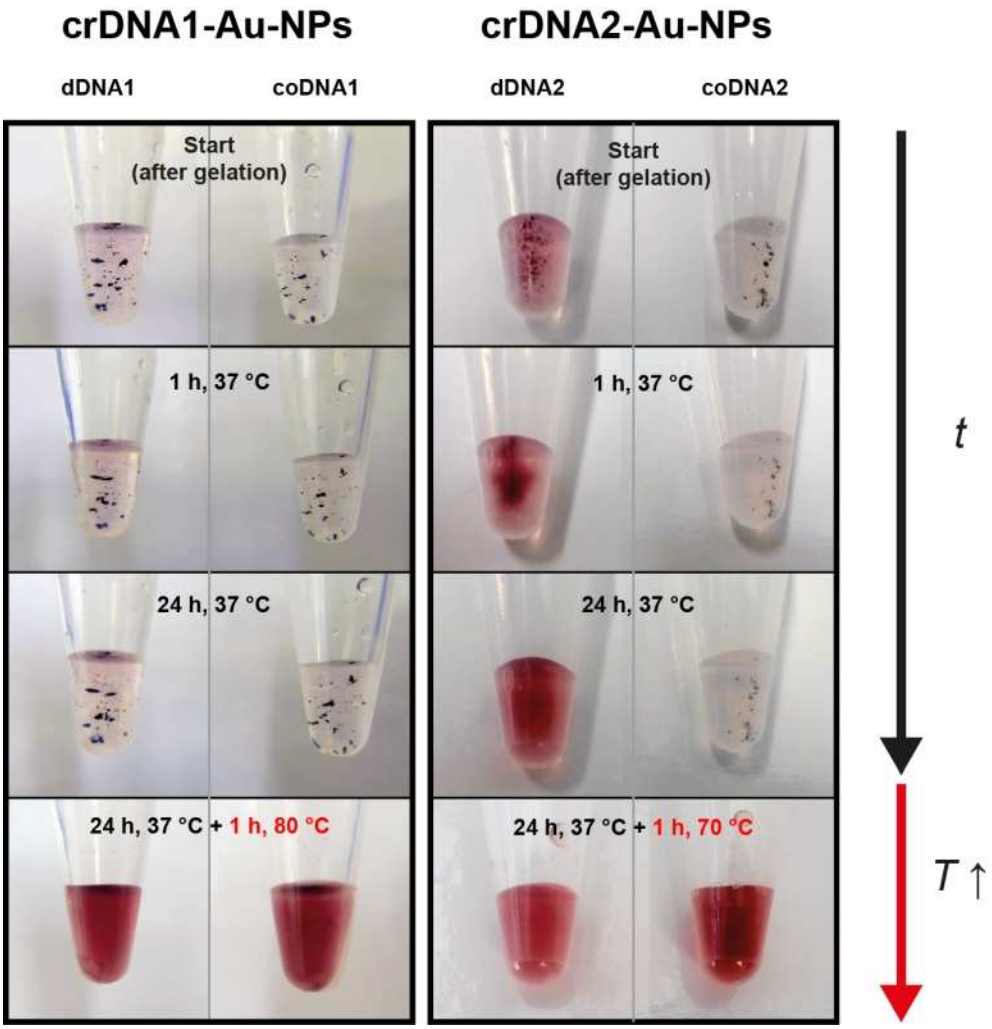

Figure 35 DNA-mediated disaggregation of DNA-crosslinked Au-NP-aggregates. When incorporated into agarose gels, crDNA2-crosslinked Au-NP-aggregates can successfully be dissolved by dDNA2 at 37 °C. Released Au-NPs introduce a red color into the gel, which makes it possible to visually follow the disaggregation process over time. Such a disaggregation process is, however, not observed when control DNA (coDNA) or the crDNA1/dDNA1 constructs are used. In all cases, heating the samples for 1 h to temperatures above the T_m of the corresponding crDNA induced full disaggregation.

Surprisingly, even though both crDNA sequences induce efficient Au-NP-aggregation and both sets of DNA sequences should be able to form dDNA/crDNA complexes as suggested from gel electrophoresis, only crDNA2-cross-linked Au-NP-aggregates could be dissolved in presence of the corresponding displacement DNA (dDNA2). To demonstrate that crDNA1 cross-linked Au-NP aggregates can in principle be disaggregated as well, Au-NP aggregates incorporated into agarose gels were heated up to 80 °C for 1 h. Since this temperature is considerably above the T_m of 50.5 °C of crDNA1, thermal energy should be sufficient to induce disaggregation. As shown in **Figure 35**, this is indeed the case.

One possible explanation for the failure of dDNA1 molecules to induce such disaggregation of crDNA1 cross-linked Au-NP aggregates could be that this polynucleotide sequence might be able to form secondary structures at 37 °C, which are too stable to allow for efficient hybridization with the corresponding crDNA1 sequences within a reasonable period of time. Indeed, a calculation of free energy secondary structures for the different DNA sequences suggests that dDNA1 tends to from looped regions via intramolecular base paring, which first need to unfold before it can hybridize with the crDNA1 sequences (**Figure 34b**). This unfolding process may drastically slow down the kinetics of the crDNA1 displacement and therefore the disaggregation process. This might also be responsible for the observation that the bands from the PAGE analysis involving dDNA1 molecules are broader than those involving dDNA2, since secondary structures prevent polynucleotides from migrating strictly according to their size.[167] In this context, it is important to realize that the Au-NPs are probably stabilized via multiple crDNA/crDNA cross-links between each pair of neighboring NPs. Thus, efficient dDNA/crDNA hybridization is required for triggering NP-aggregate disassembly. In contrast, such a secondary structure formation is very unlikely for the dDNA2 construct, which agrees with the high efficiency of this displacement DNA. Thus, for the remainder of this thesis, the second set of polynucleotides is used (crDNA2, dDNA2, coDNA2).

3.3.2 Triggered Gold-Nanoparticle Release from Hydrogels

Having identified a suitable set of polynucleotide constructs for the aggregation and disaggregation of Au-NPs, the next aim was to trigger this NP-disaggregation process by inducing a controlled release of dDNA molecules into the gel. As a depot for those dDNA molecules, liposome particles were chosen as they can easily be embedded into hydrogels [108] and can be loaded with a broad range of (macro)molecules including proteins, peptides, DNA, RNA, as well as hydrophilic and hydrophobic drugs [168, 169]. When searching for a simple external trigger to induce the release of incorporated molecules from liposomes, the previously presented system of temperature sensitive liposomes cannot be applied here: Temperature sensitive liposomes release preferably small molecules, since their lipid membrane becomes merely leaky if the ambient temperature matches their phase transition temperature but remains otherwise intact. The dDNA sequences used here are rather large, this prevents the usage of this simple temperature trigger. However, when a NP-loaded gel is brought in contact with the human body, not only the temperature may change, but also other external parameters such as the pH – provided that the gel is produced and stored at non-physiological conditions. Unfortunately, employing differences in pH as a trigger for inducing molecule release from liposomes is difficult: in the context of a wound a significant deviation of gel pH from physiological levels would lead to discomfort or

even tissue damage. In turn, designing a release mechanism based on minor changes in pH would be rather challenging. Instead, it is important to recall that molecules embedded into the gel will be able to leave the gel by diffusion when the gel is applied to a different and considerable lager, water-based environment. If the gel is loaded with a control molecule, the depletion of such a control molecule from the gel can be used to trigger liposome disassembly, e.g. by inducing an osmotic pressure. Thus, applying the gel onto a body surface serving as sink for such control molecules should induce the desired dDNA release, which in turn triggers NP release from the gel through disaggregation (see **Figure 36**).

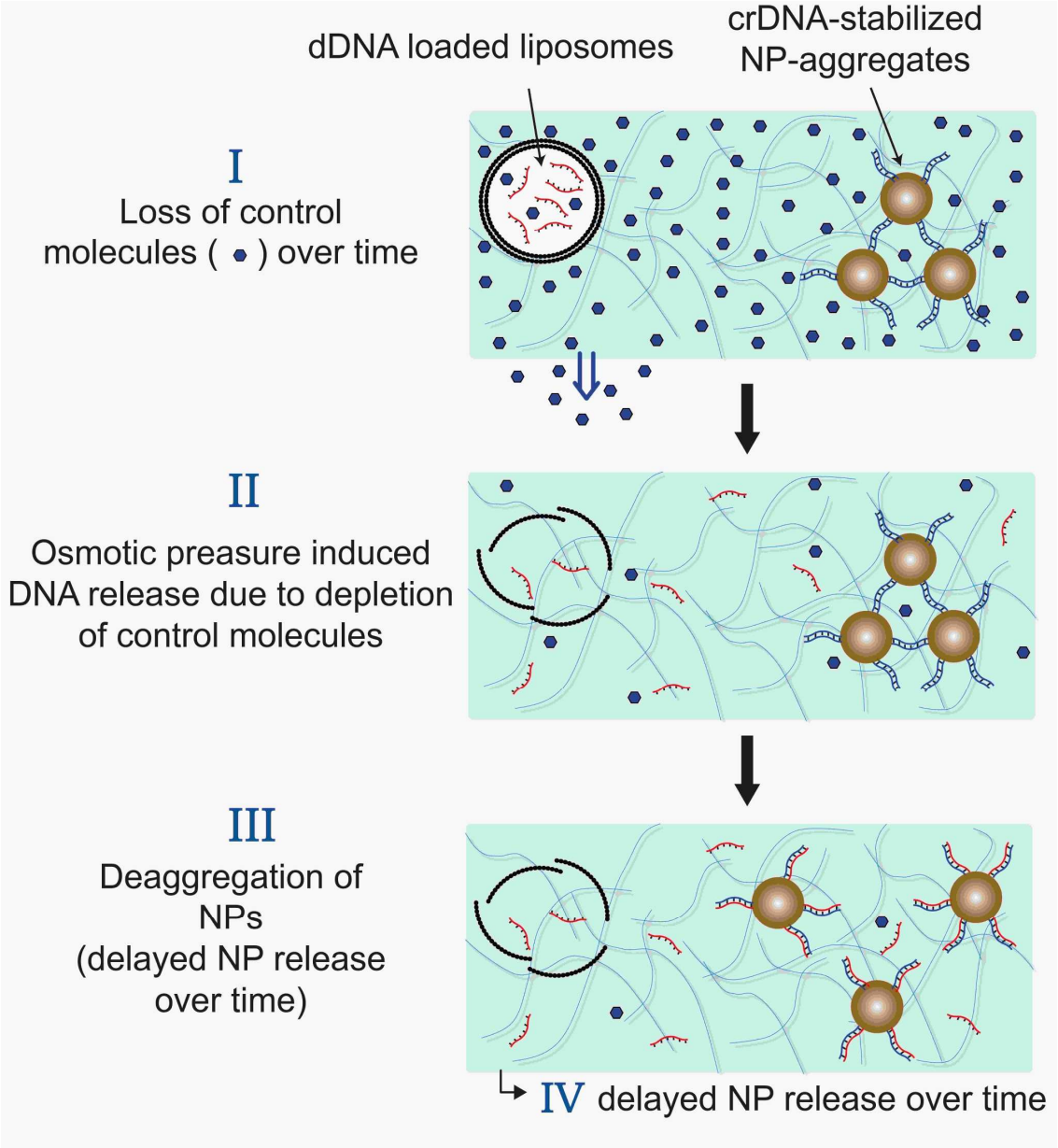

Figure 36 Schematic illustration of the triggered NP release mechanism from a gel. Two different types of NPs are embedded into the gel environment: DNA-loaded liposomes and gold nanoparticle aggregates, the latter of which are stabilized by DNA cross-links (crDNA). A depletion of control molecules from the gel entails a build-up of osmotic pressure which triggers the bursting of liposomes and thus a release of displacement DNA (dDNA) into the gel. These dDNA molecules can then diffuse through the gel, bind complementarily to the crDNA sequences and thus dissolve the crDNA-mediated cross-links. As a consequence, individual gold nanoparticles are removed from the aggregate, become mobile, and can leave the gel by diffusion.

Based on this idea, the gel was enriched with the small monosaccharide sorbitol. This molecule is harmless when applied to body surfaces but is not found in human tissue. As a consequence, when a sorbitol-enriched gel is applied to human tissue, the sorbitol molecules can leave the gel

over time by simple diffusion, as long as no interaction between the sorbitol and the gel matrix occurs. Here, due to the inert nature of the utilized agar gel, such simple diffusive flux can be assumed. However, to achieve osmotic balance as long as the agar gel is not exposed to another water-based environment, the dDNA loaded liposomes were also enriched with an identical concentration of sorbitol, which is unable to leave the interior of liposomes as long as they possess an intact lipid membrane. Thus, by depletion of the sorbitol molecules from the gel, an osmotic pressure will build up. Once a critical pressure is reached, the liposomes should burst and their incorporated cargo should be released into the agar gel. This release is independent of the size of the cargo and thus should also be suitable for the release of dDNA to trigger NP-disaggregation. As a proof of concept, DOPG liposomes were loaded with sorbitol and 1.5 mM of the fluorescent dye calcein and embedded into the gel. As shown in **Figure 37a,** after 72 h a ~3-fold higher calcein release from the agar gel is detected when an osmotic pressure is present compared to when osmatic balance is maintained, i.e. when the gel is layered with sorbitol-enriched PBS. This demonstrates that the build-up of an osmotic pressure by the depletion of a control molecule from the gel can indeed be a suitable trigger for the aim pursued here.

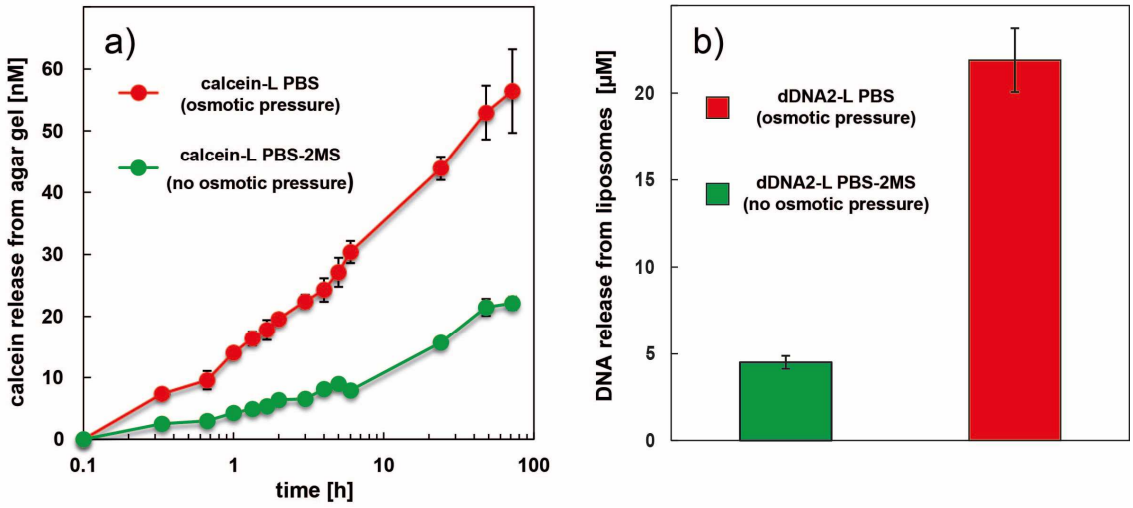

Figure 37 Release of molecules from liposomes can be triggered by a build-up of osmotic pressure**.** (a) Calcein-loaded DOPG liposomes embedded into an agar gel release more cargo in the presence of osmotic pressure than under osmotic balance. The experiment was conducted at 37 °C. (b) At 37 °C, osmotic pressure can also efficiently induce the release of larger molecules such as DNA from liposomes. The amount of released DNA was determined 30 min after the depletion of the control molecule sorbitol was initiated. In both subfigures, the error bars denote the standard deviation as obtained from at least three independent experiments.

To verify that such a build-up of an osmotic pressure is indeed sufficient to release dDNA from liposomes, dDNA2-loaded liposomes were diluted 1:10 with PBS, and dDNA release was

quantified in this liquid environment at 37 °C. The experiment showed that, even at osmotic balance a small amount of released dDNA is detected as well. A possible explanation could be, that liposomes are known to release their cargo if the lipid membrane spreads on a suitable surface; such a behavior is e.g. observed for DOTAP liposomes on silica [170] and could thus account for the low amount of dDNA release in the absence of osmotic pressure. In contrast, when osmotic pressure is present, a 4-5 times higher dDNA2 release can be observed (**Figure 37**b). The amount of liberated dDNA was >20 µM which should be sufficient to trigger NP disaggregation. Indeed, when an agar gel is enriched with both crDNA-cross-linked Au-NP aggregates and dDNA-loaded liposomes, the amount of released Au-NPs over a time period of several days is considerably higher in the presence of osmotic pressure (**Figure 38a**). In the control sample, i.e. at osmotic balance lacking the build-up of an osmotic release trigger, there is virtually no NP release detectable for the first 10 h. The occurring NP-release at later time points reflects the intrinsic life time of liposomes which are subjected to chemical and physical degradation,[171] and possibly the previously mentioned cargo release if the lipid membrane spreads on a suitable surface (such as the cuvette surface in which the experiment was conducted).

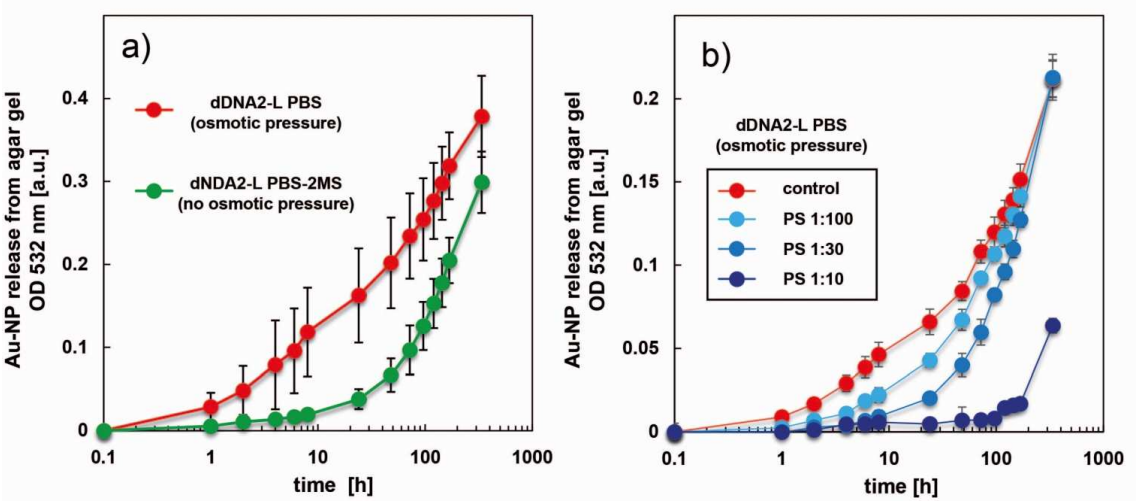

Figure 38 Release of molecules and NPs from gels can be triggered by a build-up of osmotic pressure**.** (a) Osmotic pressure induced release of dDNA from liposomes triggered by a build-up of osmotic pressure leads to liberation of individual Au-NPs (or small Au-NP complexes) from the agar gel over time. (b) By supplementing the gel with positively charged polystyrene beads (PS) acting as charge traps, the triggered liberation of Au-NPs can be retarded. In both subfigures, the error bars denote the standard deviation as obtained from at least three independent experiments.

In a further step, it was tested whether the onset of triggered NP-release can be delayed by implementing an additional control mechanism into the gel. As the dDNA molecules released from the liposomes need to reach the cross-linked NP-aggregates by diffusion, retarding the

diffusion of the DNA constructs through the gel could provide such a control mechanism. DNA molecules are highly negatively charged. Thus, distributing local 'charge traps' throughout the otherwise inert agarose gel matrix should give rise to a 'sticky diffusion' process of the DNA molecules as already observed for NPs in complex biological gels.[105] Experimentally, such local charge traps can be generated in the agar gel by adding positively charged polystyrene microparticles to the gel matrix. For this purpose, the size of those particles has to be large enough to ensure that they will be trapped in the gel. Then, the particles should engage in transient binding interactions with the diffusing DNA molecules thus retarding their diffusive spreading throughout the gel. Indeed such a behavior is observed: the onset of Au-NP particle release is delayed by compared to the gel formulation without polystyrene particles, and the strength of this effect depends on the concentration of particles added (**Figure 38b**). Though, if the binding strength between the polystyrene particles and the DNA molecules were too strong, the charge traps could permanently reduce the total amount of free DNA molecules. However, it can be observed that, at later time points, the amount of liberated NPs approaches the quantity released from the sample lacking charge traps. And after 2 weeks all samples reached the same release level of Au-NPs from the gel and remained on this final level for later time points, except for the highest concentration of polystyrene particles. Adding polystyrene beads in a ratio of 1:10 into the gel retards the amount of released Au-NPs so drastically that only a quarter of the ultimate amount of Au-NP release is reached after 2 weeks. However, from **Figure 38b** it is not clear, if the amount of liberated Au-NPs in presence of the highest concentration of charge traps will finally approach the level of the control at some point. However, a discrepancy is not expected, since all samples were prepared with the same amount of dDNA2 loaded liposomes and Au-NP-aggregates. Thus it can be assumed that, indeed, the dDNA molecules released from the liposomes are only retarded by the installed charge traps, and the amount of permanently trapped dDNA molecules is negligible.[7]

3.3.3 Conclusion to Chapter 3.3

Here, a mechanism was introduced, which combines a triggered build-up of osmotic pressure causing the rupture of liposomes and the subsequent liberation of synthetic DNA constructs to evoke NP disaggregation and thus release of individualized NPs from a hydrogel. Au-NPs were chosen as one possible NP species that can be released from a gel through diffusion following a disaggregation process. One reason for this choice is that those Au-NPs have been extensively studied in a biological and therapeutic context, and there are already several approaches, which

[7] I want to thank Benjamin Käsdorf for pursuing the Au-NP release experiments and contributing data discussed in this part of the presented thesis.

make use of Au-NPs for the selective delivery of therapeutic agents.[172-175] Of course, the potential drug liberation system introduced here could also be transferred to other suitable drug carrier molecules/NPs – provided that they can be functionalized with DNA sequences. The combination of liposomes and cross-linked NPs already offers the possibility to release two types of molecules/particles at different time points. By depositing charge traps in the gel, it was possible to extend the time interval between DNA release into the gel and NP release from the gel. Furthermore, this time interval can also be modulated by tuning the amount of charge traps installed into the gel.

A hydrogel system with a controlled and orchestrated drug release mechanism as demonstrated here would greatly benefit wound healing approaches since it allows for the release of different therapeutic agents at distinct time points but only requires a single treatment with such a gel. Thus, the otherwise typically performed sequential drug administration and the risks involved (unnecessary irritation of the wound caused by wound gel replacement and the increased infection risk during the procedure) could be avoided. Moreover, for internal wounds after surgery, where sequential administration is no viable alternative, the developed wound gel system offers a solution for orchestrated drug release.

In addition to the orchestrated release of different drugs, the developed system could also be used to achieve prolonged drug release if liposomes and the NPs are loaded with one and the same therapeutic agent. This approach would thereby prevent a burst drug release, which is a common problem in pharmacokinetics.[176]

4 Outlook

In this thesis it was demonstrated that the antibacterial glycoprotein mucin can be combined with the mechanical adjuvant MC to genrate a biopolymer hybrid system, which possesses thermal autogelation properties at physiological pH and selective permeability properties. In addition to these selective permeability qualities, it could be shown that NPs such as thermoresponsive liposomes can be incorporated into this hydrogel to achieve controlled drug release from such a gel. Furthermore, DNA molecules released from liposomes into the gel after a triggered build-up of osmotic pressure were successfully used in combination with DNA cross-linked Au-NP aggregates to evoke NP disaggregation. This mechanism offers the possibility of orchestrated drug release, where the therapeutic agents can be released form the gel at distinct and well separated time points.

In chapter 3.2 it was demonstrated that the developed thermoresponsive MC/mucin hybrid gel provides a powerful and versatile platform for the treatment of a variety of wounds - whether they are internal or external - and remains in place even at steep tilt angles. However, if certain applications require specific mechanical properties of the biopolymer mixture that differ from the so far realized viscosity, gelation kinetic or final shear stiffness, this should be adjustable. As discussed in chapter 3.2.1 the gelation kinetics can be tuned by choosing a MC variant of appropriate molecular weight: the lower the molecular weight, the faster the gelation. The final shear stiffness, in turn, can be adjusted by the MC concentration: higher concentrations result in an increase of the shear stiffness. However, it should be considered that both parameters, the viscosity and the shear stiffness, are a result of the molecular weight of the employed MC and its concentration, and both material properties have to be coordinated to match the detailed requirements. The viscosity of such a biopolymer mixture can also be increased, if necessary, by the addition of PEG,[177] which should due to its inert nature have no strong effect on the other gel properties. A situation different from wound treatment where strengthening the local human immune defense with the hybrid gel would be highly desirable, can be found in patients at high-risk of preterm labor.[178] Here, the mucus plug sealing the entrance of the uterus can be compromised. This decreased barrier function of the mucus plug might facilitate intrauterine infections which in turn are thought to trigger preterm labor. Reinforcing the mucus plug of pregnant women with the MC/mucin solution should therefore lower the risk for preterm labor. For this application, the hybrid system offers the following features: Due to the viscous behavior of the biopolymer mixture at low temperatures, an elongated syringe could be used to deposit a drop of MC/mucin gel on

top of the compromised mucus plug, where it forms a stiff protective layer triggered by the temperature shift. Whereas boosting the protective function of compromised native mucus with a purified mucus component, the mucin glycoprotein, might appear to be an obvious choice, this is only possible by additionally harnessing the mechanical properties brought about by the adjuvant MC. Furthermore, MC cannot only provide the required gelation properties but is also not easily degraded by the human body, which should increase the lifetime of the applied MC/mucin protection layer thus reducing the necessity to repeat the treatment. The incorporated mucin, in turn, should reduce bacterial adhesion to the gel and prevent bacterial penetration into the uterus, hence decreasing the risk of intrauterine infections and preterm labor (see **Figure 39**). A next step towards a clinical application would be performing *in vivo* assays, preferably in mouse models, to investigate the clinical benefit of this method. Of course, also in this context, liberation of therapeutic agents, such as antibiotics, taking effect *in situ* over a prolonged time period may be of benefit for the patients.

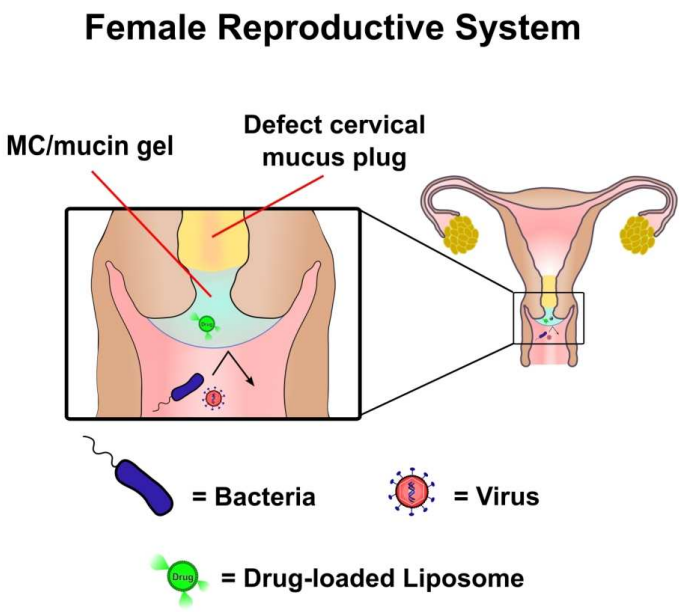

Figure 39 Schematic visualization of a compromised cervical mucus plug reinforced by the MC/mucin hybrid gel. Here, the MC/mucin hybrid gel could act as a protective layer against bacteria and viruses and could be enriched with drug-loaded nanoparticles.

To achieve this goal of prolonged and even orchestrated drug release, the strategy presented in chapter 3.3, i.e. employing osmotic pressure sensitive liposomes loaded with DNA to initiate disaggregation of gold nanoparticle clusters trapped within a gel, could be employed. However,

this strategy may also allow for installing even more complex control mechanisms into hydrogels thus enabling the orchestrated release of different molecules/particles from the gel at well-defined and separated time points. One possibility for such further adjustment of the release process could make use of the tunability of liposomes: The lipid composition of liposomes affects their sensitivity towards osmotic pressure changes.[179] Furthermore, the sequences of the cross-linking and displacement DNA molecules can be varied. This offers additional opportunities to control the dynamics of the process, e.g. by tuning the binding affinity between the crDNA sequences or between the crDNA and the corresponding dDNA sequences, or by adding competitive constructs. Introducing another step into the release cascade, e.g. triggered by a displaced crDNA which is not bound directly to NPs, but cross-links two DNA sequences bound to the surface of neighboring particles, may even offer the possibility to release more than two types of molecules/NPs at different time points. Here, the displaced crDNA could be used to trigger disaggregation of another set of DNA cross-linked NPs incorporated into the gel, now serving as dDNA itself (see **Figure 40**).

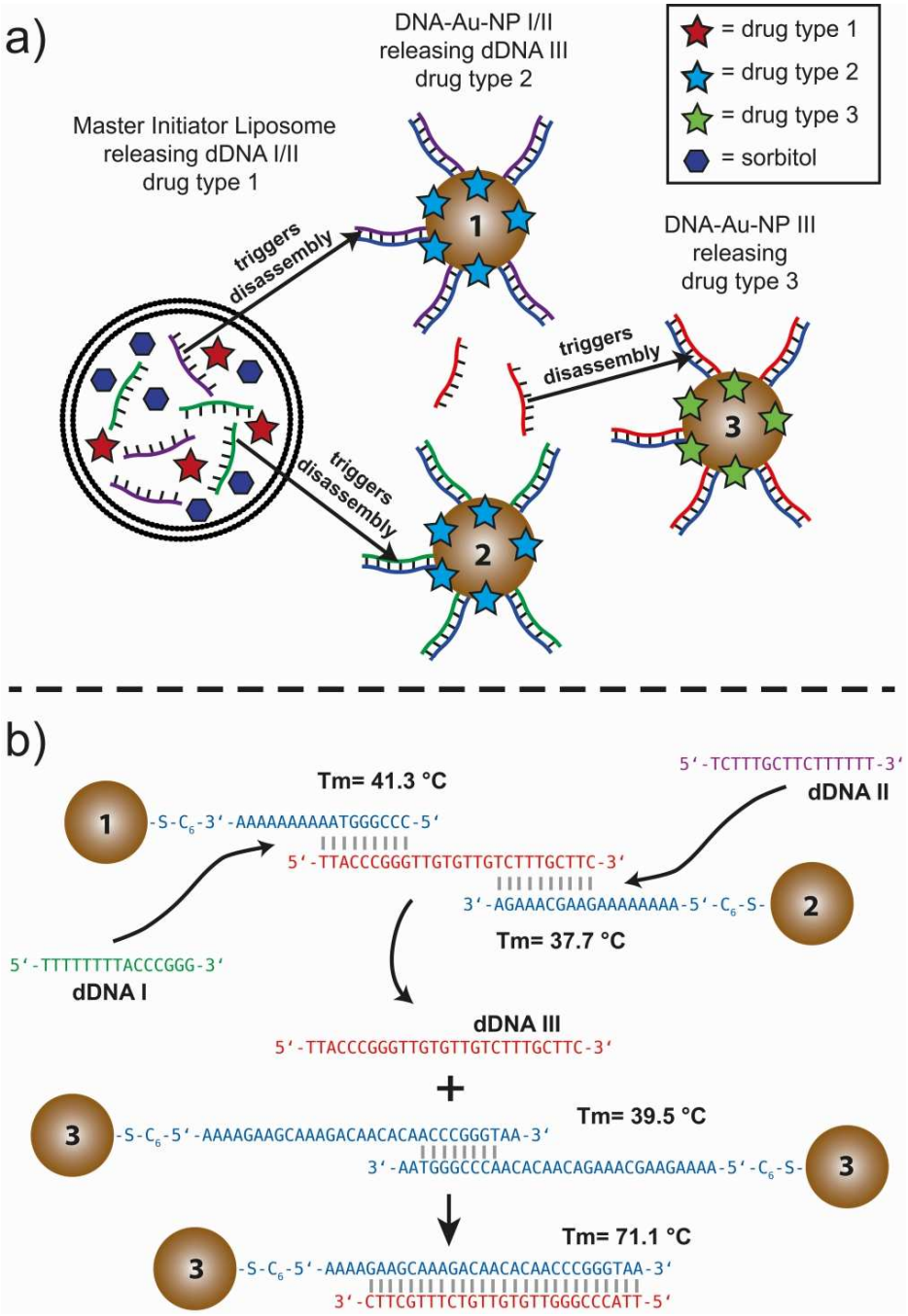

Figure 40 Schematic illustration and molecular design of NPs cross-linked by DNA, to achieve orchestrated particle release initiated by osmotic pressure induced release of only one set of displacement DNA (dDNA) sequences from liposomes. (a) Depletion of sorbitol from the gel induces an increase in osmotic pressure, thus the dDNA molecules are released from the liposomes. This set of dDNA sequences (green and purple) now trigger by competitive binding the liberation of another DNA sequence (red), which previously cross-linked the first two NP species, thus initiating their disaggregation. The released cross-linking DND (crDNA), in turn, can now serve itself as dDNA for a third species of DNA cross-linked NPs, following the mechanism illustrated previously in **Figure 33**. Thus, their disaggregation starts delayed to the first NP species, and therefore the first and the last particle species can be released from a gel at distinct and separated time points. (b) depicts a possible molecular design and the envisioned interplay of the DNA sequences required for the mechanism shown in (a). For simplicity, the NPs depicted here are only cross-linked by a single DNA linker; in reality, each NP is likely form multiple cross-links with other NPs.

Another release mechanism making use of DNA molecules and NPs to achieve control over drug release kinetics, can be realized by the combination of mesoporous silica nanoparticles (MSNs) functionalized with smart DNA molecule-gated switches.[180] Here, the DNA sequences grafted onto the MSN surface are only able to hybridize and block the pores of the MSNs in presence of Ag^+ ions, e.g. by bridging cytosine (C) mismatches through the formation of $C - Ag^+ - C$ structures. Therapeutic agents trapped within the MSN can then be liberated over time by depletion or competitive displacement of Ag^+ ions, e.g. triggered by the addition of thiol-containing molecules such as dithiothreitol (DTT). In addition to therapeutic agents, these DNA gated MSNs could be loaded with dDNA, initiating the previously described disaggregation of DNA cross-linked Au-NPs (see **Figure 41**).

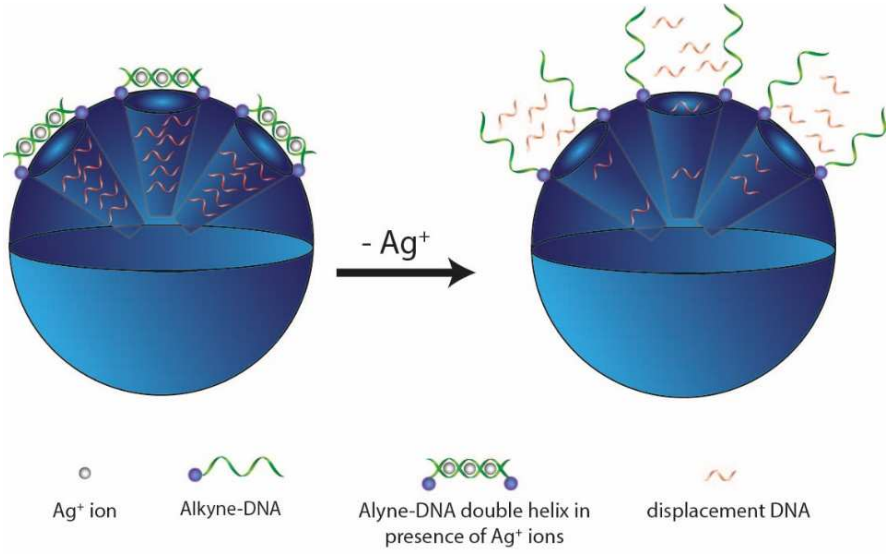

Figure 41 Schematic illustration of the release mechanism of displacement DNA from DNA-gated mesoporous silica nanoparticles after depletion of silver ions (Ag^+).[8]

These two additional release mechanisms of displaced and released crDNA serving as dDNA itself, and the DNA gated MSNs regulated by Ag^+ ions, in combination with the previously discussed system of osmotic pressure sensitive liposomes and DNA cross-linked Au-NPs, offers now theoretically the possibility to design a five-step release process from a gel. For this purpose, the wound gel has to be enriched with sorbitol and Ag^+ ions and loaded with liposomes, several DNA cross-linked Au-NP species and with DNA-gated MSNs. The crucial point here is that the liposomes have to be loaded with Ag^+ ions in addition to the first set of dDNA sequences

[8] Figure adapted from: He, D., et al., Reversible stimuli-responsive controlled release using mesoporous silica nanoparticles functionalized with a smart DNA molecule-gated switch. Journal of Materials Chemistry, 2012. **22**(29): p. 14715-14721.

(initiating, once released by osmotic pressure, the mechanism shown in **Figure 40**). This is necessary, to compensate for the depletion of Ag^+ from the Ag^+ enriched gel after application, at least until the liposomes are depleted themselves. Thus, in theory five different molecules/particles could be liberated from the gel at distinct time points: the first drug is released from the liposomes, the second and third in form of disaggregated Au-NPs, the fourth from DNA-gated MSNs, and the last drug again in the form of disaggregated Au-NPs since the MSNs can be loaded with both, a therapeutic agent and a crDNA sequence (see **Figure 42**). However, the detailed order in which the drugs are released here, will depend on the dissociation constant of Ag^+ ions bound to C:C mismatched base pairs: the MSNs have to release their content after the final Au-NP disaggregation process took place. However, whereas the dissociation constant cannot be manipulated easily, the number of C:C mismatched base pairs of the DNA locking the MSN pores can be tuned. Each C:C mismatched base pair should contribute cumulatively to the average time necessary to separate two annealed DNA strands. Thus, the release time of cargo from the MSNs should scale with the number of C:C mismatches, since Ag+ ions and C:C mismatched base pairs possess stoichiometric binding without interference and negative cooperativity.[181]

In addition, fine-tuning of the different drug release kinetics could be realized by altering the biopolymer hydrogel matrix itself into which the NPs are incorporated. Here, the same mechanism of electrostatic interaction, utilized in chapter 3.2.4 to retard the diffusion of positively charged DEAE-dextrans and in chapter 3.3.2 to retard the diffusion of DNA constructs through the gel by the distribution of oppositely charged traps throughout the gel, could be employed: the polymers that constitute the hydrogel could be modified by attaching positively or negatively charged molecules covalently to the polymer backbone, as required. With this approach, one could distribute charge traps of either charge very homogeneously throughout the matrix while maintaining the overall hydrophobic character of the polymers that allows for triggering gelation by an increase in temperature. Charge traps of negative charge could be used to retard the depletion of Ag^+ ions form the gel and thus the opening of the pores of the DNA-gated MSNs. Polymers possessing positively charged motifs, in turn, should retard the diffusive spreading of negatively charged DNA constructs, which are used to initiate Au-NP disaggregation. However, such positive charge traps will retard the diffusion of all DNA molecules. For a more specific diffusive retardation of certain DNA constructs, DNA molecules which match (to some extent) the DNA sequence of the target DNA construct (i.e. that construct whose distribution should be retarded by transient binding) could be attached to the polymer backbone constituting the gel matrix instead of positively charged molecules. Possibly, polymers modified with different DNA molecules could be used within one and the same gel to specifically retard the diffusion of several

DNA constructs thus tuning the kinetics of multiple Au-NP disaggregation processes at the same time.

The benefit for medical applications realizing such a tunable drug release system would be enormous. However, the complexity of the presented setup will probably give rise to new challenges, which have to be addressed in the future.

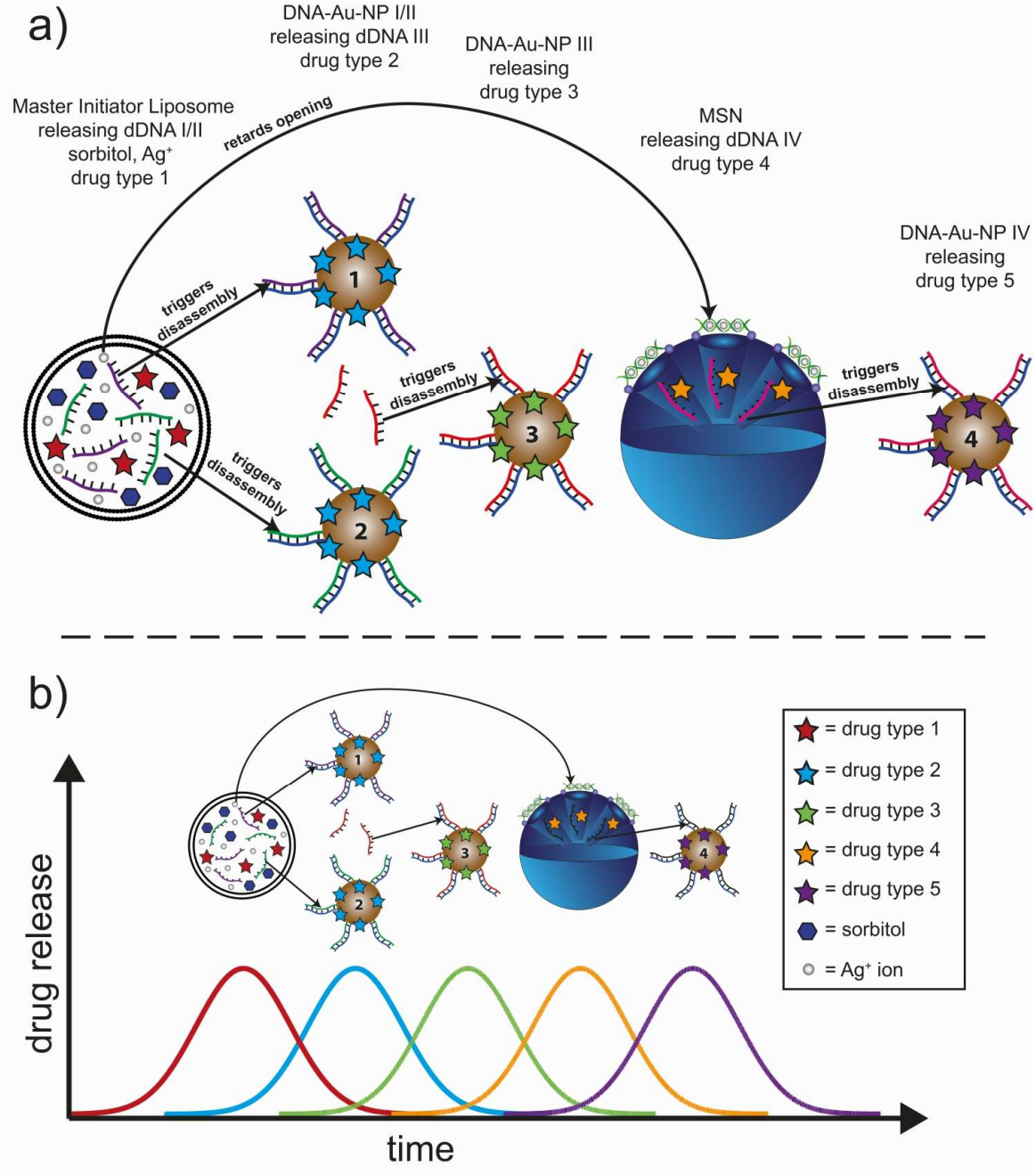

Figure 42 Schematic illustration of the interplay of nanoparticles within a hydrogel for orchestrated drug release. (a) Molecular mechanism of the interplay between liposomes, DNA cross-linked Au-NPs and DNA gated MSNs. Here, each NP is loaded with a different type of therapeutic agent. (b) shows the theoretically possible drug release kinetics of the five drug molecules, at well-defined and separate time points, which can be achieved with the setup shown in (a).

5 Appendix

Table A1 Results from mass spectroscopy analysis of the additional band of ECM1. Database: NCBInr 20140323, Taxonomy: Mus musculus, Type of search: Peptide mass fingerprint, Enzyme: Trypsin

	Mass	**Score**	**Expected**	**Matches**
gi|52858	37712	63	0.087	8
Hartl,L., Oberbaumer,I. and Deutzmann,R., *The N terminus of laminin A chain is homologous to the B chains*, Eur. J. Biochem. 173 (3), 629-635 (1988)				
gi|74224878	37746	46	4.1	8
gi|400977322	58595	31	1.5e+02	8
gi|111305466	63060	27	3.7e+02	7
gi|119226206	11651	45	5.2	5
gi|6531381	10720	32	1.2e+02	4
gi|74152705	12396	43	9.1	4
gi|74224092	15468	36	39	4
gi|148666045	54791	34	63	6
gi|15126700	33604	33	87	6
gi|19353516	48696	26	4.7e+02	6
gi|26346418	48757	26	4.7e+02	6
gi|269308251	48742	26	4.7e+02	6
gi|148694651	3714	33	95	2
gi|9837303	12897	32	1.2e+02	3
gi|347943574	6034	31	1.3e+02	3
gi|12853295	22326	30	1.7e+02	4
gi|18845005	17541	30	1.9e+02	4
gi|159162515	14644	30	1.9e+02	3
gi|148685215	33776	29	2e+02	4
gi|83627687	11276	29	2.2e+02	3
gi|289526642	4440	29	2.3e+02	2
gi|568912134	54738	29	2.3e+02	5
gi|568912132	55153	28	2.4e+02	5
gi|568912128	55368	28	2.5e+02	5
gi|568912108	60167	27	3.5e+02	5
gi|568912106	60582	27	3.7e+02	5
gi|568912104	60796	27	3.8e+02	5
gi|568912102	61195	26	3.9e+02	5
gi|568935374	102356	28	2.4e+02	6
gi|26343501	108941	27	3.1e+02	6
gi|164519057	108914	27	3.1e+02	6
gi|2558835	108928	27	3.1e+02	6
gi|50511047	64568	28	2.5e+02	6
gi|18044474	55932	28	3e+02	5
gi|67010061	56108	27	3.2e+02	5
gi341940401	55727	27	3.6e+02	5

6 List of Abbreviations

Ag-NP	silver nanoparticle
AM	acetoxymethyl
Au-NP	gold nanoparticle
BSA	bovine serum albumin
CM	carboxymethyl
CO_2	carbon dioxide
coDNA	control DNA
crDNA	cross-linker DNA
D	diffusion constant
dDNA	displacement DNA
DEAE	diethylaminoethyl
DMEM	Dulbecco's Modified Eagle's Medium
DMSO	dimethylsulfoxide
dNTP	deoxynucleoside triphosphate
DOPC	1,2-dioleoyl-sn-glycero-3-phosphocholine
DOPE-Rhod	1,2-dioleoyl-sn-glycero-3-phosphoethanolamine-N-(lissamine rhodamine B sulfonyl)
DOPG	1,2-dioleoyl-sn-glycero-3-phospho-(1'rac-glycerol)
DOTAP	1,2-dioleoyl-3-trimethylammonium-propane
Dox	doxorubicin
DPPC	1,2-dipalmitoy-sn-glycero-3-phosphocholine
DTT	dithiothreitol
ECM	extracellular matrices
ED	euclidean distance
EDTA	ethylenediaminetetraacetic acid
Egg-PC	L-α-phosphatidylcholine from egg yolk
FBS	fetal bovine serum
FDA	Food and Drug Administration
FITC	fluorescein isothiocyanate
fMLP	N-formyl-methionine-leucine-phenylalanine
GFP	green fluorescent protein
gfr	growth factor reduced
HEPES	4-(2-hydroxyethyl)-1-piperazineethanesulfonic acid
IL-8	interleukin-8

IMDM	Iscove’s Modified Dulbecco’s Medium
MALDI	matrix-assisted laser desorption/ionization
MC	methylcellulose
MFE	minimum free energy
MSD	mean-square displacement
MSN	mesoporous silica nanoparticles
NaCl	sodium chloride
NaN3	sodium azide
NaOH	sodium hydroxide
NP	nanoparticle
PAGE	polyacrylamide gel electrophoresis
PBS	phosphate-buffer saline
PBS-2MS	PBS containing 2 M sorbitol
PDGF	platelet-derived growth factor
PDI	polydispersity index
PDMS	polydimethylsiloxane
PEG	polyethylene glycol
PFG-NMR	pulsed-field-gradient nuclear magnetic resonance
PMSF	phenylmethane sulfonyl fluoride
PS	polystyrene beads
RT	room temperature
SDS	sodium dodecyl sulfate
SEC	size exclusion chromatography
SEM	scanning electron microscopy
TAMRA	carboxytetramethylrhodamine
TBE	tris-Borat-EDTA
TCEP	tris-(2-carboxyethyl)-phosphin hydrochlorid
TGF-ß	transforming growth factor-beta
TiO2	titanium dioxide
TOF	time-of-flight
Tris/HCl	tris-(hydroxymethyl)-aminomethanhydrochlorid
TRITC	tetramethylrhodamine isothiocyanate
VEGF	vascular endothelial cell growth factor
vWF	von Willebrand factor

7 List of Figures

8 List of Tables

9 References

1. Rosiak, J.M. and F. Yoshii, *Hydrogels and their medical applications.* Nuclear Instruments and Methods in Physics Research Section B: Beam Interactions with Materials and Atoms, 1999. **151**(1–4): p. 56-64.
2. Vashist, A. and S. Ahmad, *Hydrogels in Tissue Engineering: Scope and Applications.* Current Pharmaceutical Biotechnology, 2015. **16**(7): p. 606-620.
3. Eisenbud, D., et al., *Hydrogel wound dressings: where do we stand in 2003?* Ostomy Wound Manage, 2003. **49**(10): p. 52-7.
4. Nguyen, K.T. and J.L. West, *Photopolymerizable hydrogels for tissue engineering applications.* Biomaterials, 2002. **23**(22): p. 4307-14.
5. Ingber, D.E., *Cellular mechanotransduction: putting all the pieces together again.* FASEB J, 2006. **20**(7): p. 811-27.
6. Engler, A.J., et al., *Matrix elasticity directs stem cell lineage specification.* Cell, 2006. **126**(4): p. 677-89.
7. Gulrez, S.K.H., S. Al-Assaf, and G.O. Phillips, *Hydrogels: Methods of Preparation, Characterisation and Applications, Progress in Molecular and Environmental Bioengineering - From Analysis and Modeling to Technology Applications,* ed. P.A. Carpi. 2011, InTech.
8. da Silva, M.A., et al., *Exploring the kinetics of gelation and final architecture of enzymatically cross-linked chitosan/gelatin gels.* Biomacromolecules, 2015. **16**(4): p. 1401-9.
9. Johnson, P.J., et al., *Controlled release of neurotrophin-3 and platelet-derived growth factor from fibrin scaffolds containing neural progenitor cells enhances survival and differentiation into neurons in a subacute model of SCI.* Cell Transplant, 2010. **19**(1): p. 89-101.
10. Antoine, E.E., P.P. Vlachos, and M.N. Rylander, *Review of collagen I hydrogels for bioengineered tissue microenvironments: characterization of mechanics, structure, and transport.* Tissue Eng Part B Rev, 2014. **20**(6): p. 683-96.
11. Butcher, J.T. and R.M. Nerem, *Porcine aortic valve interstitial cells in three-dimensional culture: comparison of phenotype with aortic smooth muscle cells.* J Heart Valve Dis, 2004. **13**(3): p. 478-85; discussion 485-6.
12. Masters, K.S., et al., *Designing scaffolds for valvular interstitial cells: cell adhesion and function on naturally derived materials.* J Biomed Mater Res A, 2004. **71**(1): p. 172-80.
13. Aurand, E.R., K.J. Lampe, and K.B. Bjugstad, *Defining and designing polymers and hydrogels for neural tissue engineering.* Neurosci Res, 2012. **72**(3): p. 199-213.
14. Martens, P. and K.S. Anseth, *Characterization of hydrogels formed from acrylate modified poly(vinyl alcohol) macromers.* Polymer, 2000. **41**(21): p. 7715-7722.
15. Chirila, T.V., et al., *Poly(2-hydroxyethyl methacrylate) sponges as implant materials: in vivo and in vitro evaluation of cellular invasion.* Biomaterials, 1993. **14**(1): p. 26-38.
16. Tibbitt, M.W. and K.S. Anseth, *Hydrogels as extracellular matrix mimics for 3D cell culture.* Biotechnol Bioeng, 2009. **103**(4): p. 655-63.
17. Cukierman, E., et al., *Taking cell-matrix adhesions to the third dimension.* Science, 2001. **294**(5547): p. 1708-12.
18. Abbott, A., *Cell culture: biology's new dimension.* Nature, 2003. **424**(6951): p. 870-2.
19. Kleinman, H.K., et al., *Use of extracellular matrix components for cell culture.* Anal Biochem, 1987. **166**(1): p. 1-13.
20. Lutolf, M.P. and J.A. Hubbell, *Synthetic biomaterials as instructive extracellular microenvironments for morphogenesis in tissue engineering.* Nat Biotechnol, 2005. **23**(1): p. 47-55.
21. Rowley, J.A., G. Madlambayan, and D.J. Mooney, *Alginate hydrogels as synthetic extracellular matrix materials.* Biomaterials, 1999. **20**(1): p. 45-53.

22. Drury, J.L. and D.J. Mooney, *Hydrogels for tissue engineering: scaffold design variables and applications.* Biomaterials, 2003. **24**(24): p. 4337-51.
23. Alberts, B., et al. , *Molecular Biology of the Cell*. 4th ed. 2002: Garland Science.
24. Kleinman, H.K. and G.R. Martin, *Matrigel: Basement membrane matrix with biological activity.* Seminars in Cancer Biology, 2005. **15**(5): p. 378-386.
25. Temenoff, J.S. and A.G. Mikos, *Review: tissue engineering for regeneration of articular cartilage.* Biomaterials, 2000. **21**(5): p. 431-40.
26. Yurchenco, P.D. and B.L. Patton, *Developmental and pathogenic mechanisms of basement membrane assembly.* Curr Pharm Des, 2009. **15**(12): p. 1277-94.
27. Nicosia, R.F. and A. Ottinetti, *Modulation of microvascular growth and morphogenesis by reconstituted basement membrane gel in three-dimensional cultures of rat aorta: a comparative study of angiogenesis in matrigel, collagen, fibrin, and plasma clot.* In Vitro Cell Dev Biol, 1990. **26**(2): p. 119-28.
28. Philp, D., et al., *Complex extracellular matrices promote tissue-specific stem cell differentiation.* Stem Cells, 2005. **23**(2): p. 288-96.
29. Kleinman, H.K., D. Philp, and M.P. Hoffman, *Role of the extracellular matrix in morphogenesis.* Curr Opin Biotechnol, 2003. **14**(5): p. 526-32.
30. Kleinman, H.K., et al., *Isolation and characterization of type IV procollagen, laminin, and heparan sulfate proteoglycan from the EHS sarcoma.* Biochemistry, 1982. **21**(24): p. 6188-93.
31. Kleinman, H.K., et al., *Basement membrane complexes with biological activity.* Biochemistry, 1986. **25**(2): p. 312-8.
32. Odland, G.F., *The fine structure of the interrelationship of cells in the human epidermis.* J Biophys Biochem Cytol, 1958. **4**(5): p. 529-38.
33. Prevention, C.f.D.C.a., *Antibiotic resistance threats in the United Stats.* U.S. Department of Health and Human Services, 2013.
34. Proksch, E., J.M. Brandner, and J.M. Jensen, *The skin: an indispensable barrier.* Exp Dermatol, 2008. **17**(12): p. 1063-72.
35. Elias, P.M., *The skin barrier as an innate immune element.* Seminars in Immunopathology, 2007. **29**(1): p. 3-14.
36. Danzmann, L., et al., *Health care workers causing large nosocomial outbreaks: a systematic review.* BMC Infect Dis, 2013. **13**: p. 98.
37. Yanaga, K., et al., *Hepatitis-C Virus-Infection among Japanese General Surgical Patients.* World Journal of Surgery, 1995. **19**(5): p. 694-697.
38. Straccia, M.C., et al., *Alginate Hydrogels Coated with Chitosan for Wound Dressing.* Marine Drugs, 2015. **13**(5): p. 2890-2908.
39. Linden, S.K., et al., *Mucins in the mucosal barrier to infection.* Mucosal Immunol, 2008. **1**(3): p. 183-97.
40. Turner, B.S., et al., *Cysteine-rich regions of pig gastric mucin contain von willebrand factor and cystine knot domains at the carboxyl terminal(1).* Biochim Biophys Acta, 1999. **1447**(1): p. 77-92.
41. Bell, S.L., G. Xu, and J.F. Forstner, *Role of the cystine-knot motif at the C-terminus of rat mucin protein Muc2 in dimer formation and secretion.* Biochem J, 2001. **357**(Pt 1): p. 203-9.
42. Perez-Vilar, J. and R.L. Hill, *The structure and assembly of secreted mucins.* J Biol Chem, 1999. **274**(45): p. 31751-4.
43. Sheehan, J.K., et al., *Identification of molecular intermediates in the assembly pathway of the MUC5AC mucin.* J Biol Chem, 2004. **279**(15): p. 15698-705.
44. Bansil, R. and B.S. Turner, *Mucin structure, aggregation, physiological functions and biomedical applications.* Current Opinion in Colloid & Interface Science, 2006. **11**(2–3): p. 164-170.
45. Shi, L., et al., *Mucin coating on polymeric material surfaces to suppress bacterial adhesion.* Colloids and Surfaces B-Biointerfaces, 2000. **17**(4): p. 229-239.

46. Pan, Q., et al., *Enhanced Membrane-tethered Mucin 3 (MUC3) Expression by a Tetrameric Branched Peptide with a Conserved TFLK Motif Inhibits Bacteria Adherence.* Journal of Biological Chemistry, 2013. **288**(8): p. 5407-5416.
47. Lieleg, O., et al., *Mucin Biopolymers As Broad-Spectrum Antiviral Agents.* Biomacromolecules, 2012. **13**(6): p. 1724-1732.
48. Bansil, R., E. Stanley, and J.T. LaMont, *Mucin biophysics.* Annu Rev Physiol, 1995. **57**: p. 635-57.
49. Co, J.Y., T. Crouzier, and K. Ribbeck, *Probing the Role of Mucin-Bound Glycans in Bacterial Repulsion by Mucin Coatings.* Advanced Materials Interfaces, 2015.
50. Crouzier, T., et al., *Modulating Mucin Hydration and Lubrication by Deglycosylation and Polyethylene Glycol Binding.* Advanced Materials Interfaces, 2015: p. n/a-n/a.
51. Celli, J., et al., *Viscoelastic properties and dynamics of porcine gastric mucin.* Biomacromolecules, 2005. **6**(3): p. 1329-1333.
52. Lieleg, O., I. Vladescu, and K. Ribbeck, *Characterization of Particle Translocation through Mucin Hydrogels.* Biophysical Journal, 2010. **98**(9): p. 1782-1789.
53. Pfeiffer, C.J., *Experimental-Analysis of Hydrogen-Ion Diffusion in Gastrointestinal Mucus Glycoprotein.* American Journal of Physiology, 1981. **240**(2): p. G176-G182.
54. Li, L., et al., *A microfluidic in vitro system for the quantitative study of the stomach mucus barrier function.* Lab on a Chip, 2012. **12**(20): p. 4071-4079.
55. Celli, J.P., et al., *Rheology of gastric mucin exhibits a pH-dependent sol-gel transition.* Biomacromolecules, 2007. **8**(5): p. 1580-1586.
56. Levental, I., P.C. Georges, and P.A. Janmey, *Soft biological materials and their impact on cell function.* Soft Matter, 2007. **3**(3): p. 299-306.
57. Duffy, C.V., L. David, and T. Crouzier, *Covalently-crosslinked mucin biopolymer hydrogels for sustained drug delivery*. Acta Biomater, 2015. **20**: p. 51-9.
58. Strous, G.J. and J. Dekker, *Mucin-type glycoproteins.* Crit Rev Biochem Mol Biol, 1992. **27**(1-2): p. 57-92.
59. Sellers, L.A., et al., *Mechanical characterization and properties of gastrointestinal mucus gel.* Biorheology, 1987. **24**(6): p. 615-23.
60. Matsui, H., et al., *A physical linkage between cystic fibrosis airway surface dehydration and Pseudomonas aeruginosa biofilms.* Proceedings of the National Academy of Sciences of the United States of America, 2006. **103**(48): p. 18131-18136.
61. Hirrien, M., et al., *Thermogelation of methylcelluloses: new evidence for understanding the gelation mechanism.* Polymer, 1998. **39**(25): p. 6251-6259.
62. Tate, M.C., et al., *Biocompatibility of methylcellulose-based constructs designed for intracerebral gelation following experimental traumatic brain injury.* Biomaterials, 2001. **22**(10): p. 1113-1123.
63. De la Riva, B., et al., *Local controlled release of VEGF and PDGF from a combined brushite-chitosan system enhances bone regeneration.* J Control Release, 2010. **143**(1): p. 45-52.
64. Roberts, A.B., et al., *Transforming growth factor type beta: rapid induction of fibrosis and angiogenesis in vivo and stimulation of collagen formation in vitro.* Proc Natl Acad Sci U S A, 1986. **83**(12): p. 4167-71.
65. Diegelmann, R.F. and M.C. Evans, *Wound healing: an overview of acute, fibrotic and delayed healing.* Front Biosci, 2004. **9**: p. 283-9.
66. Hameedaldeen, A., et al., *FOXO1, TGF-beta regulation and wound healing.* Int J Mol Sci, 2014. **15**(9): p. 16257-69.
67. Massague, J., *TGF[beta] signalling in context.* Nat Rev Mol Cell Biol, 2012. **13**(10): p. 616-630.
68. Bao, P., et al., *The role of vascular endothelial growth factor in wound healing.* J Surg Res, 2009. **153**(2): p. 347-58.
69. Ferrara, N., H.P. Gerber, and J. LeCouter, *The biology of VEGF and its receptors.* Nat Med, 2003. **9**(6): p. 669-76.

70. Sung, J.H., et al., *Gel characterisation and in vivo evaluation of minocycline-loaded wound dressing with enhanced wound healing using polyvinyl alcohol and chitosan.* Int J Pharm, 2010. **392**(1-2): p. 232-40.
71. Caló, E. and V.V. Khutoryanskiy, *Biomedical applications of hydrogels: A review of patents and commercial products.* European Polymer Journal, 2015. **65**: p. 252-267.
72. Lau, H.K. and K.L. Kiick, *Opportunities for multicomponent hybrid hydrogels in biomedical applications.* Biomacromolecules, 2015. **16**(1): p. 28-42.
73. Singh, B., S. Sharma, and A. Dhiman, *Design of antibiotic containing hydrogel wound dressings: biomedical properties and histological study of wound healing.* Int J Pharm, 2013. **457**(1): p. 82-91.
74. Enoch, S., J.E. Grey, and K.G. Harding, *ABC of wound healing. Non-surgical and drug treatments.* BMJ, 2006. **332**(7546): p. 900-3.
75. Hess, C.T. and R.S. Kirsner, *Orchestrating wound healing: assessing and preparing the wound bed.* Adv Skin Wound Care, 2003. **16**(5): p. 246-57; quiz 258-9.
76. Song, J., et al., *Sequential Drug Release and Enhanced Photothermal and Photoacoustic Effect of Hybrid Reduced Graphene Oxide-Loaded Ultrasmall Gold Nanorod Vesicles for Cancer Therapy.* ACS Nano, 2015. **9**(9): p. 9199-209.
77. Hudson, S.P., et al., *Injectable in situ cross-linking hydrogels for local antifungal therapy.* Biomaterials, 2010. **31**(6): p. 1444-52.
78. Hasan, A., et al., *Injectable Hydrogels for Cardiac Tissue Repair after Myocardial Infarction.* Advanced Science, 2015. **2**(11): p. n/a-n/a.
79. Kamata, H., et al., *Design of Hydrogels for Biomedical Applications.* Adv Healthc Mater, 2015. **4**(16): p. 2360-74.
80. Hoare, T.R. and D.S. Kohane, *Hydrogels in drug delivery: Progress and challenges.* Polymer, 2008. **49**(8): p. 1993-2007.
81. Paavola, A., et al., *Controlled release of lidocaine from injectable gels and efficacy in rat sciatic nerve block.* Pharm Res, 1995. **12**(12): p. 1997-2002.
82. Bayramoglu, G., et al., *Examination of fabrication conditions of acrylate-based hydrogel formulations for doxorubicin release and efficacy test for hepatocellular carcinoma cell.* J Biomater Sci Polym Ed, 2014. **25**(7): p. 657-78.
83. Barzegar-Jalali, M., et al., *Kinetic analysis of drug release from nanoparticles.* J Pharm Pharm Sci, 2008. **11**(1): p. 167-77.
84. Mohammed, A.R., et al., *Liposome formulation of poorly water soluble drugs: optimisation of drug loading and ESEM analysis of stability.* Int J Pharm, 2004. **285**(1-2): p. 23-34.
85. Ahuja, G. and K. Pathak, *Porous carriers for controlled/modulated drug delivery.* Indian J Pharm Sci, 2009. **71**(6): p. 599-607.
86. Kawashita, M., et al., *In vitro apatite formation and drug loading/release of porous TiO2 microspheres prepared by sol-gel processing with different SiO2 nanoparticle contents.* Mater Sci Eng C Mater Biol Appl, 2015. **50**: p. 317-23.
87. Wang, T., et al., *Potential application of functional porous TiO2 nanoparticles in light-controlled drug release and targeted drug delivery.* Acta Biomater, 2015. **13**: p. 354-63.
88. Bharti, C., et al., *Mesoporous silica nanoparticles in target drug delivery system: A review.* Int J Pharm Investig, 2015. **5**(3): p. 124-33.
89. Yufang, Z., *Mesoporous Silica Nanoparticles with a Core-Shell Structure for Drug Delivery.* Journal of Bioanalysis and Biomedicine, 2013. **- 5**(3): p. - -.
90. Ahmadi, E., et al., *Synthesis and surface modification of mesoporous silica nanoparticles and its application as carriers for sustained drug delivery.* Drug Deliv, 2014. **21**(3): p. 164-72.
91. Natarajan, S.K. and S. Selvaraj, *Mesoporous silica nanoparticles: importance of surface modifications and its role in drug delivery.* RSC Advances, 2014. **4**(28): p. 14328-14334.

92. Caldorera-Moore, M., et al., *Designer nanoparticles: incorporating size, shape and triggered release into nanoscale drug carriers.* Expert Opin Drug Deliv, 2010. **7**(4): p. 479-95.
93. Wang, J.J., et al., *Recent advances of chitosan nanoparticles as drug carriers.* Int J Nanomedicine, 2011. **6**: p. 765-74.
94. Prabaharan, M., *Chitosan-based nanoparticles for tumor-targeted drug delivery.* International Journal of Biological Macromolecules, 2015. **72**: p. 1313-1322.
95. Wasiak, I., et al., *Dextran Nanoparticle Synthesis and Properties.* PLoS One, 2016. **11**(1): p. e0146237.
96. Thambi, T., et al., *Bioreducible carboxymethyl dextran nanoparticles for tumor-targeted drug delivery.* Adv Healthc Mater, 2014. **3**(11): p. 1829-38.
97. Ge, J., et al., *Protein-polymer hybrid nanoparticles for drug delivery.* Small, 2012. **8**(23): p. 3573-8.
98. Rafat, M., et al., *Nanoparticles incorporated collagen hydrogels for sustained release of EGF.* Acta Ophthalmologica, 2013. **91**: p. 0-0.
99. Zhu, J. and R.E. Marchant, *Design properties of hydrogel tissue-engineering scaffolds.* Expert Rev Med Devices, 2011. **8**(5): p. 607-26.
100. Zou, H., W. Guo, and W.Z. Yuan, *Supramolecular hydrogels from inclusion complexation of alpha-cyclodextrin with densely grafted chains in micelles for controlled drug and protein release.* Journal of Materials Chemistry B, 2013. **1**(45): p. 6235-6244.
101. Liu, Z.J. and P. Yao, *Versatile injectable supramolecular hydrogels containing drug loaded micelles for delivery of various drugs.* Polymer Chemistry, 2014. **5**(3): p. 1072-1081.
102. Arends, F., et al., *The biophysical properties of Basal lamina gels depend on the biochemical composition of the gel.* PLoS One, 2015. **10**(2): p. e0118090.
103. Hughes, C.S., L.M. Postovit, and G.A. Lajoie, *Matrigel: A complex protein mixture required for optimal growth of cell culture.* Proteomics, 2010. **10**(9): p. 1886-1890.
104. Schuster, B.S., et al., *Nanoparticle diffusion in respiratory mucus from humans without lung disease.* Biomaterials, 2013. **34**(13): p. 3439-46.
105. Arends, F., R. Baumgartel, and O. Lieleg, *Ion-specific effects modulate the diffusive mobility of colloids in an extracellular matrix gel.* Langmuir, 2013. **29**(51): p. 15965-73.
106. Schilling, J., E. Sackmann, and A.R. Bausch, *Digital imaging processing for biophysical applications.* Review of Scientific Instruments, 2004. **75**(9): p. 2822-2827.
107. Collins, S.J., R.C. Gallo, and R.E. Gallagher, *Continuous growth and differentiation of human myeloid leukaemic cells in suspension culture.* Nature, 1977. **270**(5635): p. 347-9.
108. Nowald, C., et al., *A Selective Mucin/Methylcellulose Hybrid Gel with Tailored Mechanical Properties.* Macromol Biosci, 2016.
109. Sandberg, T., H. Blom, and K.D. Caldwell, *Potential use of mucins as biomaterial coatings. I. Fractionation, characterization, and model adsorption of bovine, porcine, and human mucins.* J Biomed Mater Res A, 2009. **91**(3): p. 762-72.
110. Mc, M.J., *Histological demonstration of mucin after periodic acid.* Nature, 1946. **158**: p. 202.
111. Cauda, V., et al., *Multiple Core-Shell Functionalized Colloidal Mesoporous Silica Nanoparticles.* J Am Chem Soc, 2009. **131**(32): p. 11361-11370.
112. Zheng, G. and W.S. Price, *Simultaneous convection compensation and solvent suppression in biomolecular NMR diffusion experiments.* J Biomol NMR, 2009. **45**(3): p. 295-9.
113. Pichert, A., et al., *Characterization of the interaction of interleukin-8 with hyaluronan, chondroitin sulfate, dermatan sulfate and their sulfated derivatives by spectroscopy and molecular modeling.* Glycobiology, 2012. **22**(1): p. 134-145.

114. Fritze, A., et al., *Remote loading of doxorubicin into liposomes driven by a transmembrane phosphate gradient.* Biochimica Et Biophysica Acta-Biomembranes, 2006. **1758**(10): p. 1633-1640.
115. Cinelli, S., et al., *Properties of mixed DOTAP-DPPC bilayer membranes as reported by differential scanning calorimetry and dynamic light scattering measurements.* Journal of Physical Chemistry B, 2007. **111**(33): p. 10032-10039.
116. Michel, N., et al., *Determination of phase transition temperatures of lipids by light scattering.* Chemistry and Physics of Lipids, 2006. **139**(1): p. 11-19.
117. Owczarzy, R., et al., *IDT SciTools: a suite for analysis and design of nucleic acid oligomers.* Nucleic Acids Research, 2008. **36**: p. W163-W169.
118. Zadeh, J.N., et al., *NUPACK: Analysis and Design of Nucleic Acid Systems.* Journal of Computational Chemistry, 2011. **32**(1): p. 170-173.
119. Taton, T.A., *Preparation of gold nanoparticle-DNA conjugates.* Curr Protoc Nucleic Acid Chem, 2002. **Chapter 12**: p. Unit 12 2.
120. Demers, L.M., et al., *A fluorescence-based method for determining the surface coverage and hybridization efficiency of thiol-capped oligonucleotides bound to gold thin films and nanoparticles.* Anal Chem, 2000. **72**(22): p. 5535-41.
121. Aumailley, M., *The laminin family.* Cell Adh Migr, 2013. **7**(1): p. 48-55.
122. Lieleg, O. and K. Ribbeck, *Biological hydrogels as selective diffusion barriers.* Trends in Cell Biology, 2011. **21**(9): p. 543-551.
123. Lieleg, O., R.M. Baumgärtel, and A.R. Bausch, *Selective Filtering of Particles by the Extracellular Matrix: An Electrostatic Bandpass.* Biophysical Journal, 2009. **97**(6): p. 1569-1577.
124. Lieleg, O., R.M. Baumgartel, and A.R. Bausch, *Selective filtering of particles by the extracellular matrix: an electrostatic bandpass.* Biophys J, 2009. **97**(6): p. 1569-77.
125. Otsuka, H., Y. Nagasaki, and K. Kataoka, *PEGylated nanoparticles for biological and pharmaceutical applications.* Adv Drug Deliv Rev, 2003. **55**(3): p. 403-19.
126. Jokerst, J.V., et al., *Nanoparticle PEGylation for imaging and therapy.* Nanomedicine (Lond), 2011. **6**(4): p. 715-28.
127. Owens, D.E., 3rd and N.A. Peppas, *Opsonization, biodistribution, and pharmacokinetics of polymeric nanoparticles.* Int J Pharm, 2006. **307**(1): p. 93-102.
128. Wong, R.S., M. Ashton, and K. Dodou, *Effect of Crosslinking Agent Concentration on the Properties of Unmedicated Hydrogels.* Pharmaceutics, 2015. **7**(3): p. 305-19.
129. Lieleg, O., M.M.A.E. Claessens, and A.R. Bausch, *Structure and dynamics of cross-linked actin networks.* Soft Matter, 2010. **6**(2): p. 218-225.
130. Lieleg, O., et al., *Mechanics of bundled semiflexible polymer networks.* Physical Review Letters, 2007. **99**(8).
131. Charras, G. and E. Sahai, *Physical influences of the extracellular environment on cell migration.* Nat Rev Mol Cell Biol, 2014. **15**(12): p. 813-24.
132. Aumailley, M., R. Timpl, and W. Risau, *Differences in laminin fragment interactions of normal and transformed endothelial cells.* Exp Cell Res, 1991. **196**(2): p. 177-83.
133. Miyazaki, T., et al., *Laminin E8 fragments support efficient adhesion and expansion of dissociated human pluripotent stem cells.* Nat Commun, 2012. **3**: p. 1236.
134. Desban, N., et al., *alpha1beta1-integrin engagement to distinct laminin-1 domains orchestrates spreading, migration and survival of neural crest cells through independent signaling pathways.* J Cell Sci, 2006. **119**(Pt 15): p. 3206-18.
135. Chung, A.E. and M.E. Durkin, *Entactin: structure and function.* Am J Respir Cell Mol Biol, 1990. **3**(4): p. 275-82.
136. Niederman, R., P.C. Amrein, and J. Hartwig, *3-Dimensional Structure of Actin-Filaments and of an Actin Gel Made with Actin-Binding Protein.* Journal of Cell Biology, 1983. **96**(5): p. 1400-1413.
137. Maccioni, R.B. and V. Cambiazo, *Role of Microtubule-Associated Proteins in the Control of Microtubule Assembly.* Physiological Reviews, 1995. **75**(4): p. 835-864.

138. Patenaude, M., N.M.B. Smeets, and T. Hoare, *Designing Injectable, Covalently Cross-Linked Hydrogels for Biomedical Applications.* Macromolecular Rapid Communications, 2014. **35**(6): p. 598-617.
139. Cho, J.Y., et al., *Physical gelation of chitosan in the presence of beta-glycerophosphate: The effect of temperature.* Biomacromolecules, 2005. **6**(6): p. 3267-3275.
140. Chenite, A., et al., *Novel injectable neutral solutions of chitosan form biodegradable gels in situ.* Biomaterials, 2000. **21**(21): p. 2155-2161.
141. Elkins, T.E., et al., *Adhesion Prevention by Solutions of Sodium Carboxymethylcellulose in the Rat .2.* Fertility and Sterility, 1984. **41**(6): p. 929-932.
142. Tate, M.C., et al., *Biocompatibility of methylcellulose-based constructs designed for intracerebral gelation following experimental traumatic brain injury.* Biomaterials, 2001. **22**(10): p. 1113-23.
143. Desbrieres, J., M. Hirrien, and S.B. Ross-Murphy, *Thermogelation of methylcellulose: rheological considerations (vol 41, pg 2451, 2000).* Polymer, 2000. **41**(14): p. 5547-5547.
144. Bain, M.K., et al., *Effect of PEG-salt mixture on the gelation temperature and morphology of MC gel for sustained delivery of drug.* Carbohydrate Polymers, 2013. **91**(2): p. 529-536.
145. Kuang, Q.L., et al., *Thermogelation hydrogels of methylcellulose and glycerol-methylcellulose systems.* Journal of Applied Polymer Science, 2006. **100**(5): p. 4120-4126.
146. Vagenende, V., M.G.S. Yap, and B.L. Trout, *Mechanisms of Protein Stabilization and Prevention of Protein Aggregation by Glycerol.* Biochemistry, 2009. **48**(46): p. 11084-11096.
147. Kunz, W., J. Henle, and B.W. Ninham, *'Zur Lehre von der Wirkung der Salze' (about the science of the effect of salts): Franz Hofmeister's historical papers.* Current Opinion in Colloid & Interface Science, 2004. **9**(1-2): p. 19-37.
148. Rossettoa, H.L., M.F. de Souza, and V.C. Pandolfelli, *Chaotropic Substances and their Effects on the Mechanical Strength of Portland Cement-Based Materials.* Materials Research-Ibero-American Journal of Materials, 2008. **11**(2): p. 183-185.
149. Clapham, D.E., *Calcium signaling.* Cell, 2007. **131**(6): p. 1047-58.
150. Li, L.D., et al., *Spatial configuration and composition of charge modulates transport into a mucin hydrogel barrier.* Biophys J, 2013. **105**(6): p. 1357-65.
151. Arends, F., et al., *A microfluidics approach to study the accumulation of molecules at basal lamina interfaces.* Lab Chip, 2015.
152. Al-Baradi, A.M., et al., *Diffusion of dextran within poly(methacrylic acid) hydrogels.* Journal of Polymer Science Part B-Polymer Physics, 2012. **50**(18): p. 1286-1292.
153. Kingsnorth, A.N. and J. Slavin, *Peptide growth factors and wound healing.* Br J Surg, 1991. **78**(11): p. 1286-90.
154. Argyo, C., et al., *Multifunctional Mesoporous Silica Nanoparticles as a Universal Platform for Drug Delivery.* Chemistry of Materials, 2014. **26**(1): p. 435-451.
155. Cazes, J., *Encyclopedia of Chromatography.* Vol. Two. 2005: Taylor & Francis Group. 1121.
156. Patel, H.S., D., *A Comparative Study Of Hydrogel Dressing Versus Conventional Dressing In Burns.* The Internet Journal of Surgery, 2006. **13**(2).
157. Artimo, P., et al., *ExPASy: SIB bioinformatics resource portal.* Nucleic Acids Res, 2012. **40**(Web Server issue): p. W597-603.
158. Venegas, B. and P.L.G. Chong, *Drug Release from Liposomes can be Modulated by the Extent of Cholesterol Superlattice in the Lipid Membrane.* Biophysical Journal, 2010. **98**(3): p. 273a-273a.
159. van der Meel, R., et al., *Extracellular vesicles as drug delivery systems: Lessons from the liposome field.* Journal of Controlled Release, 2014.

160. Mouritsen, O.G. and K. Jorgensen, *Micro-, nano- and meso-scale heterogeneity of lipid bilayers and its influence on macroscopic membrane properties.* Mol Membr Biol, 1995. **12**(1): p. 15-20.
161. Prados, J., et al., *Doxorubicin-loaded nanoparticles: new advances in breast cancer therapy.* Anticancer Agents Med Chem, 2012. **12**(9): p. 1058-70.
162. Tian, P., M. Brandl, and R. Mandrell, *Porcine gastric mucin binds to recombinant norovirus particles and competitively inhibits their binding to histo-blood group antigens and Caco-2 cells.* Letters in Applied Microbiology, 2005. **41**(4): p. 315-320.
163. Shi, L., et al., *Bacterial adhesion to a model surface with self-generated protection coating of mucin via jacalin.* Biotechnology Letters, 2001. **23**(6): p. 437-441.
164. Walker, M. and D. Parsons, *The biological fate of silver ions following the use of silver-containing wound care products - a review.* International Wound Journal, 2014. **11**(5): p. 496-504.
165. Agnihotri, S., S. Mukherji, and S. Mukherji, *Size-controlled silver nanoparticles synthesized over the range 5-100 nm using the same protocol and their antibacterial efficacy.* Rsc Advances, 2014. **4**(8): p. 3974-3983.
166. Dreaden, E.C., et al., *Size matters: gold nanoparticles in targeted cancer drug delivery.* Ther Deliv, 2012. **3**(4): p. 457-78.
167. Aranda, P.S., D.M. LaJoie, and C.L. Jorcyk, *Bleach gel: a simple agarose gel for analyzing RNA quality.* Electrophoresis, 2012. **33**(2): p. 366-9.
168. Akbarzadeh, A., et al., *Liposome: classification, preparation, and applications.* Nanoscale Res Lett, 2013. **8**(1): p. 102.
169. Eloy, J.O., et al., *Liposomes as carriers of hydrophilic small molecule drugs: strategies to enhance encapsulation and delivery.* Colloids Surf B Biointerfaces, 2014. **123**: p. 345-63.
170. Richter, R.P., J.L.K. Him, and A. Brisson, *Supported lipid membranes.* Materials Today, 2003. **6**(11): p. 32-37.
171. Toh, M.-R. and G.N.C. Chiu, *Liposomes as sterile preparations and limitations of sterilisation techniques in liposomal manufacturing.* Asian Journal of Pharmaceutical Sciences, 2013. **8**(2): p. 88-95.
172. Zavaleta, C.L., et al., *Multiplexed imaging of surface enhanced Raman scattering nanotags in living mice using noninvasive Raman spectroscopy.* Proc Natl Acad Sci U S A, 2009. **106**(32): p. 13511-6.
173. Dreaden, E.C., et al., *Tamoxifen-poly(ethylene glycol)-thiol gold nanoparticle conjugates: enhanced potency and selective delivery for breast cancer treatment.* Bioconjug Chem, 2009. **20**(12): p. 2247-53.
174. Dhar, S., et al., *Polyvalent Oligonucleotide Gold Nanoparticle Conjugates as Delivery Vehicles for Platinum(IV) Warheads (vol 131, pg 14652, 2009).* Journal of the American Chemical Society, 2010. **132**(48): p. 17335-17335.
175. Giljohann, D.A., et al., *Gene Regulation with Polyvalent siRNA-Nanoparticle Conjugates.* Journal of the American Chemical Society, 2009. **131**(6): p. 2072-+.
176. Xiang, Z., P. Sarazin, and B.D. Favis, *Controlling burst and final drug release times from porous polylactide devices derived from co-continuous polymer blends.* Biomacromolecules, 2009. **10**(8): p. 2053-66.
177. Fruijtier-Pölloth, C., *Safety assessment on polyethylene glycols (PEGs) and their derivatives as used in cosmetic products.* Toxicology, 2005. **214**(1–2): p. 1-38.
178. Critchfield, A.S., et al., *Cervical mucus properties stratify risk for preterm birth.* PLoS One, 2013. **8**(8): p. e69528.
179. Nagamachi, E., et al., *Studies on osmotic stability of liposomes prepared with bacterial membrane lipids by carboxyfluorescein release.* Microbiol Immunol, 1992. **36**(3): p. 231-4.

180. He, D., et al., *Reversible stimuli-responsive controlled release using mesoporous silica nanoparticles functionalized with a smart DNA molecule-gated switch.* Journal of Materials Chemistry, 2012. **22**(29): p. 14715-14721.
181. Torigoe, H., et al., *Thermodynamic properties of the specific binding between Ag+ ions and C:C mismatched base pairs in duplex DNA.* Nucleosides Nucleotides Nucleic Acids, 2011. **30**(2): p. 149-67.

10 Acknowledgements

Jetzt kommt der Teil meiner Doktorarbeit, auf den ich mich beim Schreiben schon die ganze Zeit gefreut habe. Jetzt darf ich allen danken, die mir beim Gelingen dieser Arbeit geholfen haben.

Ganz besonders möchte ich mich bei meinem Doktorvater Prof. Lieleg bedanken, der mich in seine Arbeitsgruppe aufgenommen hat und mir damit überhaupt erst ermöglicht hat, diese Arbeit anzufertigen. Eine bessere Betreuung kann man sich von seinem Mentor nicht erhoffen, seine Türe stand mir stets und damit meine ich wirklich täglich offen, sei es um Daten zu diskutieren oder mir physikalisches Wissen näherzubringen. Im Besonderen möchte ich mich auch dafür bedanken, dass er stets ein offenes Ohr für meine Ideen hatte und ich mich im Labor entfalten durfte.

Man kann wahrscheinlich auch alleine eine praktische Doktorarbeit im Labor zustande bringen, mit einer tollen Arbeitsgruppe wie die der Biomechanik ist man aber vermutlich deutlich erfolgreicher und garantiert macht es viel mehr Spaß. Deshalb ein ganz großes Dankeschön an alle, mit denen ich während meiner Zeit am IEMTUM zusammen arbeiten durfte, ihr wart spitze. Ich danke Bärchen für die Lachkrämpfe und für die Hilfe an Rheolotta und dem Rheonauten. Auch Kathrin danke ich für die Hilfe bei rheologischen Fragen und es tut mir leid, dass ich nicht immer gleich den richtigen Stift parat hatte. Ohne Fabi hätte ich mir wahrscheinlich öfters mal die Zähne an kniffligen Fragestellungen ausgebissen und ohne sie hätte mir ein knallharter Diskussionspartner gefehlt, danke dafür. Und ohne Benni wäre das Labor im Chaos versunken und ich hätte nie die Bekanntschaft mit dem Krümelmonster gemacht, ich werde sie beide im nächsten Labor vermissen.

Zum Schluss möchte ich auch allen anderen danken, im Besonderen meiner Familie samt Tigger und Schucki, Lisa und meinen Freunden, die mir während der Doktorarbeit zur Seite gestanden haben.

11 List of Publications

CN, B. Käsdorf, O. Lieleg,

Controlled nanoparticle release from a hydrogel by DNA-mediated particle disaggregation,

Journal of Controlled Release, submitted

CN, A. Penk, H. Chiu, T. Bein, D. Huster, O. Lieleg,

A Selective Mucin/Methylcellulose Hybrid Gel with Tailored Mechanical Properties,

Macromolecular Bioscience, 16(4), 567-579, doi:10.1002/mabi.201500353 (2016)

F. Arends, **CN**, K. Pflieger, K. Boettcher, S. Zahler, O. Lieleg,

The biophysical properties of basal lamina gels depend on the biochemical composition of the gel,

PLoS ONE, 10(2), e0118090, doi:10.1371/journal.pone.0118090 (2015)